MODELING AND CONTROL OF SOLID OXIDE FUEL CELL – GAS TURBINE POWER PLANT SYSTEMS

by

Adam Hahn

BS, University of Pittsburgh, 2000

Submitted to the Graduate Faculty of

School of Engineering in partial fulfillment

of the requirements for the degree of

Master of Science in Mechanical Engineering

University of Pittsburgh

2004

UNIVERSITY OF PITTSBURGH

SCHOOL OF ENGINEERING

This thesis was presented

by

Adam Hahn

It was defended on

April 8, 2004

and approved by

Sung Kwon Cho, Assistant Professor, Department of Mechanical Engineering

William Clark, Associate Professor, Department of Mechanical Engineering

Thesis Advisor: Jeffrey Vipperman, Assistant Professor, Department of Mechanical Engineering

MODELING AND CONTROL OF SOLID OXIDE FUEL CELL – GAS TURBINE POWER PLANT SYSTEMS

Adam Hahn, MSME

University of Pittsburgh, 2004

There is extensive research taking place involving fuel cell – gas turbine combined power plant systems. These systems use a high temperature fuel cell and a gas turbine to achieve higher overall performance and efficiency than a single mode power plant. Due to the high temperature of the exhaust gasses of the fuel cell, heat can be recuperated and used to drive a gas turbine. The turbine creates additional power and is a means of utilizing the exhaust energy of the fuel cell. Despite the research being done on integrating these systems, little work has been done to characterize the dynamics of the integrated systems. Due to the high response of the fuel cell and the relatively sluggish response of the turbine, control of the system needs to be understood. This thesis develops dynamic models of the individual components that comprise a fuel cell – gas turbine hybrid system (axial flow compressor, combustor, turbine, fuel cell, and heat exchanger). These models are incorporated to produce a complete dynamic hybrid model. The models are analyzed with respect to dynamics and basic control techniques are used to control various parameters. It is shown that the system can be controlled using hydrogen input flow rate control for the fuel cell and controlled turbine inlet temperature for the gas turbine.

TABLE OF CONTENTS

LIST OF TABLES

LIST OF FIGURES

To Susan

1.0 INTRODUCTION

1.1 FUEL CELL POWER PLANTS

Fuel cells have been receiving a lot of attention lately due to their potential as becoming a new energy source with a large range of applications. The benefits of fuel cell energy are primarily the high efficiency with which they can run and their environmentally friendly by-products. Fuel cells use a chemical reaction to convert hydrogen and oxygen into water, releasing electrons (energy) in the process. Essentially, the hydrogen fuel is being "burnt" in a simple reaction to produce water. Instead of releasing energy, however, the reaction releases an electric current. A typical fuel cell consists of two electrodes (anode and cathode) where the reactions take place. The electrodes are also the mediums that the current flows between. Sandwiched between the electrodes is an electrolyte material which the ions flow through to keep the reactions continuous. There are several types of fuel cells being researched at present. These include alkaline, proton exchange membrane, phosphoric acid, molten carbonate, and solid oxide. They differ in electrode and electrolyte materials, chemical reactions, catalysts, and operating temperatures and pressures [8].

Fuel cells can be incorporated with other components to create high efficiency industrial power plants. These power plants usually consist of a pump or blower to circulate the working fluids through the fuel cell, a reformer to convert the fuel into hydrogen, pressure regulators, and power conditioners. Most fuel cells do not use straight hydrogen as fuel. Therefore they must incorporate a reformer to convert the fuel being used into hydrogen. Fuels that can be reformed are methane, ammonia, methanol, ethanol, or gasoline. Storage of the fuel for power plants is a significant issue in fuel cell power plant design. Typically, the fuel cell takes up a small percentage of the overall size of a fuel cell power plant.

1.2 GAS TURBINES

Gas turbines have been used to produce power for many years. They are the main source of power for jet aircraft and can be used to create industrial power in gas turbine power plants. The concept is similar to that of a combustion engine: to convert chemical energy of a fuel into mechanical energy. The fluid cycle is similar to a combustion engine. A working fluid (usually air) is compressed, fuel is added and the mixture is ignited to initiate combustion. The combustion releases energy and the fluid expands moving a physical barrier. The moving of the barrier is the mechanical work out of the cycle. A portion of this mechanical energy is then used to compress the fluid in the next cycle. The difference between a gas turbine and a combustion engine is that the gas turbine cycle runs continuously instead of in iterative cycles (one after the other). The basic components of a gas turbine are a compressor, combustor or heat exchanger, and a turbine. The compressor is typically an axial flow or centrifugal design. The working

fluid flows through the compressor and the pressure is increased. Heat energy is then added to the fluid via combustion or a heat exchanger. The fluid then expands through a turbine (doing work on it) to create energy. The turbine is used to run the compressor. The difference between the power it takes to run the compressor and the total power out of the turbine is the net power produced by the cycle. Gas turbine power plants can be designed for a multitude of cycles using multiple compressors and turbines as well as heat exchangers and throttling devices [6], [14].

1.3 COMBINED FUEL CELL GAS TURBINE POWER PLANTS

As stated above, some fuel cells, specifically solid oxide (SOFC) and molten carbonate (MCFC), operate at elevated temperatures [11]. Therefore, their exhaust gasses (steam and air) exit with high heat energy content. These high temperature gasses can be used to run a gas turbine bottoming cycle and extract even more energy. Fuel Cell Gas Turbine (FCGT) hybrid systems can be configured in a number of ways. Heat exchangers can be used to transfer energy from one stream to another or the working fluid of the gas turbine can be used to supply the fuel cell air input. These systems are capable of delivering power at very high efficiencies [8], [11]. Current research is being done to incorporate fuel cells and gas turbines into power plants in a number of ways. A number of technical papers have been written about the design and modeling of these systems. Specifically the National Energy Technology Laboratory in Morgantown WV is currently building and analyzing a hybrid system [12], [13], [20].

One of the issues with the hybrid design is there must be a means to control the power output of the entire system as well as protect the individual components from unstable conditions that could damage the power plant. This entails understanding the dynamics of each of the components used in the hybrid system and controlling the power output of entire plant. These components include a compressor, combustor, turbine, fuel cell, and heat exchanger. The main unstable conditions of the compressor are rotating stall and surge. Rotating stall is a condition where the flow over individual blades of the compressor is not constant. If a stall condition develops in one of the channels, a decrease in flow rate through that channel will occur. The stall will then become induced in the adjacent channel while recovering in the original channel. The stall will propagate about the axis of the compressor and will affect the overall flow rate through the compressor [2]. Surge is also a common unstable condition in axial flow compressors; this is where the flow rate through the entire compressor is reversed due to the pressure drop being in the opposite direction of the flow. This can severely damage compressors and affect the overall power cycle [2]. As well as compressor concerns, fuel cells need to be maintained at specific temperatures and pressures to operate safely and efficiently. Also the humidity needs to be kept at certain levels to ensure proper operation. These are things that need to be addressed when dealing with the control of FCGT systems. There is research being done concerning the steady state operation of the systems [10], [19], [21]. However, limited research has been performed concerning the dynamics and transients of the systems including a controls study.

1.4 CURRENT STUDY AND ORGANIZATION

This paper will develop independent dynamic models of an axial flow compressor, combustor, turbine, heat exchanger, and solid oxide fuel cell. The models will be arranged in state space format and analyzed independently. They can then be combined into any configuration of a combined cycle and analyzed. Two configurations will be developed and simulated using MATLAB and Simulink software. Basic controls will be applied to one configuration and simulated to show stability.

The components of the gas turbine will be developed first starting with the axial flow compressor. This is a complicated dynamic model that can be used to simulate rotating stall and surge conditions. It will also calculate the flow rate and pressure drop across the compressor as well as the angular velocity of the compressor. This angular velocity will also be the angular velocity of the turbine since they are rigidly coupled [1]. A combustor model will be developed in section 2.2. It is based on a "well stirred reactor" model that uses methane and air as the reactants [5]. It calculates the mass fractions of reactants and products in the reactor as well as the output temperature rise of the products of combustion. Section 2.3 will develop a turbine model that calculates the power output of the turbine and the torque developed [4], [6]. This torque will be fed back into the compressor model and drive the compressor. Section 3.1 will develop a counter flow heat exchanger model to be used in the final hybrid model [7], [17]. It is based on a log mean temperature difference profile and calculates the output temperature and flow rates of hot and cold fluid streams. Section 3.2 explains a simple fuel cell model that is used to determine the power output of a solid oxide fuel cell based on inlet flow rates of hydrogen and air [9]. It assumes a constant operating temperature. Section 4.1 uses the gas

turbine components to form an integrated gas turbine power plant and simulates the operating conditions. Section 4.2 integrates all the components to form two possible configurations of a FCGT hybrid system. Section 5 simulates one FCGT configuration with respect to step inputs and applies a basic control scenario to the system.

2.0 GAS TURBINE MODELS

The components of a typical gas turbine will be developed in this section. These components include a compressor, combustor, and a turbine. The working fluid (usually air) enters the compressor where work is added to bring it to a higher pressure and temperature. It then enters a combustor where it is burned with fuel to raise it to a higher temperature and higher enthalpy. It then expands through the turbine and creates mechanical energy. A portion of the energy produced is used to run the compressor which is rigidly coupled to the turbine. The models developed here are an axial flow compressor, a well stirred reaction (WSR) combustor, and a turbine. The axial flow compressor will contain the dynamics of the velocity of the rotor, which is the coupled compressor, turbine, and generator.

2.1 AXIAL FLOW COMPRESSOR

The compressor is an integral component of the FCGT model. Rotodynamic pumps are difficult to model due to their complicated flow characteristics and various unstable conditions they can encounter [2]. The compressor characteristics will also be a key factor of the controllability of the entire integrated system. The compressor, and hence the gas turbine, will be sluggish and slower to react to control input than the other components of the system. An ideal compressor

model would be as simple as possible but complete enough to describe the various phenomenons that would affect its controllability.

2.1.1 Main Operating Theory

An axial flow compressor works by causing a working fluid to pass through a series of expanding passages. The passages are formed by the profile of annular blades fixed to a circular shaft. The fluid velocity is normal to the blades and moves through the compressor axially. The fluid pressure increases as the axial velocity decreases. In order to maintain the axial velocity at a constant level, the annulus diameter increases in proportion to the pressure increase.

Axial compressors are made up of several stages, each having a stator blade row and a rotor blade row. The fluid passes through the rotor which transfers kinetic energy and accelerates the fluid. It is then diffused through the expanding blade passages of the stator. The stator also redirects the fluid to a suitable entry angle for the next rotor. Figure 1 displays a typical compressor stage with relative fluid velocities where C1, C2, and C3 are the fluid velocity directions before the rotor, after the rotor, and after the stator respectively and R is the rotor velocity direction. Along with the rotors and stators, there are entry and exit guide vanes at the beginning and end of the entire compressor.

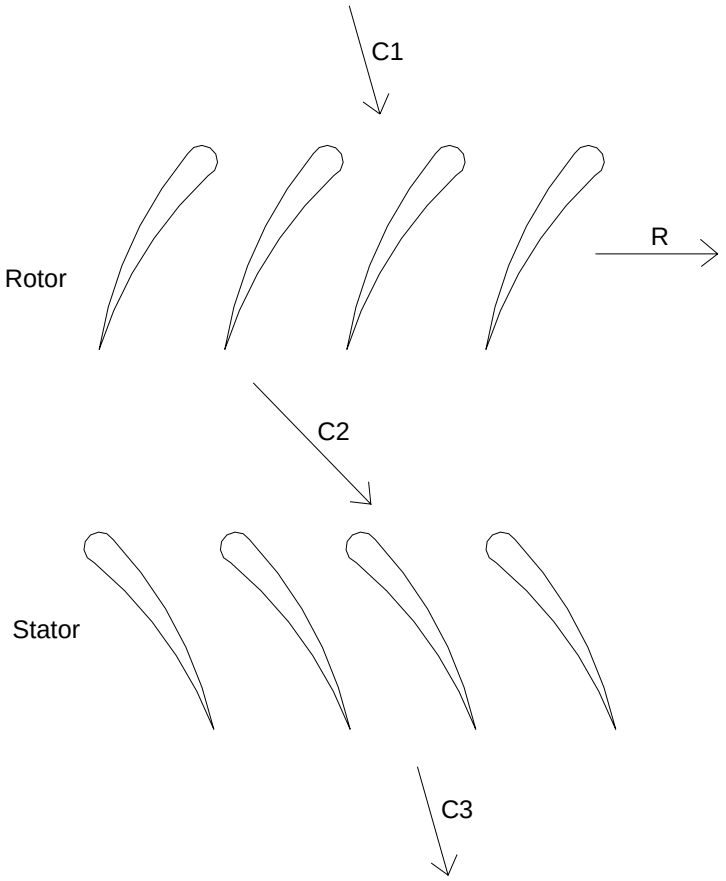

Figure 1: Axial Compressor Rotor and Stator Diagrams

The two main dynamic conditions that the compressor model should estimate, along with normal operation, are surge and rotating stall. Surge is an axi-symetric instability condition which can occur near the pressure ratio limit in an axial or centrifugal compressor. Surge is induced if there is a sudden decrease in mass flow rate or increase in system demand. Axial flow compressors are inherently unstable because the flow is moving in the direction of increased pressure. If the pressure on one side of the overall compressor changes rapidly, the pressure gradient will be too high for the compressor to handle, and the overall flow direction reverses (i.e. the compressor

"surges"). This induces an oscillatory flow behavior that could, if not controlled, compromise the performance of the entire system or destroy the compressor [14].

Stall is similar to the stalling that can occur in a single airfoil (such as in an airplane). It occurs when the angle of attack of the airfoil is too aggressive and the flow of the working fluid is completely separated from the backside of the blade (Figure 2).

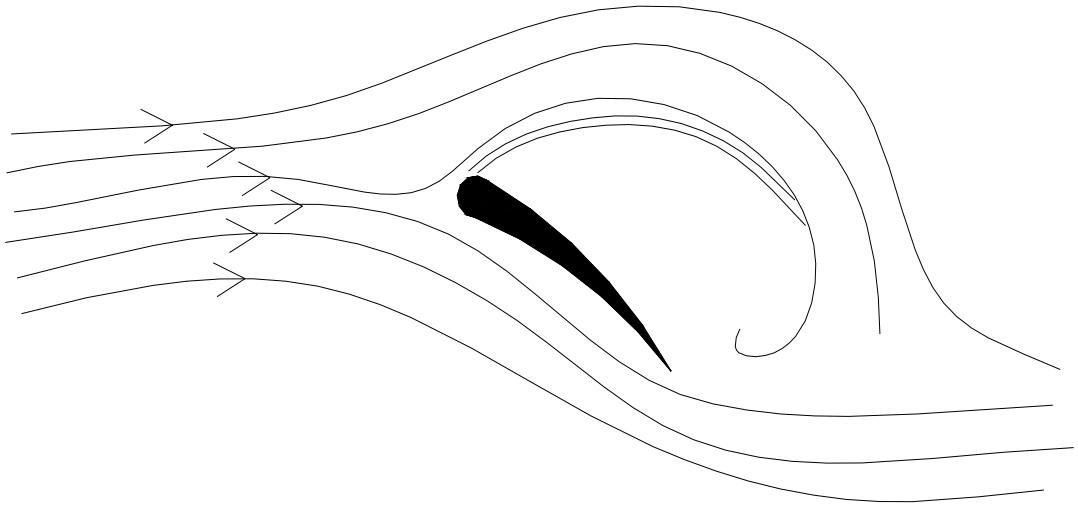

Figure 2: Airflow Around a Stalled Airfoil

If there is a minor flow disturbance in one vane and stalling occurs, it will alter the inlet flow angle of the adjacent vane. This disturbance will then cause stalling in that vane, enabling the original vane to recover. The disturbance will propagate radially around the entire blade row. The phenomenon is called rotating stall.

The fluid dynamics associated with these two phenomenon's are complicated and not fully understood [14]. It is thought that they are related and the onset of one can cause the other to occur. Surge and stall are an integral part of gas turbine modeling and control, and will be accounted for in the models developed below.

2.1.2 Compressor Characteristics

Using non-dimensional techniques, overall compressor performance can be represented by two graphs. These graphs are obtained through testing of the compressor. A sample axial flow compressor characteristic is shown in Figure 3. The graph shows the pressure ratio vs. the dimensionless flow rate. A surge line can be drawn by connecting each maxima on the different speed curves. The stable operating area of the compressor is to the right of the surge line. In this region, a flow rate decrease would result in an increase in pressure ratio. If the operating point moves to the left of the surge line, oscillation of the flow direction (surge) will occur as described above.

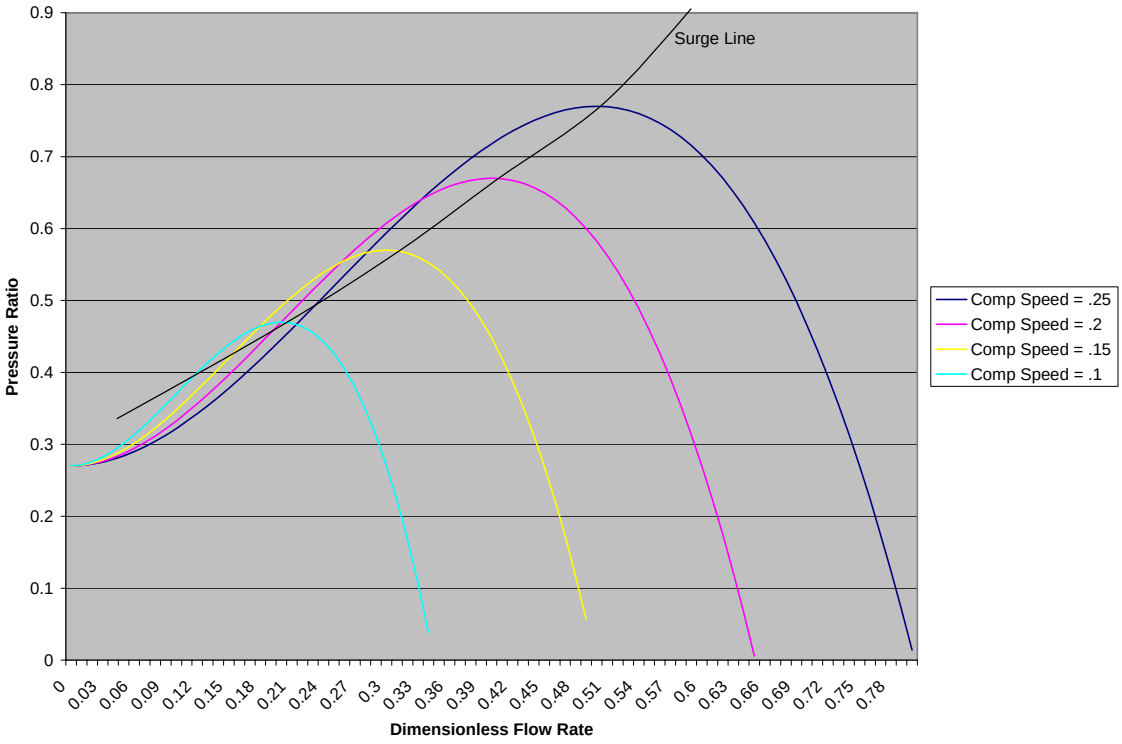

Figure 3: Typical Axial Flow Compressor Characteristic

2.1.3 Moore Greitzer Model

The standard model for axial flow compressors is the Moore – Greitzer model [1]. It accurately models compressor behavior as well as transients such as surge and stall. The compressor is simulated using the following model (Figure 4).

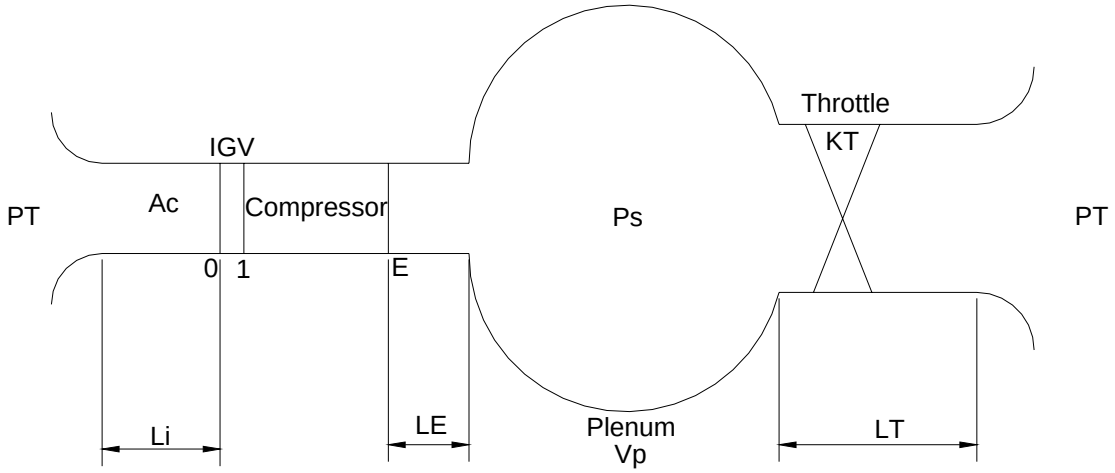

Figure 4: Moore – Greitzer Compressor Model

Figure 4 terms are defined as:

P_T: total pressure ahead of entrance and after throttle

Ac: compressor duct area

IGV: inlet guide vanes

L_i, L_E, L_T: length of inlet, exit, and throttle ducts, respectively

0: compressor entrance

1: inlet guide vane exit

E: compressor exit

Ps: static pressure at the end of exit duct and pressure in plenum

Vp: volume of plenum

K_T: throttle coefficient

The model consists of a compressor operating in a duct that discharges to a downstream plenum. Velocities and accelerations in the plenum are considered negligible and its pressure can be assumed constant spatially but varying in time. Due to this time pressure variation, the plenum could be treated as a gas spring. The flow through the system is controlled by the throttle coefficient (K_T), which is analogous to the loss through a turbine. Incompressible flow can be assumed everywhere except the plenum, due to small mach numbers and the oscillation frequency being below the acoustic resonance of the system. The compressor can be treated as two dimensional in longitudinal axis and rotor angle if a high hub to tip ratio is assumed. This means that the flow variations occurring radially are negligible if the hub radius, which is the radius of the center core of the compressor, is not much smaller than the outer radius of the rotor and stator blades.

In the development of the compressor equations, all distances are non-dimensionalized by the mean compressor radius.

$$\eta = \frac{X}{R}: \text{ axial coordinate} \tag{1}$$

where X: actual axial coordinate

R: compressor mean radius

θ: angular coordinate (already non-dimensional)

Time is non-dimensionalized by

$$\xi = \frac{Ut}{R} \tag{2}$$

where U: rotor speed at mean diameter (dist / time)

t: time

The pressure rise across a compressor of N stages (not including the inlet and exit guide vanes) is described by [1]:

$$\frac{p_E - p_1}{\rho U^2} = NF(\varphi) - \frac{1}{2a}\left(2\frac{\partial \varphi}{\partial \xi} + \frac{\partial \varphi}{\partial \theta}\right), \tag{3}$$

where: p_E: pressure coefficient at the exit of core compressor

p_1: pressure coefficient at the entrance of the core compressor

ρ: density

$F(\varphi)$: axi-symetric performance of the blade row

$\varphi = \frac{C_x}{U}$: local unsteady axial velocity coefficient (4)

$$a \equiv \frac{R}{N\tau U} \tag{5}$$

where τ: time constant, internal lag of the compressor

The average φ around the circumference of the compressor is defined as Φ:

$$\Phi(\xi) = \frac{1}{2\pi}\int_0^{2\pi} \varphi(\xi,\theta)d\theta \tag{6}$$

Assuming that any circumferential non-uniformity persists along the axis of the compressor, then:

$$\varphi = \Phi(\xi) + g(\xi,\theta), \text{ and} \tag{7}$$

$$h = h(\xi,\theta), \tag{8}$$

where g: disturbance of axial flow coefficient at a specific radial location

h: circumferential flow coefficient

Note that the circumferential averages of both g and h are zero.

The pressure across the inlet guide vanes (IGV) is computed as:

$$\frac{p_1 - p_0}{\rho U^2} = \frac{1}{2} K_G h^2 \tag{9}$$

where: K_G: loss coefficient of the IGV (=1 if no loss, <1 if loss)

p_0: static pressure to the entrance of the IGV

The velocity potential upstream of the IGV is defined, the gradient of which will give the axial and circumferential velocity coefficients everywhere in the entrance duct as:

$$\tilde{\varphi}_\eta = \frac{v}{U} \qquad \tilde{\varphi}_\theta = \frac{u}{U}, \tag{10a,b}$$

where v and u are the axial and circumferential velocities, respectively

where the subscript denotes partial differentiation

These velocity coefficients satisfy Laplace's equation due to the assumption of irrotational flow upstream of the IGV, such that:

$$\nabla^2 \tilde{\varphi} = 0 . \tag{11}$$

Using LaPlace's equation with Bernoulli's equation [2], the pressure drop across the inlet is:

$$\frac{p_T - p_0}{\rho U^2} = \frac{1}{2}\left(\varphi^2 + h^2\right) + \left(\tilde{\varphi}_\xi\right)_0 , \tag{12}$$

where $\tilde{\phi}_\xi$: represents the unsteadiness in Φ and g.

2.1.4 Exit Ducts and Guide Vanes

In the exit duct, a rotational flow occurs when the axial flow varies with θ. Using a simplifying assumption that the pressure in the exit duct differs only slightly from the pressure in the plenum (p_S), it can be shown that the Laplace equation is satisfied. Using the Euler equation, the pressure drop between the plenum and the exit is computed as follows:

$$\frac{p_s - p_E}{\rho U^2} = \left(P\right)_E = -L_E \frac{\partial \Phi}{\partial \theta} - \left(m - 1\right)\left(\tilde{\varphi}'_\xi\right)_0 \quad , \tag{13}$$

where m is a parameter to specify the length of the exit duct (2 for long, 1 for short).

Finally, the overall pressure rise from the upstream reservoir (p_T) to the plenum (p_S) can be derived by combining the above equations (3, 9, 11, 12), defining new parameters and making a simplifying assumption that $\frac{dh}{d\theta} = \quad g$.

$$\Psi(\xi) = \psi_c(\Phi - Y_{\theta\theta}) - L_c \frac{d\Phi}{d\xi} - mY_{\xi} + \frac{1}{2a}(2Y_{\xi\theta\theta} + Y_{\theta\theta\theta}), \tag{14}$$

where $\Psi(\xi) \equiv \frac{p_s - p_T}{\rho U^2}$ (15)

where Ψ : the dimesionless pressure rise and,

$$\psi_c(\varphi) = NF(\varphi) - \frac{1}{2}\varphi^2 \tag{16}$$

is the compressor performance that would be expected if no angle or time dependence were permitted.

$$Y(\xi,\theta) \equiv \left(\tilde{\varphi}'\right)_0 \tag{17}$$

$$Y_{\theta\theta} = \left(\tilde{\varphi}'_{\eta}\right)_0 \tag{18}$$

The overall pressure balance of the entire system can now be derived by developing the equations for the plenum and throttle. The plenum will eliminate any spatial variation in pressure. The mass entering the plenum will be different than the mass leaving, causing the

plenum to act as a gas spring. The rate of density change in the plenum will be equal to the ratio of dp_s / dt to the square of the speed of sound. The mass balance of the plenum is:

$$L_c \frac{d\Psi}{d\xi} = \frac{1}{4B^2}[\Phi(\xi) - \Phi_T(\xi)] \tag{19}$$

where L_c: total length of the compressor and ducts

$$B \equiv \frac{U}{2a_s}\sqrt{\frac{V_P}{A_C L_C}} \qquad \text{(B parameter)} \tag{20}$$

where: a_s - speed of sound

The throttle discharges to p_T which is at the same pressure as the inlet reservoir. The momentum balance of the plenum is then:

$$\Psi(\xi) = F_T(\Phi_T) + L_T \frac{d\Phi_T}{d\xi} \tag{21}$$

where F_T is the throttle characteristic equation. A reasonable characteristic could be in parabolic form [1]:

$$F_T = \frac{1}{2} K_T \Phi_T^2 \tag{22}$$

where K_T is a constant throttle coefficient

These equations complete the system of equations for the system as shown in Figure 4. They are summarized below. The first is the local momentum balance of the system (from (14)), the second is the annulus averaged momentum balance (from (6), (7), (8)), and the third is the mass balance of the plenum (from (21), (22)):

$$\Psi(\xi) + L_C \frac{d\Phi}{d\xi} = \psi_C(\Phi - Y_{\theta\theta}) - mY_{\xi} + \frac{1}{2a}(2Y_{\xi\theta\theta} + Y_{\theta\theta\theta}) \tag{23}$$

$$\Psi(\xi) + L_C \frac{d\Phi}{d\xi} = \frac{1}{2\pi}\int_0^{2\pi} \Psi_C(\Phi - Y_{\theta\theta})d\theta \tag{24}$$

$$L_C \frac{d\Psi}{d\xi} = \frac{1}{4B^2}[\Phi(\xi) - F_T{}^{-1}(\Psi)] \tag{25}$$

where $\Phi = \frac{C_X}{U}$ - annulus averaged dimensionless axial flow coefficient

Ψ - is given by equation (15)

ξ - is given by equation (2)

2.1.5 Compressor Characteristic

A function for the characteristic of the compressor (ψ_C) must be chosen arbitrarily since it is an inherent feature of any given compressor. The characteristic is usually measured for any individual compressor. As stated above, the characteristic usually takes on the form of a smooth

cubic equation. The following is a generic form of this equation with user-defined parameters Ψ_{C0}, W, and H which can be specified to create a unique characteristic curve to match the curve of any compressor.

$$\psi_C(\varphi) = \psi_{C0} + H\left[1 + \frac{3}{2}\left(\frac{\varphi}{W} - 1\right) - \frac{1}{2}\left(\frac{\varphi}{W} - 1\right)^3\right] \tag{26}$$

where ψ_{C0} - shut off value of axisymetric characteristic

H - Height of characteristic

W - Width of characteristic

$\varphi = \Phi - Y_{\theta\theta}$ accounts for departures from the averaged velocity coefficient Φ.

2.1.6 Galerkin Procedure

The system of equations above is highly non-linear and would be difficult to solve. The derivatives are third order in θ and first order in ξ. The Galerkin procedure of nonlinear mechanics is applied to effectively reduce the order of θ. The Galerkin procedure represents the solution of the differential equation by a sequence of basic functions. This solution is similar to a Fourier series. The variable Y will be represented as a single harmonic function.

$$Y = WA(\xi)\sin(\theta - r(\xi)) \tag{27}$$

where $r(\xi)$ - phase angle

A - amplitude of harmonic function

Introducing a new variable J where:

$$J(\xi) \equiv A^2(\xi) \tag{28}$$

The final simplified equations according to [1] are:

$$\frac{d\Psi}{d\xi} = \frac{W/H}{4B^2}\left[\frac{\Phi}{W} - \frac{1}{W}F_T^{-1}(\Psi)\right]\frac{H}{L_C} \tag{29}$$

$$\frac{d\Phi}{d\xi} = \left[-\frac{\Psi \quad \psi_{C0}}{H} + 1 + \frac{3}{2}\left(\frac{\Phi}{W} - 1\right)\left(1 - \frac{1}{2}J\right) - \frac{1}{2}\left(\frac{\Phi}{W} - 1\right)^3\right]\frac{H}{L_C} \tag{30}$$

$$\frac{dJ}{d\xi} = J\left[1 - \left(\frac{\Phi}{W} - 1\right)^2 - \frac{1}{4}J\right]\frac{3aH}{(1+ma)W} \tag{31}$$

where J - squared amplitude of angular variation (if >0, rotating stall is occurring)

parameters that will govern equations (29) – (31) are repeated here:

H/W: diagram steepness

ψ_{C0}/H: shut off head

L_C: compressor duct length

m: compressor slope

a: internal compressor lag

B: B – parameter dependent on plenum volume and compressor annulus area

F_T: throttle characteristic function

The model above is the most complete axial compressor model to date that simulates surge and rotating stall. However, it assumes a constant angular velocity. This is unsuitable for the current study as the velocity of the compressor must be known to control the overall power output of the entire system. The next section addresses this issue.

2.1.7 Spool Dynamics

The model by Gravdahl and Egeland [3] incorporates spool dynamics into the Moore-Greitzer model. The updated model takes the *B* parameter, which is proportional to compressor speed and defined in equation (20), and makes it a fourth variable. A fourth equation is derived from the momentum balance of the compressor. The three equations above now become four and are put into state space format:

$$\begin{bmatrix} \dot{\Phi} \\ \dot{\Psi} \\ \dot{J} \\ \dot{B} \end{bmatrix} = f \begin{pmatrix} \Phi \\ \Psi \\ J \\ B \end{pmatrix} \tag{32}$$

In the Moore – Greitzer model [1], time was non-dimensionalized using the constant spool speed. Since this quantity will vary, non-dimensionalized time will be updated to incorporate the "desired" angular velocity of the compressor.

$$\xi = \frac{U_d t}{R} \tag{33}$$

where U_d: desired compressor speed at mean radius

The momentum balance of the compressor spool can be written using the momentum equation [3]:

$$I \frac{d\omega}{dt} = \tau_t - \tau_c \tag{34}$$

where ω - compressor angular velocity

I - compressor moment of inertia

$\tau_{t,c}$ - turbine and compressor torque

The angular velocity and the torques can be non-dimensionalized by the following:

$$\omega = \frac{2U}{R}, \text{ and} \tag{35}$$

$$\Gamma = \Gamma_t - \Gamma_c = \frac{\tau_t - \tau_c}{\rho A_c R U^2} . \tag{36}$$

Rewriting equation (34), the momentum balance in non-dimensional form can be written as:

$$\frac{dB}{d\xi} = \Lambda_1 B^2 (\Gamma_t - \Gamma_c) \quad , \tag{37}$$

where $\Lambda_1 \equiv \frac{\rho R^3 A_c b}{2 I U_d}$ and (38)

$$b \equiv 2 a_s \sqrt{\frac{A_c L_c}{V_p}} . \tag{39}$$

The compressor torque can be found by a momentum balance. The torque that is imparted to the compressor equals the change in angular momentum of the fluid.

$$\tau_c = m_c R_{tip} C_{tip} , \tag{40}$$

where $m_c = \rho A_c U \varphi$ - mass flow rate of the working fluid

R_{tip} - radius of the rotor

C_{tip} - tangential velocity of the fluid upon exit of the rotor

The slip factor (σ) can be defined as the ratio of the velocity of the rotor blades and the tangential velocity of the fluid. It can be thought of as a kind of efficiency of the compressor on the fluid and is defined as:

$$\sigma \equiv \frac{C_{tip}}{U_{tip}} \tag{41}$$

Considering equations (40) and (41), the non-dimensionalized torque can then be written as:

$$\Gamma_c = \sigma\left(\frac{R_{tip}}{R}\right)^2 \varphi \tag{42}$$

Incorporating equations (29). (30), (31), (37), and (42), based on the above analysis, produces the four state space equations that will simulate the behavior of an axial compression system.

$$\frac{d\Phi}{d\xi} = \frac{H}{\ell_c B}\left(-\frac{\Psi - \psi_{c0}}{H} + 1 + \frac{3}{2}\left(\frac{\varphi}{W} - 1\right)\left(1 - \frac{J}{2}\right) - \frac{1}{2}\left(\frac{\varphi}{W} - 1\right)^3 - \frac{\ell_E U_d \Gamma \Lambda_1}{bH}\Phi\right) \tag{43}$$

$$\frac{d\Psi}{d\xi} = \frac{\Lambda_2}{B}(\Phi - \Phi_T) - 2\Lambda_1 \Gamma B \Psi \tag{44}$$

$$\frac{dJ}{d\xi} = J\left(1 - \left(\frac{\varphi}{W} - 1\right)^2 - \frac{J}{4} - \frac{2U_d \Gamma \Lambda_1 (m - 10W)}{3bH}\right)\frac{3aH}{(1 - m_B a)W} \tag{45}$$

$$\frac{dB}{d\xi} = \Lambda_1 \Gamma B^2 = \Lambda_1 (u - \tau_c) B^2 \tag{46}$$

ℓ_c - non dimensional compressor duct length

where $\Phi_T = \gamma\sqrt{\Psi}$ is the throttle characteristic (47)

where γ is the throttle gain

This model uses the torque of the turbine as the input u. This can be used as a speed control using the desired compressor speed U_d. This would be analogous to controlling the throttle coefficient K_T in the Moore Greitzer model.

2.1.8 Compressor Model Simulation

A script file was created in MATLAB using an ODE solver function to simulate the model with the added spool dynamics in [3]. The simulation parameters are summarized in Table 1.

Table 1: Compressor Simulation Parameters

R	0.1 m
l_E	8
V_p	1.5 m^3
H	0.18
I	0.03 kgm^2
ρ	1.15 kg/m^3
l_I	2
A_C	0.01 m^2
W	0.25
m	1.75
a_s	340 m/s
L_c	3 m
a	0.3
Ψ_{C0}	0.3
σ	0.9

Results of this model corroborated with the results of reference [3]. The speed control in the paper is a simple proportional type controller that is governed by the following equation.

$$\Gamma_t = c(U_d - U) \tag{47}$$

where c is the proportional gain of the controller

The two simulations discussed in the paper were simulated using the MATLAB model and the results verified. The first is the unstable condition with the proportional gain c set to 1 and the throttle gain (γ) set at 0.5. These conditions set the operating point of the compressor to the left of the local maximum on the characteristic and, therefore in the surge condition. Figures 5-8 present the results of the simulation. Figure 5 gives the dimensionless flow rate, Figure 6 gives the dimensionless pressure ratio, Figure 7 gives the rotating stall coefficient, and Figure 8 gives the dimensionless compressor speed.

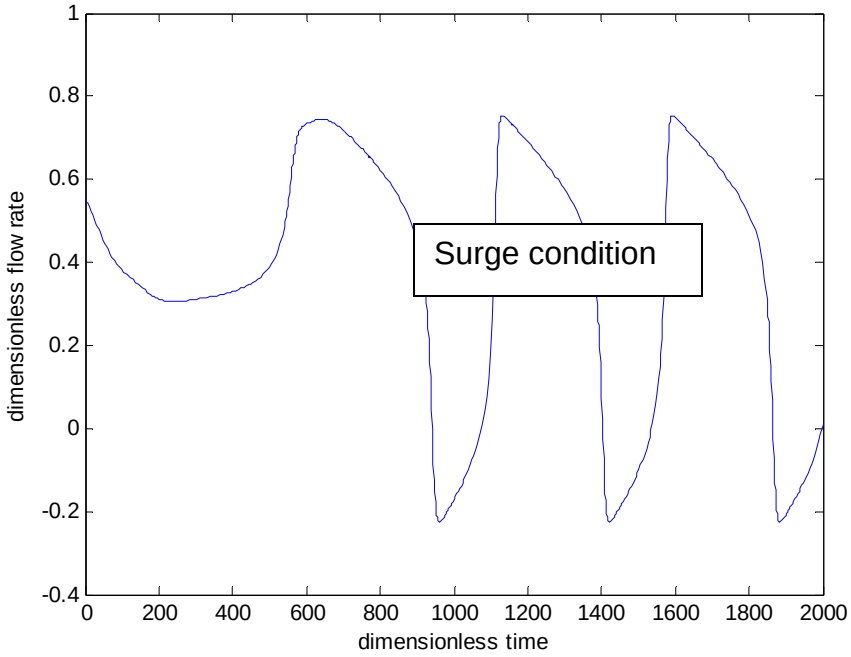

Figure 5: Dimensionless Flow Rate (*Φ*), Unstable Condition

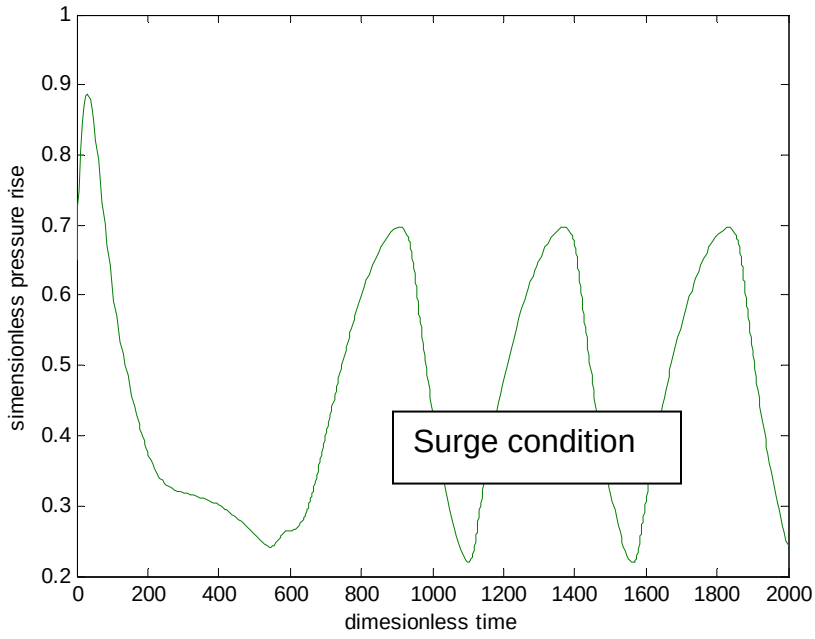

Figure 6: Dimensionless Pressure Ratio (*Ψ*), Unstable Condition

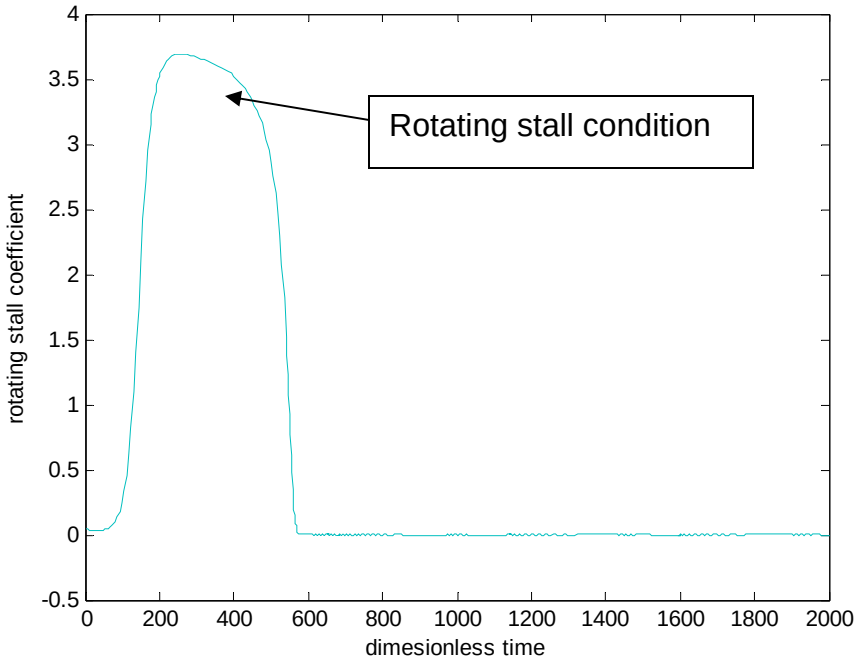

Figure 7: Stall Coefficient (*J*), Unstable Condition

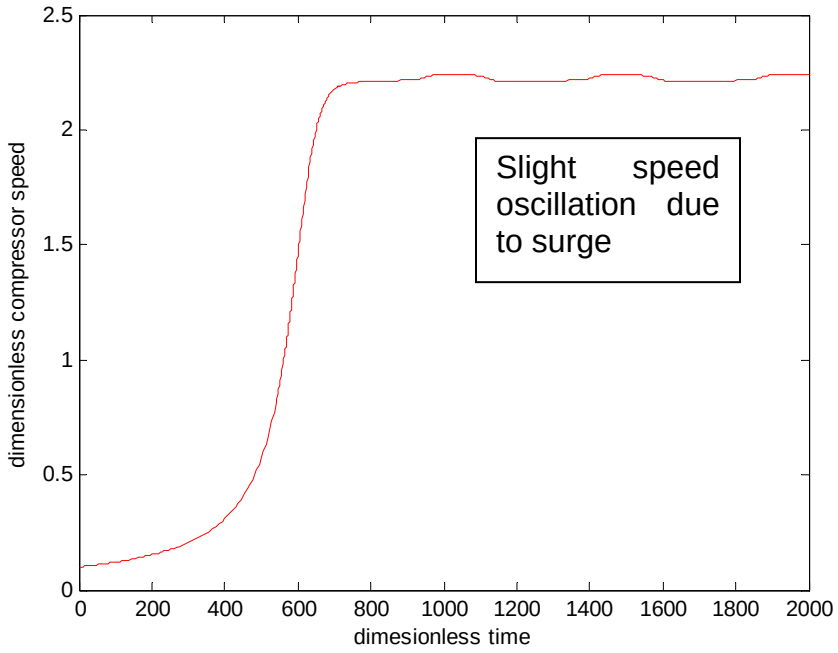

Figure 8: Dimensionless Compressor Speed (*B*), Unstable Condition

As shown from Figure 7, the compressor starts in a rotating stall position since the J value is greater than zero. The pressure (Figure 6) is decreasing at this stage, however the flow rate (Figure 5) is staying relatively constant. This is due to the fact that even though individual compressor blades are experiencing reduced flow, the average flow around the entire compressor is constant. As the time increases the input torque begins to increase the speed of the compressor due to the proportional control algorithm (Figure 8). As the speed increases, the stall is damped out and the compressor goes into axial surge. This can be seen by the oscillating flow rate and pressure starting around $\xi = 600$ on the abscissa. Figure 5 shows the flow rate dropping below zero which implies that the flow is actually reversing through the compressor. This is consistent with the definition of surge in a compressor and shows that the model can simulate both unstable conditions. The results in Figures 5-8 match those reported in [3].

The second simulation discussed in [3] is a stable condition. This displays the model starting in rotating stall and recovering to steady state equilibrium. The throttle coefficient (γ) is set to 0.65 and the proportional gain, P, is set to 2. Figures 9-12 are similar to Figures 5-8 respectively.

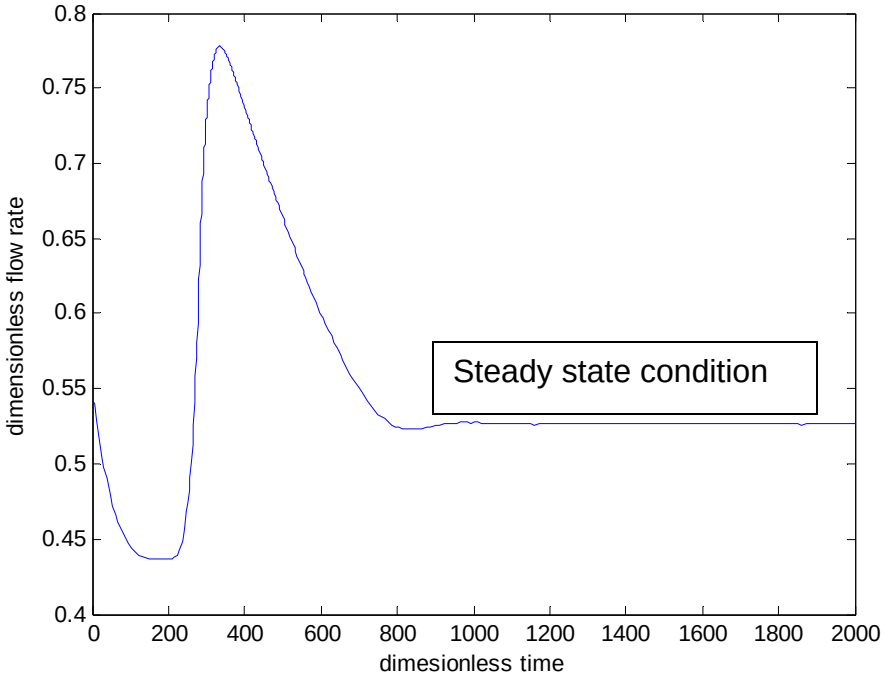

Figure 9: Dimensionless Flow Rate (Φ), Stable Condition

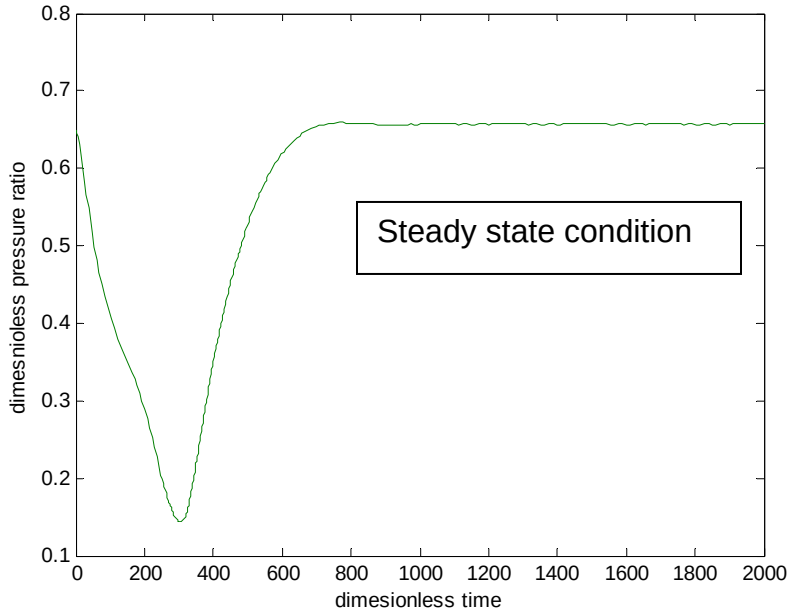

Figure 10: Dimensionless Pressure Ratio (Ψ), Stable Condition

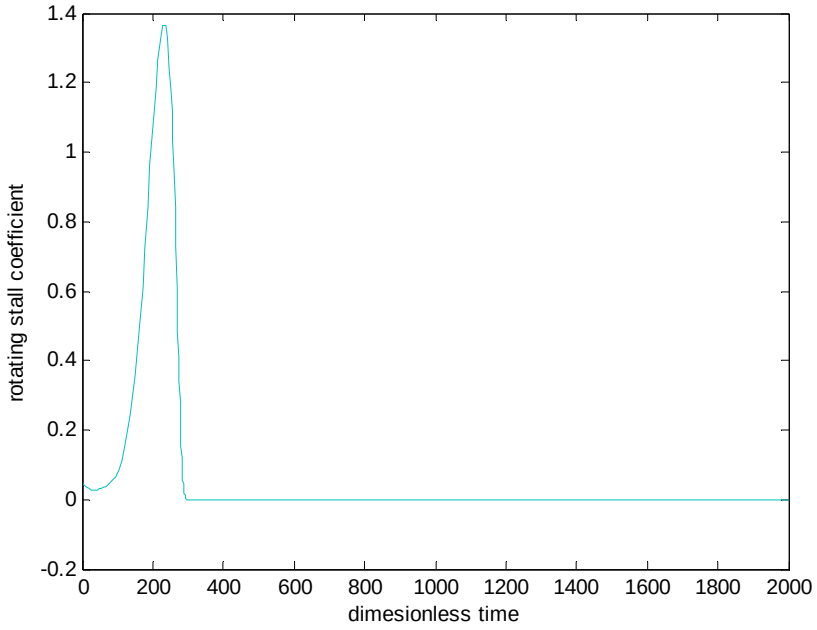

Figure 11: Stall Coefficient (*J*), Stable Condition

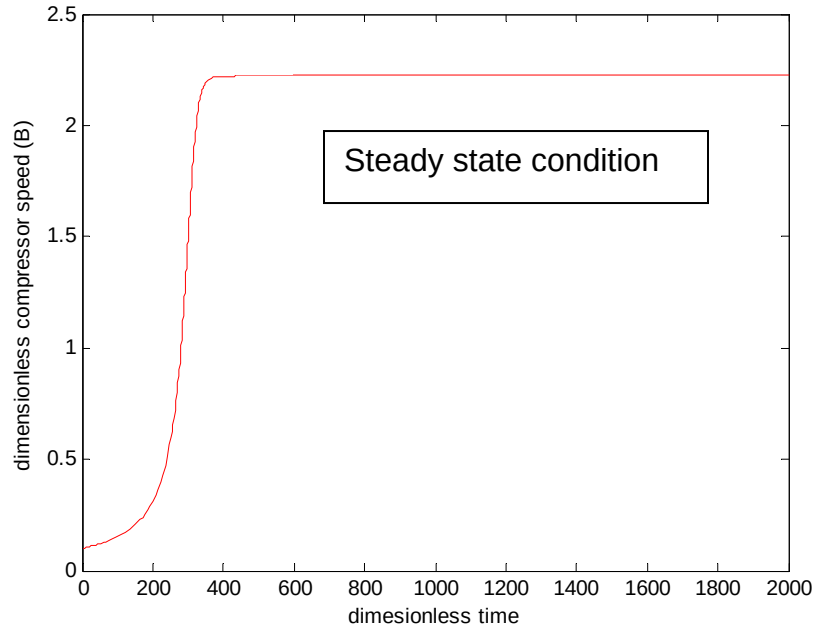

Figure 12: Dimensionless Compressor Speed (*B*), Stable Condition

As shown in figures 9-12, the compressor enters rotating stall at the onset of the simulation (ξ = 200) when the speed (B) is low. This can be seen by the positive stall coefficient (J) in Figure 11. As the input torque gain increases and the compressor gets up to speed, the stall damps out and the compressor enters a steady state condition. Flow rate, speed, and pressure rise all stabilize to a constant value with the stall coefficient at zero. Therefore, the model can simulate a recovery from a stalled condition as well as a steady state condition. These results duplicate those given in [3] and provide confidence that the compressor model is sufficient for incorporation into the entire power plant model.

It was desired to be able to simulate and study the entire model in Simulink. This will allow a more thorough means for a control study and an intuitive feel for the complete model itself. However, due to the complexity of the compressor model, it would be difficult to simulate in Simulink using the standard library of tools. Therefore, a custom Simulink block called an S-function was created. Simulink uses these functions to call lower functions to simulate the block and incorporate it with other Simulink blocks. The S-function uses a set of coupled nonlinear 1st order ODE's that can be solved numerically. The following model is used:

$$y = \begin{bmatrix} \Phi \\ \Psi \\ B \\ J \end{bmatrix} \tag{48}$$

$$[\dot{y}] = f(y) \tag{49}$$

where f - the non-linear compressor model described above

y - output

The controller was again based on a proportional (P) type controller used previously. However this is broken out of the model and used as the input in a feedback loop. This P type controller could be replaced with a PID or more advanced control algorithm (to be studied later). Figure 13 shows the Simulink model for the compressor:

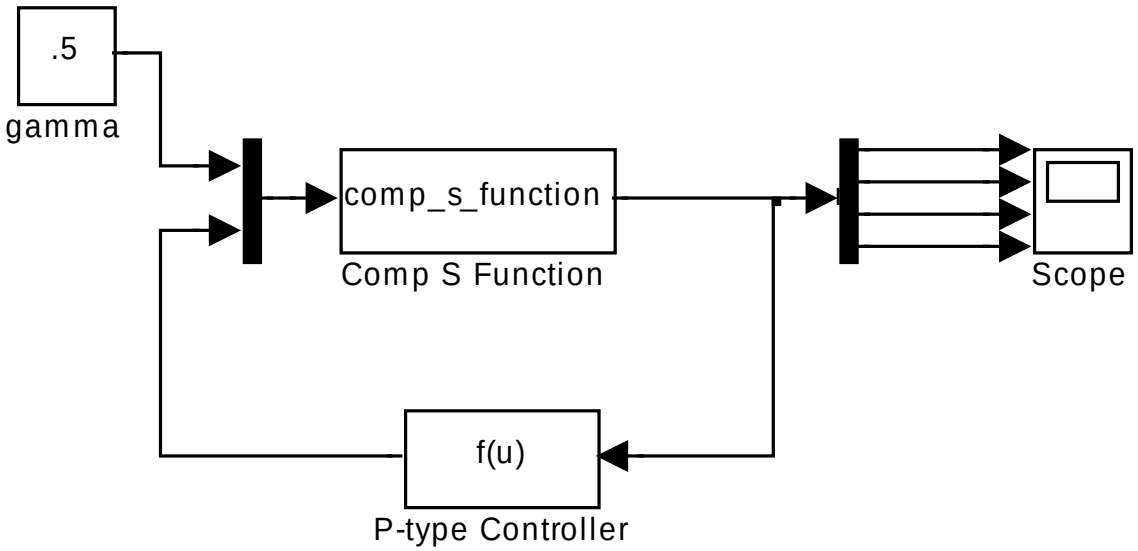

Figure 13: Simulink Model of Axial Flow Compressor

The function in the P-type controller is:

$$c(U_d - b * u[3]),$$

where c is the proportional gain,

$$b = 2a_s\sqrt{\frac{A_c L_c}{V_p}}, \tag{50}$$

and u[3] is the third state variable in the vector output of the *s*-function (*B*).

The model was simulated using the above parameters for stable and unstable conditions to verify the results (Figures 14 - 21):

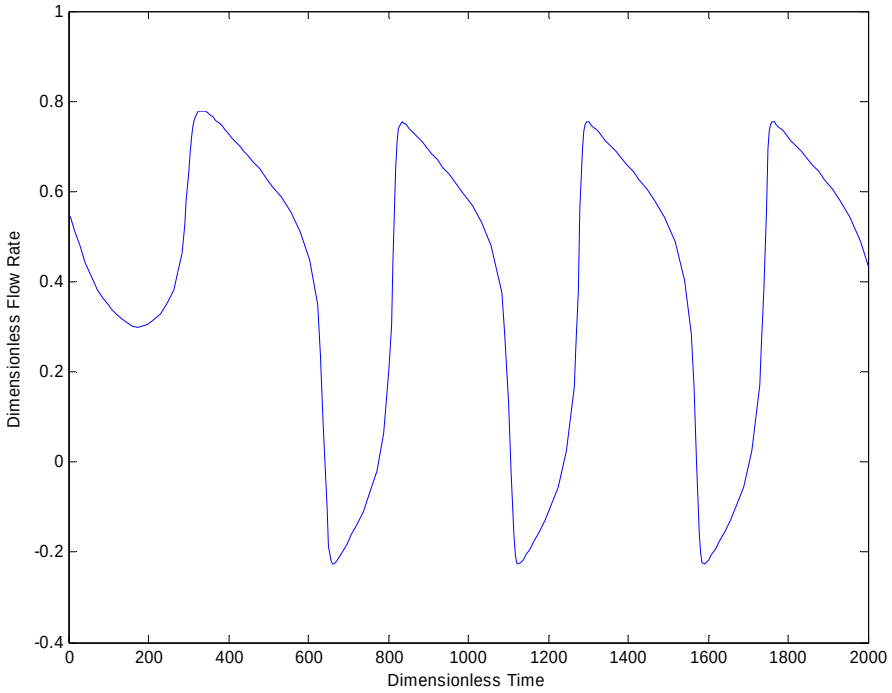

Figure 14: Simulink Compressor Model Results, Flow Rate (Φ), Unstable Condition

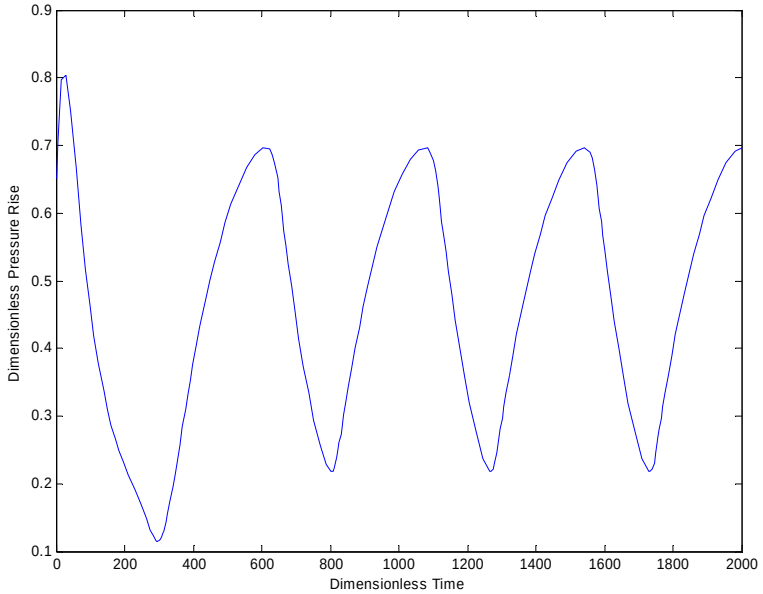

Figure 15: Simulink Compressor Model Results, Pressure Ratio (Ψ), Unstable Condition

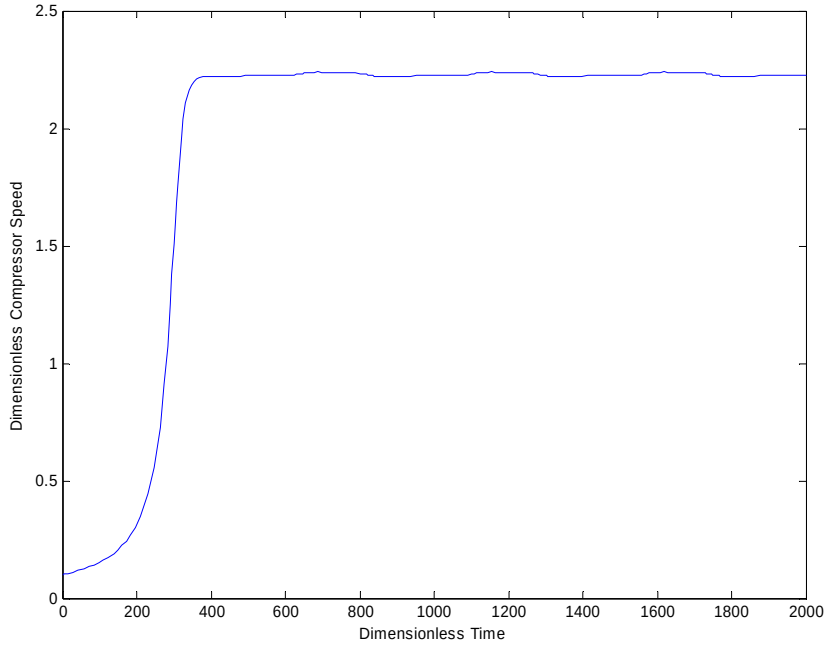

Figure 16: Simulink Compressor Model Results, Compressor Speed (*B*), Unstable Condition

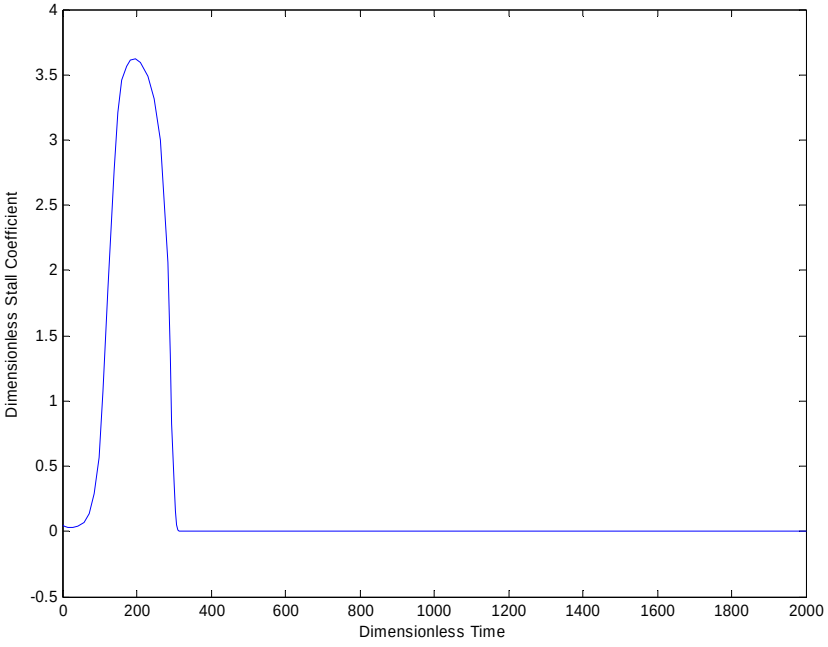

Figure 17: Simulink Compressor Model Results, Stall Coefficient (*J*), Unstable Condition

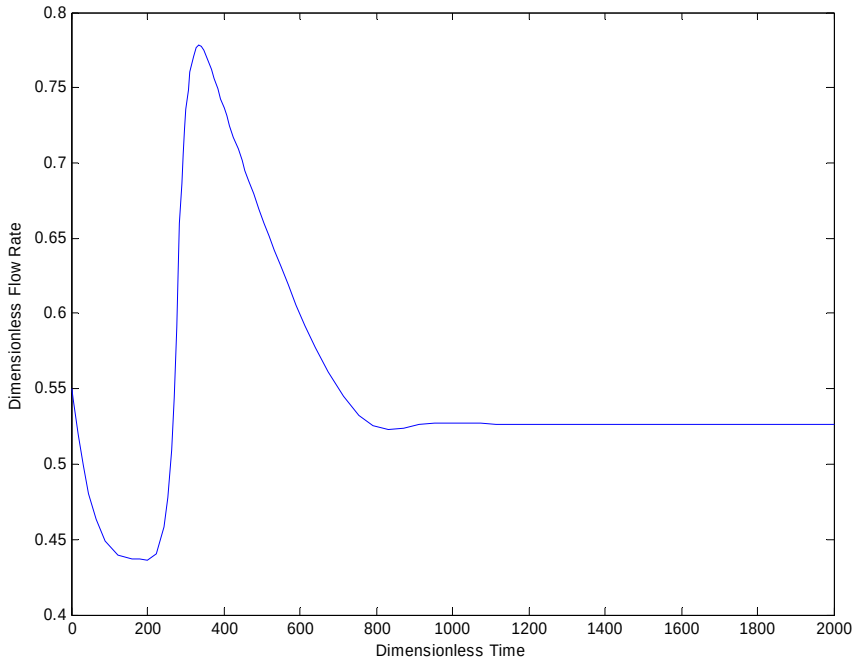

Figure 18: Simulink Compressor Model Results, Flow Rate (*Φ*), Stable Condition

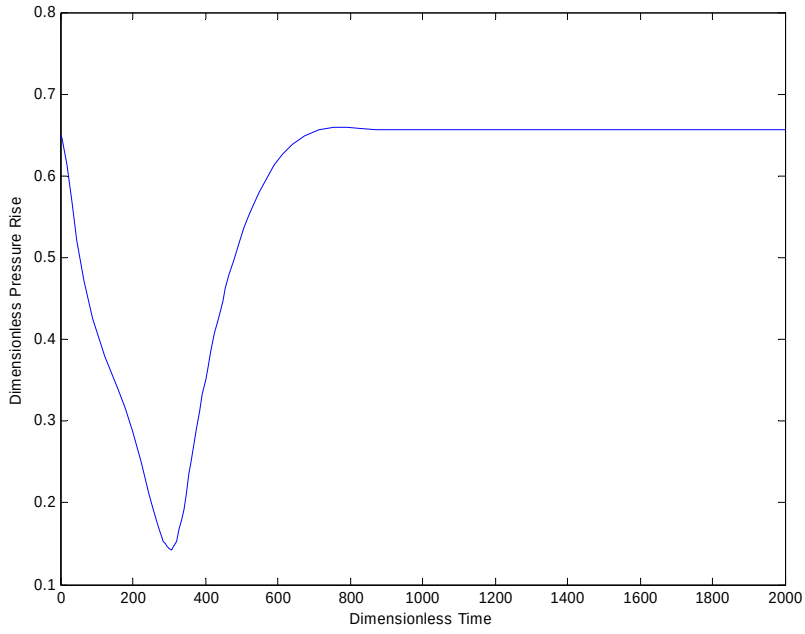

Figure 19: Simulink Compressor Model Results, Pressure Ratio (*Ψ*), Stable Condition

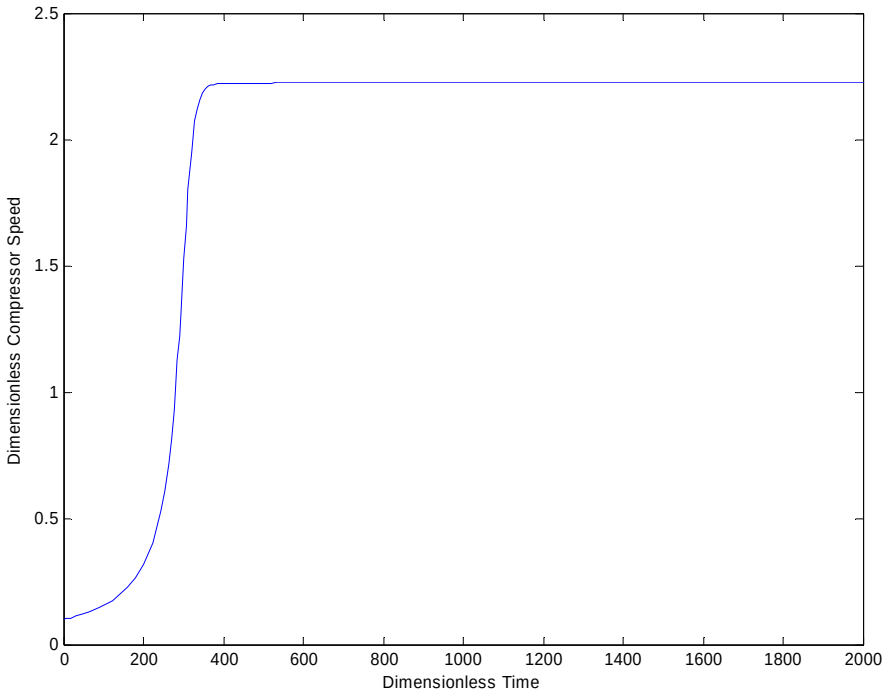

Figure 20: Simulink Compressor Model Results, Compressor Speed (*B*), Stable Condition

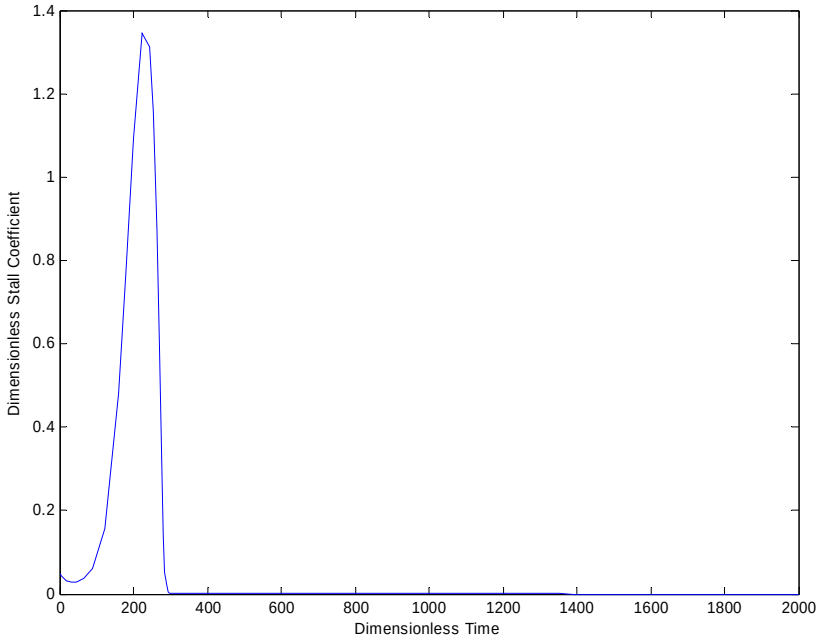

Figure 21: Simulink Compressor Model Results, Stall Coefficient (*J*), Stable Condition

Comparing Figure 14 to Figures 5-8 and Figure 15 to Figures 9-12, the results of the s-function match the script file and the results quoted in [3].

2.2 COMBUSTOR

Combustors are typically used in gas turbine cycles to heat the working fluid between the compressor and the turbine. This process increases the enthalpy and temperature of the working fluid. This additional energy is then extracted by the turbine. This is why the turbine can produce more power than it takes to run the compressor and is the source of the net power output of the entire gas turbine power plant. Figure 22 shows the location of the combustor in a typical gas turbine system. Figure 23 shows the temperature – entropy (s) diagram of a typical gas turbine cycle with respect to the different locations of the working fluid (a, b, c, d). The section of the graph between b and c is the combustor section. The rise in temperature and entropy (and enthalpy) provides the additional energy to the fluid to be extracted by the turbine. Without the combustor, or some form of heat addition to the fluid, the turbine would simply produce enough energy to run the compressor and no additional energy would be created. From a conservation of energy viewpoint, the additional heat energy (or chemical energy of the fuel) is converted to mechanical energy by the turbine [6].

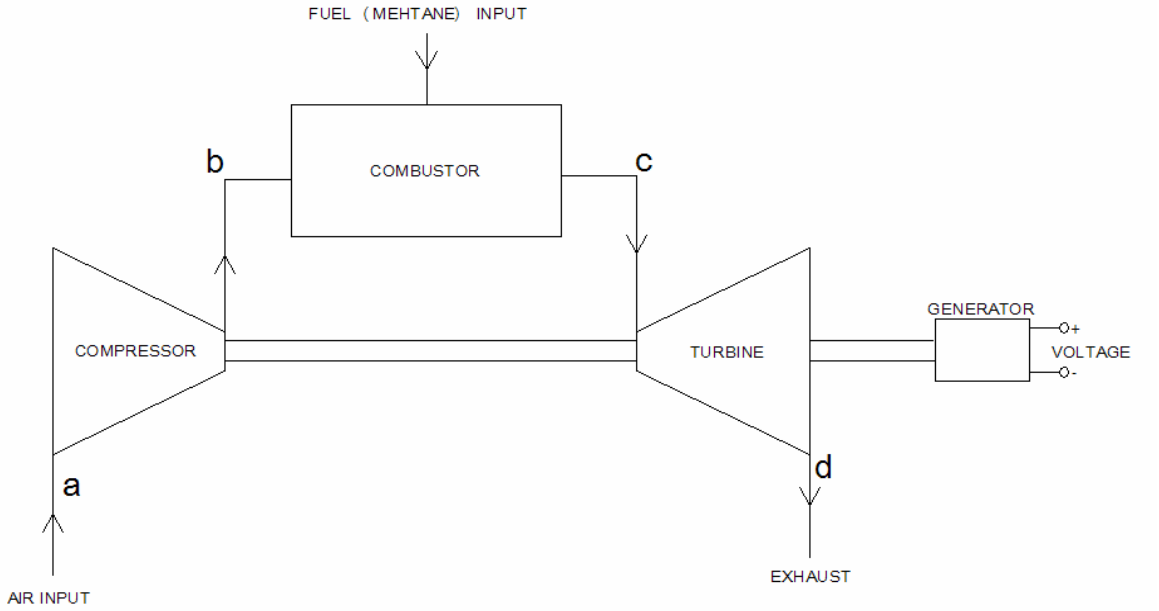

Figure 22: Typical Gas Turbine Cycle

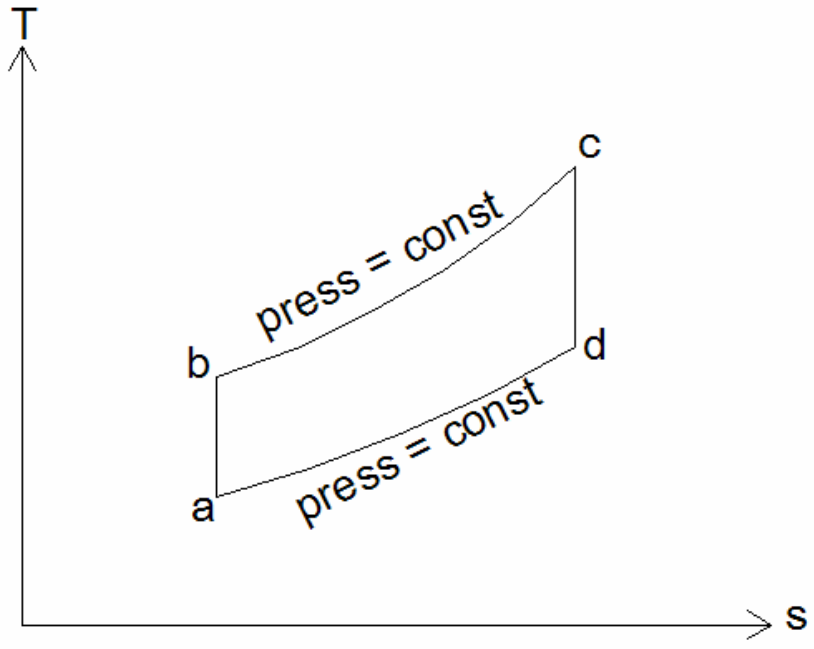

Figure 23: Temperature – Entropy Diagram of Typical Gas Turbine Cycle

2.2.1 Combustor Model

A simple combustor model is needed to incorporate into the overall fuel cell – gas turbine system. The model must be able to simulate the temperature rise to the working fluid when it is combusted with the compressed air exiting the compressor. The model assumes the fuel input to the combustor to be methane. However, it is possible to burn the excess hydrogen straight from the fuel cell output. This information will then be used to calculate the power extracted by the turbine as well as the speed of the compressor and turbine shaft (they are rigidly connected) and the torque on the turbine.

The combustor model used was developed by Fannin [5]. It is called an "unsteady well stirred reactor" (WSR) model. It assumes methane (CH_4) as the fuel and air as the oxidizer. The balanced combustion reaction is as follows:

$$CH_4 + 2(O_2 + 3.76N_2) \Rightarrow CO_2 + 2H_2O + 7.52N_2 \tag{51}$$

A non-linear state space model can be constructed using conservation of species and energy in the control volume of the combustor. The conservation of species equations are based on the three species present inside the combustor. They are the fuel (methane), the oxidizer (air), and the products of combustion. A conservation equation can be written for each species in terms of the mass fractions inside the control volume:

$$Y_{fuel} = \frac{m_{fuel}}{m_{fuel} + m_{oxid} + m_{products}} \tag{52}$$

$$Y_{oxid} = \frac{m_{oxid}}{m_{fuel} + m_{oxid} + m_{products}} \tag{53}$$

$$Y_{prod} = \frac{m_{prod}}{m_{fuel} + m_{oxid} + m_{products}} \tag{54}$$

where Y_{fuel}, Y_{oxid}, Y_{prod} – mass fraction of fuel, oxidizer, and products inside the combustor

m_{fuel}, m_{oxid}, m_{prod} – mass of fuel, oxidizer, and products inside the control volume

In words, the conservation of species equation is stated: The change in the amount of species in the control volume is equal to the amount of species in, minus the amount of species out, plus the amount of species created. For the oxidizer and fuel, the amount created inside the control volume will be negative. For the products of combustion, the amount of species created will be positive. This can be visualized by Figure 24.

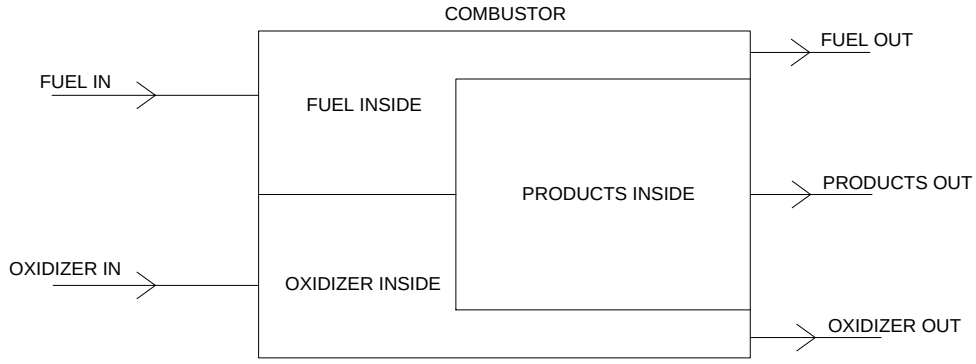

Figure 24: Conservation of Species of Combustor

The amount of species created in the control volume will be driven by the Arrhenius rate term for chemical kinetics of combustion. The conservation of species equations for the fuel and oxidizer are as follows:

$$\rho V \frac{dY_{fuel}(t)}{dt} = \dot{m}_{in} Y_{fuel,in}(t) - \dot{m}_{out} Y_{fuel}(t) + MW_{fuel} \dot{\omega}_{fuel}(t) V \tag{55}$$

$$\rho V \frac{dY_{oxid}(t)}{dt} = \dot{m}_{in} Y_{oxid,in}(t) - \dot{m}_{out} Y_{oxid}(t) + MW_{fuel} \frac{Y_{oxid,in}(t)}{Y_{fuel,in}(t)} \dot{\omega}_{fuel}(t) V \tag{56}$$

where

$$\dot{\omega}_{fuel} = \left(-24{,}100 \frac{kmol}{kg * s} \right) \rho Y_{fuel}^{\ 0.3} \left(0.233 Y_{oxid}\right)^{1.3} e^{\frac{15{,}098}{R_u T(t)}} \tag{57}$$

and ρ – density inside combustor

V – volume of combustor

$\dot{m}_{in}$ - total mass flow rate into combustor

$Y_{fuel,in}$, $Y_{oxid,in}$ - mass fraction of fuel & oxidizer into combustor respectively

$\dot{m}_{out}$ - total mass flow rate out of combustor

MW_{fuel} – molecular weight of fuel (methane)

$\dot{\omega}_{fuel}$ - Arrhenius rate term for consumption of species due to combustion

Due to the definition of the mass fraction, the equation for the mass fraction of the products is simply

$$Y_{prod} = 1 - Y_{fuel} - Y_{oxid}, \tag{58}$$

and is not a differential equation. The state variables of the system to this point are Y_{fuel} and Y_{oxid}. The third state variable will be temperature and is described by the energy equation.

The conservation of energy equation completes the model and is described as the amount of energy entering the combustor minus the amount of energy leaving the combustor balanced by a storage term.

$$\rho V \frac{d}{dt}\sum_{i=1}^{3} Y_i(t)e_i(t) = \dot{m}_{in}(Y_{oxid,in}h_{oxid,in} + Y_{fuel,in}h_{fuel,in}) - \dot{m}_{out}\sum_{i=1}^{3} Y_i(t)h_{i,out}(t) \qquad (59)$$

where e_i – specific internal energy for i = 1-fuel, 2-oxidizer, 3-products

$h_{oxid,in}$, $h_{fuel,in}$ – specific enthalpy of oxidizer and fuel into the combustor

$h_{i,out}$ – specific enthalpy for i = 1-fuel, 2-oxidizer, 3-products out of combustor

The right side of equation (59) is the total change in internal energy of the three species inside the combustor. The left hand side is the energy associated with the enthalpy of the input species and output species. All of these quantities are dependent on temperature, which is the desired output variable from the combustor model. Therefore, equation (59) is converted to be in terms of temperature rather than internal energy and enthalpy.

As stated above, the left hand side of equation (59) represents the change in internal energy of the species inside the combustion chamber. In order to make this term an expression of temperature only (and not Y_{fuel}, and Y_{oxid}) it is assumed that the majority of the species inside the combustor are products (CO_2, H_2O, and N_2), such that:

$$\rho V \frac{d}{dt} e(t)_{prod} = \dot{m}_{in}(Y_{oxid,in} h_{oxid,in} + Y_{fuel,in} h_{fuel,in}) - \dot{m}_{out} \sum_{i=1}^{3} Y_i(t) h_{i,out}(t) \quad (60)$$

A linear curve fit based on the ideal gas properties of the products can be approximated, giving a relationship between the specific internal energy and the temperature of the combustor products. This same technique can be applied to the enthalpy terms on the right side of equation (59). Therefore, equation (59) can be analyzed in terms of temperature (*T*) as a function of time. This will be the third state variable and will complete the combustor model.

The linear curve-fits of the internal energy and enthalpy data are shown in Figures 25 and 26. The actual data was obtained from ideal gas tables [6]. A linear equation was fit to the data. These equations will be incorporated into equation (60) to obtain a state equation for temperature. The enthalpy and internal energy of the products can be obtained by summing each of the contributions of the product species on a mass fraction basis. The mass fractions of the product species (CO_2, H_2O, and N_2) can be obtained using the stiochiometry in equation (51) along with their respective molecular masses.

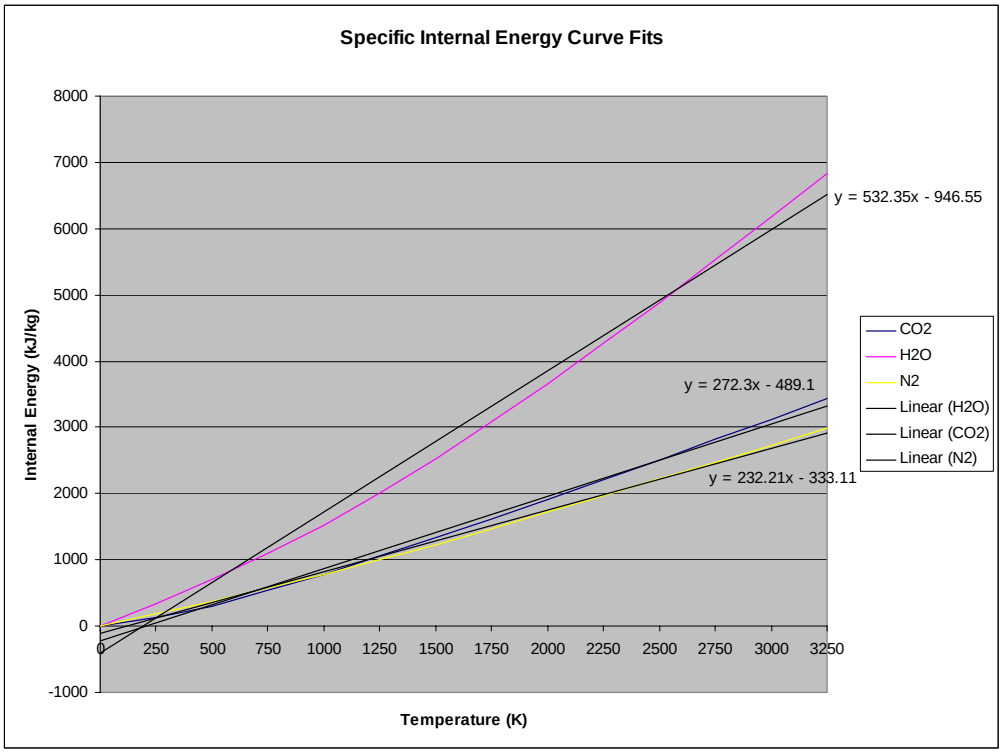

Figure 25: Linear Curve Fit of Internal Energy of Products

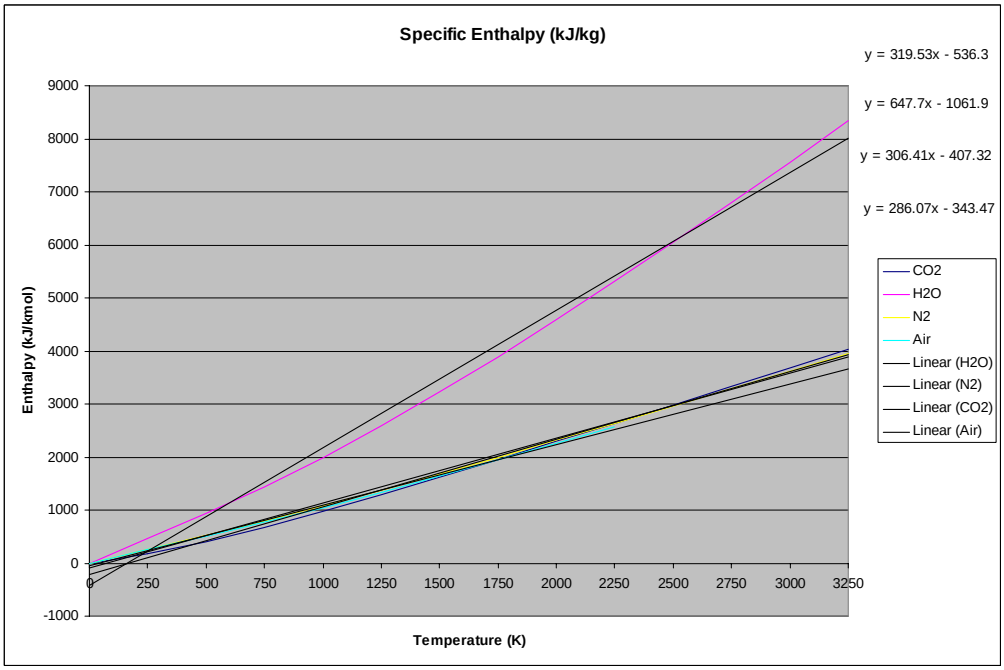

Figure 26: Linear Curve Fit of Enthalpy of Products and Air

The enthalpy equation used in the model for the fuel (methane) is as follows:

$$h_{fuel} = h_f + c_p T \tag{61}$$

where h_f - enthalpy of formation

$c_{p,fuel}$ - constant pressure specific heat

Equation (60) then becomes (61)

$$\rho V \frac{d}{dt} e(t)_{prod} = \dot{m}_{in}(Y_{oxid,in} h_{oxid,in} + Y_{fuel,in} h_{fuel,in}) - \dot{m}_{out}[\sum_{i=2}^{3} Y_i(t) h_{i,out}(t) + Y_1(t)(h_1 + c_{p,fuel} T)] \tag{61}$$

2.2.2 Combustor Model Simulation

A script file was written in MATLAB to simulate the model. The results are displayed in Figures 27 – 29. The outputs of the system are the combustor temperature (Figure 27), which is assumed to be the exit flow temperature, and the mass fractions of the fuel and oxidizer inside the combustor (Figures 28 and 29, respectively). This simulation uses constant fuel and oxidizer input flow rates. The parameters of the simulation are summarized in Table 1. The air to fuel mass ratio is close to the stoichiometric value of 17.123.

Table 2: Combustor Simulation Model Parameters

Mass flow rate of fuel in (kg/s)	1
Mass flow rate of oxidizer in (kg/s)	20
Temperature of fuel in (K)	300
Temperature of oxidizer in (K)	600
Initial conditions	
Y fuel	0.05
Y oxid	0.95
T (K)	1000

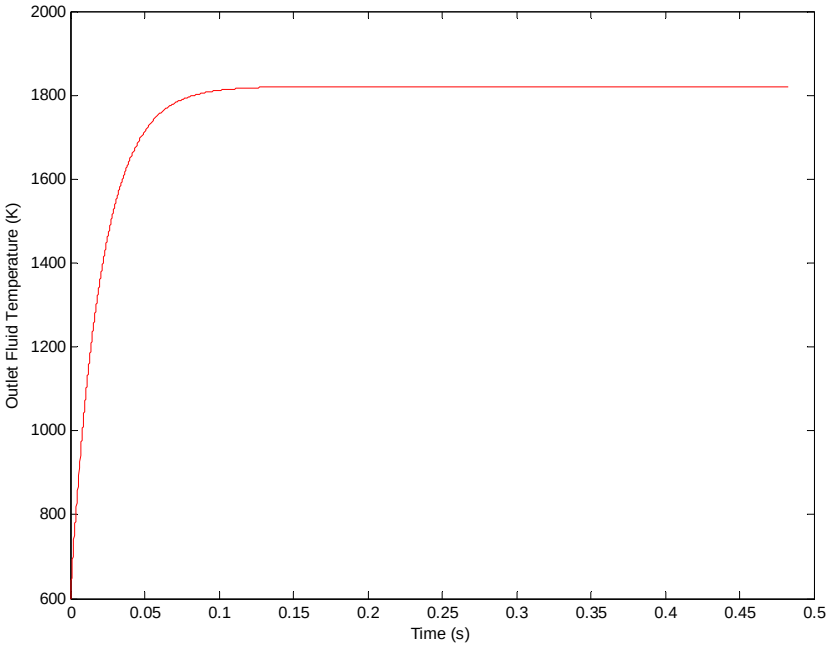

Figure 27: Outlet Fluid Temperature

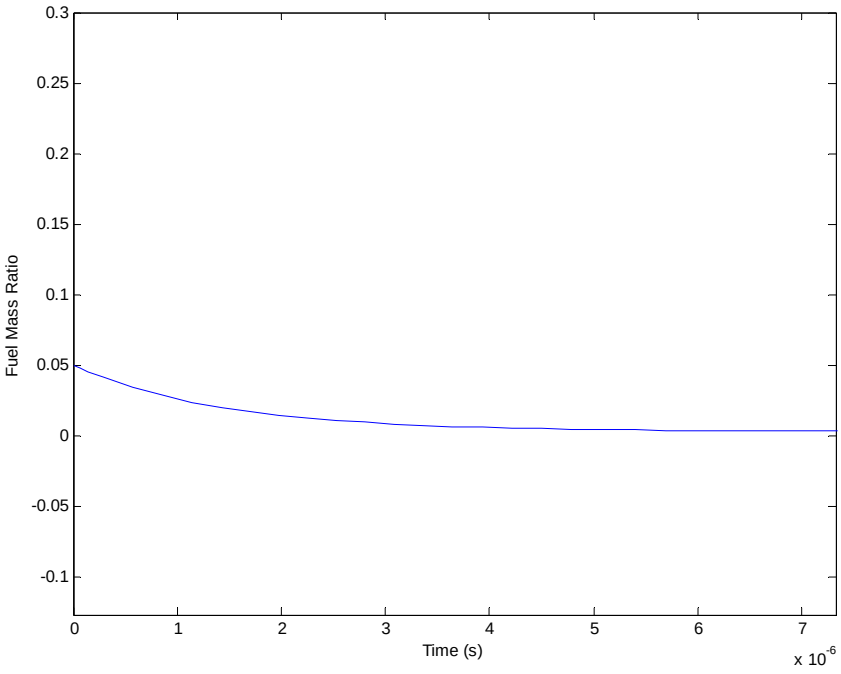

Figure 28: Fuel Mass Fraction Inside Combustor

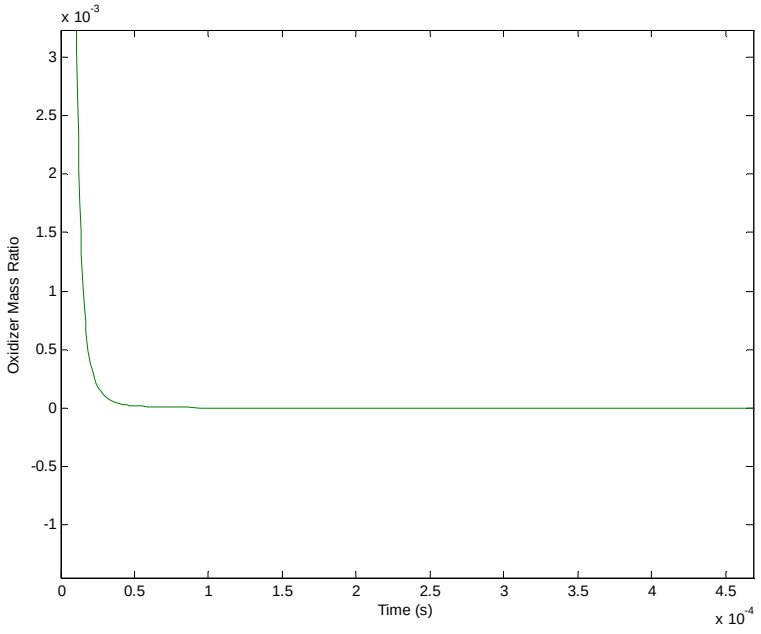

Figure 29: Oxidizer Mass Fraction Inside Combustor

As can be observed from Figure 21, the combustor raises the temperature of the working fluid from 600K to approximately 1800K. These results are consistent with the test data provided in [5]. The mass fractions of the fuel and the oxidizer fall rapidly and eventually stabilize near zero. This result implies that nearly all of the fuel and the oxidizer are being converted to products, which is consistent with the ratio of the fuel and oxidizer, which was chosen to be close to the stoichiometric value. The value of the product mass fraction inside the combustor would be close to unity according to equation (58). This gives credence to the assumption that the exit fluid consists of mostly products of combustion.

A Simulink model was created based on the script file discussed above. It uses a user defined s-function [15] to simulate the combustor model (Figure 30). The inputs are the same as the above model but the outputs have been changed to reflect the mass flow rate out of the combustor along with the temperature of those products (63).

$$\dot{m}_{in,fuel} + \dot{m}_{oxid} = \dot{m}_{in,total} = \dot{m}_{out,total} \tag{63}$$

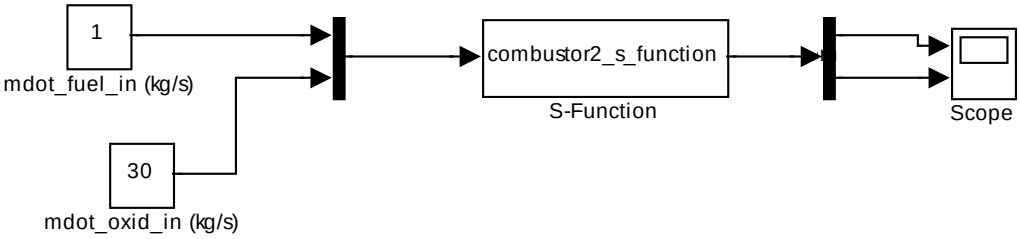

Figure 30: Combustor Model in Simulink Using S-Function

By running the same simulation parameters as above, the temperature of the exit products can be duplicated using the simulink model (Figures 31, 32). The mass flow rate of the exit products is a simple algebraic relation (63), and can be verified by inspection. This result gives confidence to the s-function representing the model described in [5].

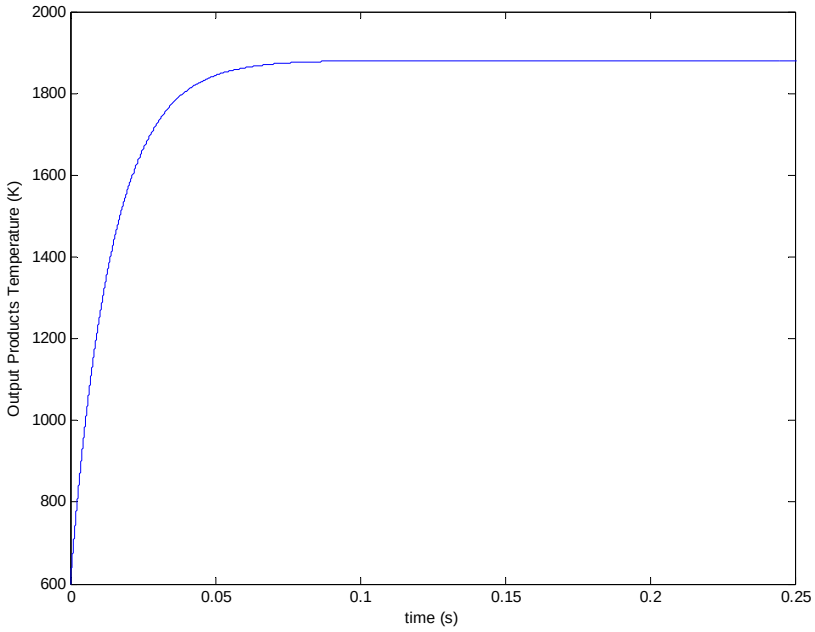

Figure 31: Output Temperature of Simulink Combustor Model

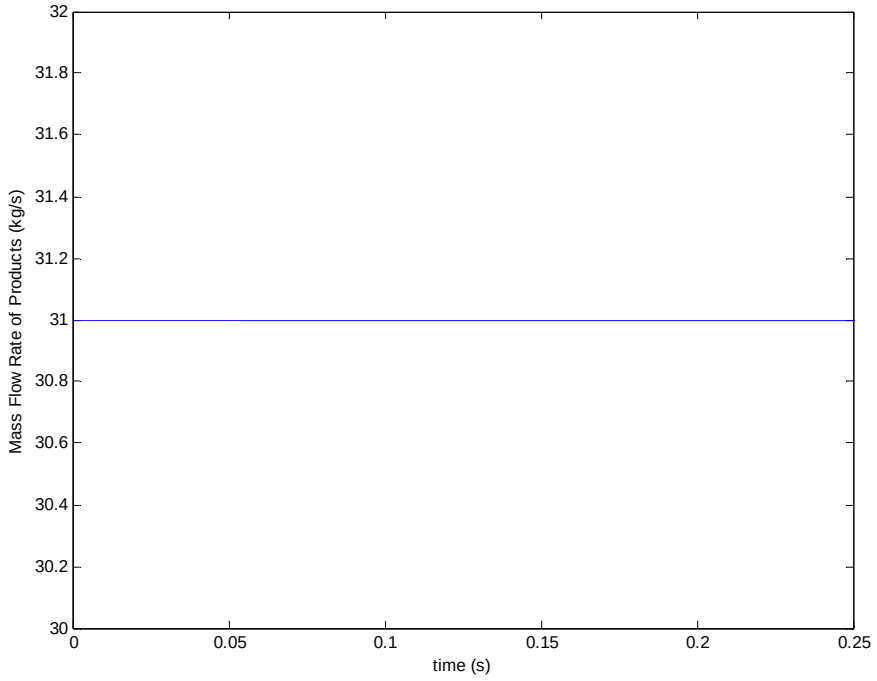

Figure 32: Output Flow Rate of Simulink Combustor Model

A second simulation was run varying the oxidizer input flow rate. The fuel input flow rate was held constant at 1 kg/s. The oxidizer flow rate was started initially at 20 kg/s, then decreased to 10 kg/s at approximately t = 0.21s, and then increased to 30 kg/s at t = 0.41s (Figure 33). The results show that the outlet temperature of the products decreases with a decrease in oxidizer mass flow rate (Figure 34). This is because the air to fuel ratio is no longer optimal so there is less combustion taking place. A second reason for the temperature decrease is that the oxidizer is entering the combustor at an elevated temperature (relative to the fuel) due to the compression stage. If the amount of fluid at the higher temperature decreases, the overall temperature of the products will decrease as well. After the subsequent increase in oxidizer flow rate, the temperature of the products increases. This is due to more high-temperature oxidizer entering the combustor, as well as more fuel reacting and releasing energy.

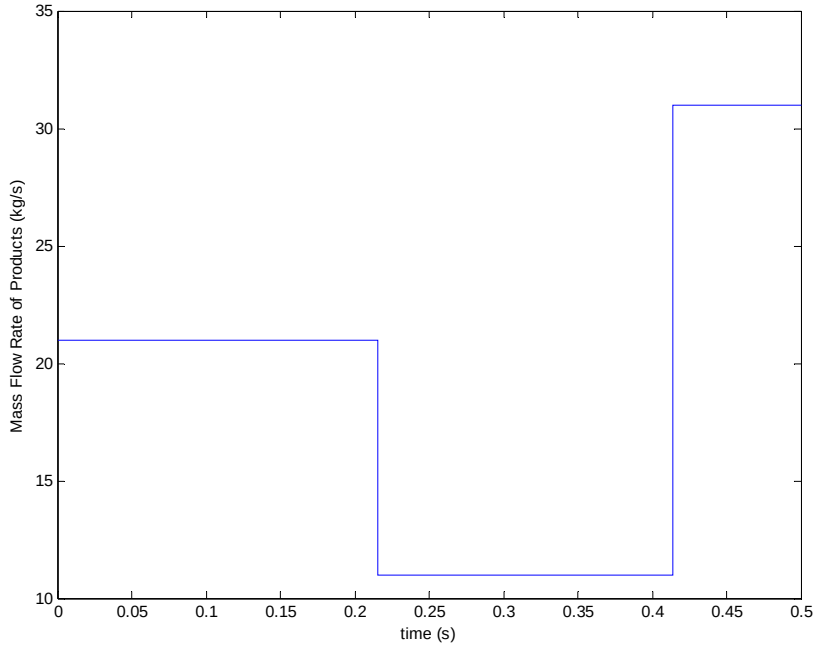

Figure 33: Mass Flow Rate of Combustor Model with Varying Input Air Flow Rate

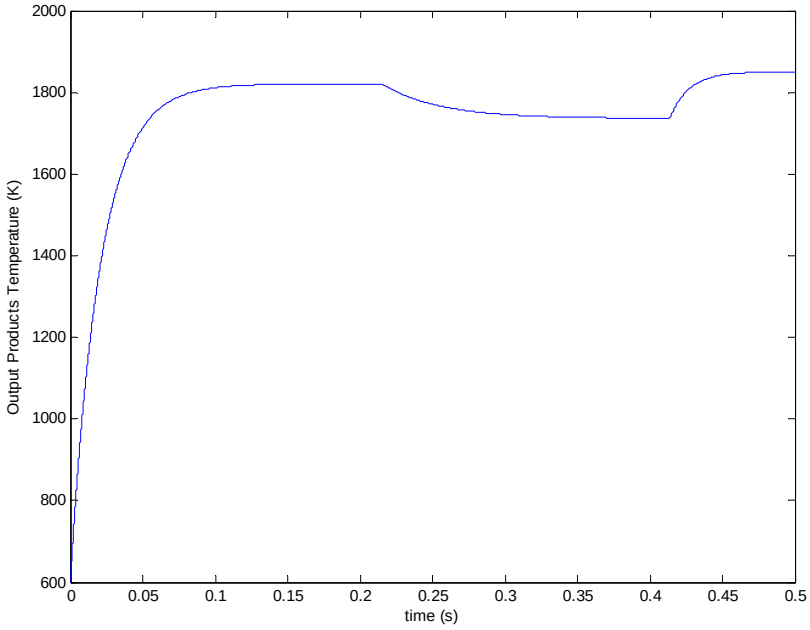

Figure 34: Output Temperature of Simulink Combustor Model with Varying Oxidizer Input Flow Rate

2.3 TURBINE

2.3.1 Turbine Theory

The turbine model is needed to simulate the torque imparted to the compressor and the generator as well as to determine the portion of the overall power developed by the gas turbine. Torque is developed in the turbine when the working fluid expands and imparts a force on the turbine blades (Figure 35). The working fluid enters the turbine stator with a velocity *CT1* and exits it with a velocity of *CT2*. When the fluid passes through the turbine rotor stage, the change in direction of the fluid to *CT3* imparts a force on the rotor, which provides the torque to the compressor and the generator and rotates the rotor with a velocity *U*. Unlike the compressor model, turbines are relatively stable and do not suffer from surge. This is because the pressure drop is in the same direction of the flow of the working fluid. Therefore there is no force to reverse the flow as in the compressor [6], [14].

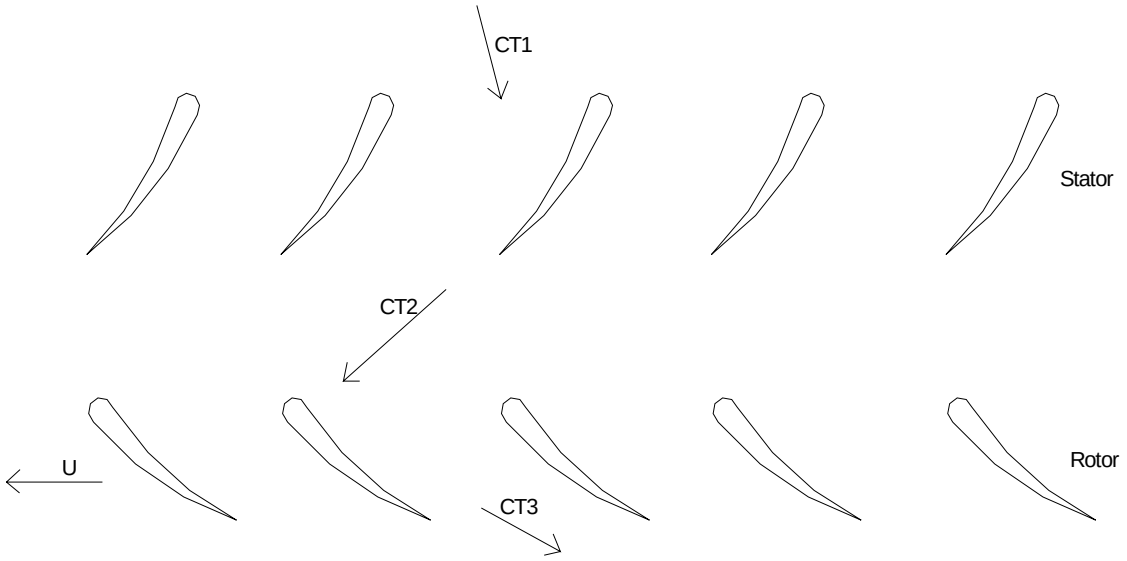

Figure 35: Example Turbine Stage

2.3.2 Turbine Function

The turbine model used here will actually be an algebraic function rather that a state space differential model. This is because the actual rotor dynamics are encompassed in the compressor model developed above (equations (34) – (42)). Since the compressor and the turbine are rigidly coupled, the speed of the turbine is extracted from the compressor model. The compressor model uses the turbine torque to calculate the speed of the rotor based on the rotational momentum balance (34).

The power developed by the turbine is calculated using the change in enthalpy in the working fluid. This enthalpy is based on the linearized enthalpy temperature relationship of the products of combustion developed for the combustor model (Figure 26) [6].

$$P_{turb} = \eta_T \dot{m}_{in} (h_{in} - h_{out}) \tag{64}$$

where P_{turb} – total power developed by the turbine

$\dot{m}_{in}$ - total mass flow rate into the turbine

η_T - isentropic efficiency of turbine

h_{in} – total specific enthalpy of the working fluid into the turbine

h_{out} – total specific enthalpy of the working fluid out of the turbine based on room temperature

The torque developed by the turbine can be calculated using the power developed by the turbine and the angular velocity of the rotor from the compressor model.

$$\tau_t = \frac{P_{turb}}{\omega} \tag{65}$$

where τ_t – total torque developed by the turbine

τ_t is fed into the compressor model to determine ω. The net torque out of the entire gas turbine is calculated using the difference between τ_t and τ_c.

$$\tau_{net} = \tau_t - \tau_c \tag{66}$$

where τ_{net} - the available torque to run the generator.

Therefore the net power out of the gas turbine is:

$$P_{out} = \tau_{net}\omega \tag{67}$$

2.3.3 Turbine Function Simulation

Figure 36 shows the turbine function created in Simulink. Figures 37, 38 show the torque and power outputs from this function using the parameters shown in Figure 36. The constant inputs and algebraic nature of equations (66) and (67) produce constant outputs.

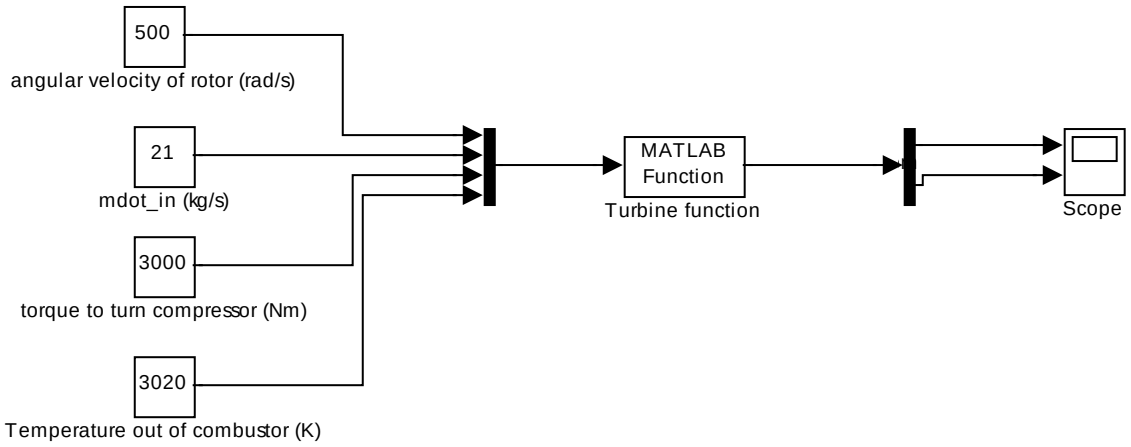

Figure 36: Simulink Turbine Function

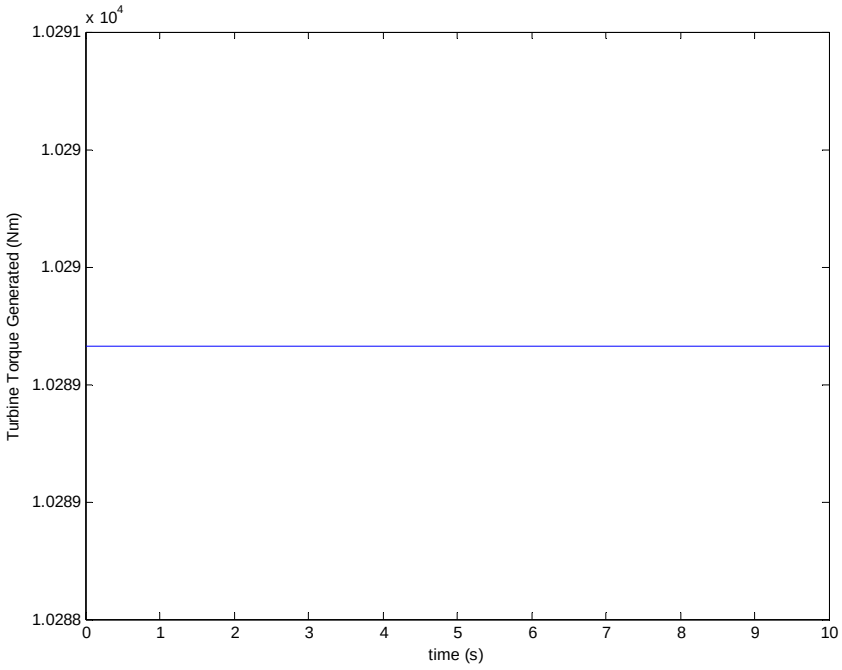

Figure 37: Turbine Torque Generated from Uncoupled Turbine Simulation

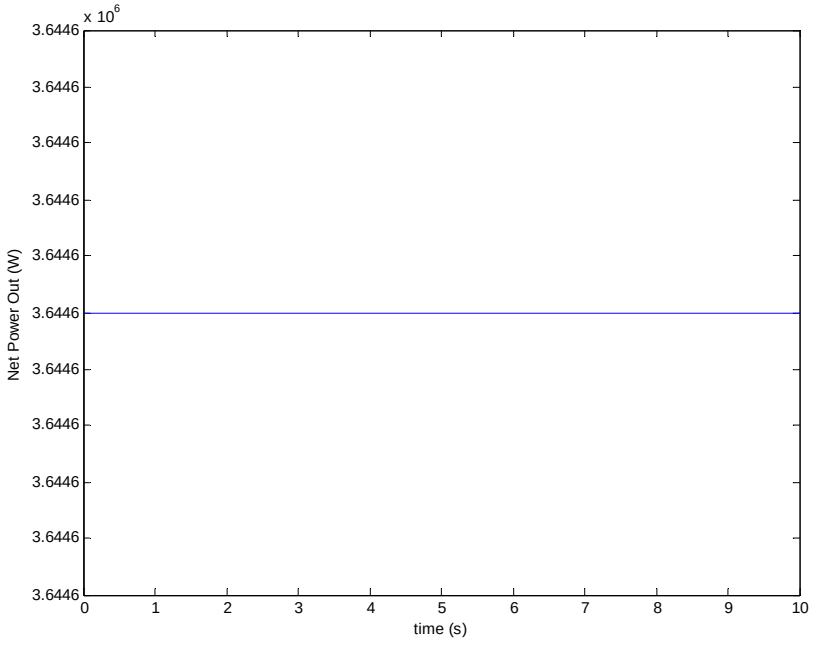

Figure 38: Net Power Out from Uncoupled Turbine Simulation

3.0 HEAT EXCHANGER AND FUEL CELL MODELS

The following sections will develop the dynamic heat exchanger and fuel cell models. These models will complete the components needed to create a FCGT hybrid power plant model.

3.1 HEAT EXCHANGER

3.1.1 Heat Exchanger Theory

A heat exchanger model will be needed to transfer the energy of the hot fuel cell fluids to the working fluid of the gas turbine. The heat exchangers can be used in various places throughout the power plant. Counter flow design is chosen, which means that the hot and cold streams flow in opposite directions through the heat exchanger. This allows the outlet temperature of the cold fluid to exceed the outlet temperature of the hot fluid (Figure 39). This is not possible in parallel flow heat exchangers. Counter flow heat exchangers are also more efficient in that they can transfer the same amount of energy between flows with a smaller surface area [7].

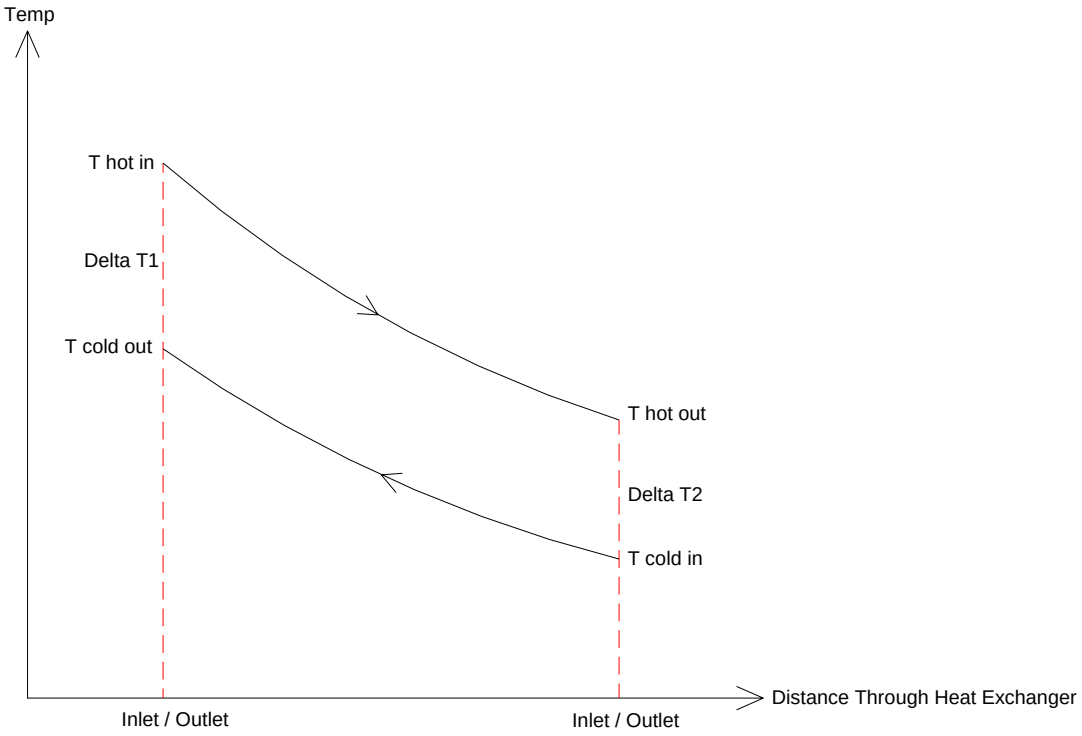

Figure 39: Temperature Graph of Counter Flow Heat Exchanger

The model will calculate the heat transfer between the hot and cold streams and will output the temperature output of each stream respectively. Since the transient time of the temperature rise of the cold stream is of interest, it will be calculated using an ODE. The temperature output of the hot stream will be calculated using an algebraic relationship to the energy transferred between streams. Therefore, the outlet temperature of the hot side will not display transients and will only show the final temperature. This will not affect the overall integrated model because it is the rise in *cold* side temperature that will be of use. The cold side will display the transients.

3.1.2 Heat Exchanger model

The following is a list of assumptions used in the heat exchanger model:

- Laminar flow
- Pressure drop through the heat exchanger (HX) is negligible
- The temperature of the cold stream equals the temperature of the HX metal
- Log mean temperature profile - Equation (68) [7]
- Both hot and cold fluids are air

$$\Delta T_{lm} = \frac{\Delta T_1 - \Delta T_2}{ln(\Delta T_1 / \Delta T_2)} \tag{68}$$

where ΔT_{lm} - log mean temp. difference of hot and cold streams

$$\Delta T_1 = T_{h,i} - T_{c,o} \tag{69}$$

$$\Delta T_2 = T_{h,o} - T_{c,i} \tag{70}$$

$T_{h,i}, T_{h,o}$ - Temp. of inlet and outlet of hot stream

$T_{c,i}, T_{c,o}$ - Temp. of inlet and outlet of cold stream

Parameters for the heat exchanger were derived from the flow rate vs. effectiveness information given by Solar Turbines via the Department of Energy (DOE). The heat transfer is given by the "ProTrax" equation [17]. The equation for the outlet temperature of the metal, which is assumed to be the outlet temperature of the cold stream, is given by equation (71) [16]:

$$\frac{\mathrm{d}\,T_{c,o}}{\mathrm{d}\,t} = \frac{1}{m_{metal} C_{p,metal}} \left[\dot{m}_{cold} C_{p,cold} (T_{c,i} - T_{c,o}) + q \right] \tag{71}$$

where m_{metal} - mass of the metal in the heat exchanger

$C_{p,metal}$ - specific heat of the heat exchanger metal

$\dot{m}_{cold}$ - mass flow rate of the cold stream

$C_{p,cold}$ - specific heat of the cold stream

q - rate of heat transfer between streams

The rate of heat transfer is calculated using the "ProTrax" equation [17]:

$$q = \frac{e^X}{\frac{e^X}{\dot{m}_{hot} C_{p,hot}} \quad \frac{1}{\dot{m}_{cold} C_{p,cold}}} \left(T_{h,i} - T_{c,i} \right) \tag{72}$$

where $\dot{m}_{hot}$ - mass flow rate of the hot stream

$C_{p,hot}$ - specific heat of the hot stream

X – dimensionless parameter defined as

$$X = k_{bulk} A_{HX} \left(\frac{1}{\dot{m}_{hot} C_{p,hot}} - \frac{1}{\dot{m}_{cold} C_{p,cold}} \right) \tag{73}$$

where k_{bulk} – bulk thermal conductivity of the streams

A_{HX} – HX surface area to gap provided by DOE

The temperature of the hot stream output is simply [7]:

$$T_{h,o} = T_{h,i} - \frac{q}{\dot{m}_{hot} C_{p,hot}} \tag{74}$$

These equations comprise the heat exchanger model and will account for variations in the hot and cold stream inlet temperatures and flow rates.

3.1.3 Heat Exchanger Model Simulation

An s-function was written in MATLAB to simulate the heat exchanger using Simulink (Figure 40). The parameters used for this simulation are summarized in Table 3.

Table 3: Heat Exchanger Simulation Parameters

m_{metal}	90 kg
$\dot{m}_{cold}$	0.7 kg/s, 1kg/s
$\dot{m}_{hot}$	0.7 kg/s
$T_{c,i}$	400 K
$T_{h,i}$	800 K

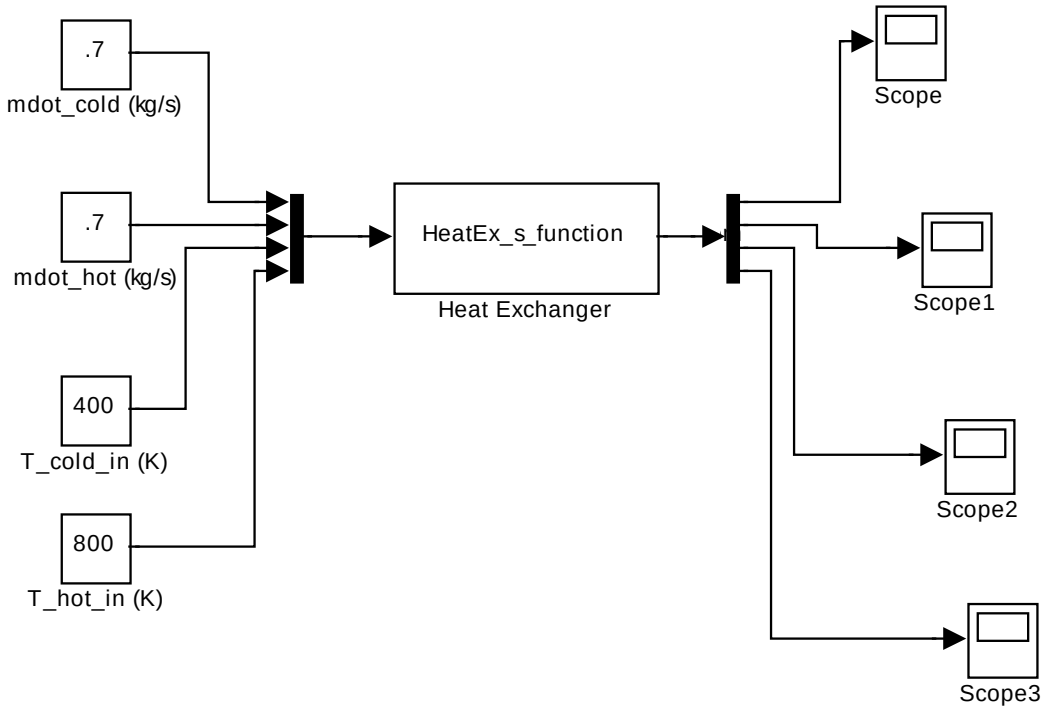

Figure 40: Heat Exchanger Simulink S-Function

The specific heat values and thermal conductivities for the hot and cold streams are calculated based on their respective temperatures [6]. Figures 41 - 44 show the outputs when the parameters shown in Figure 40 are run on the model.

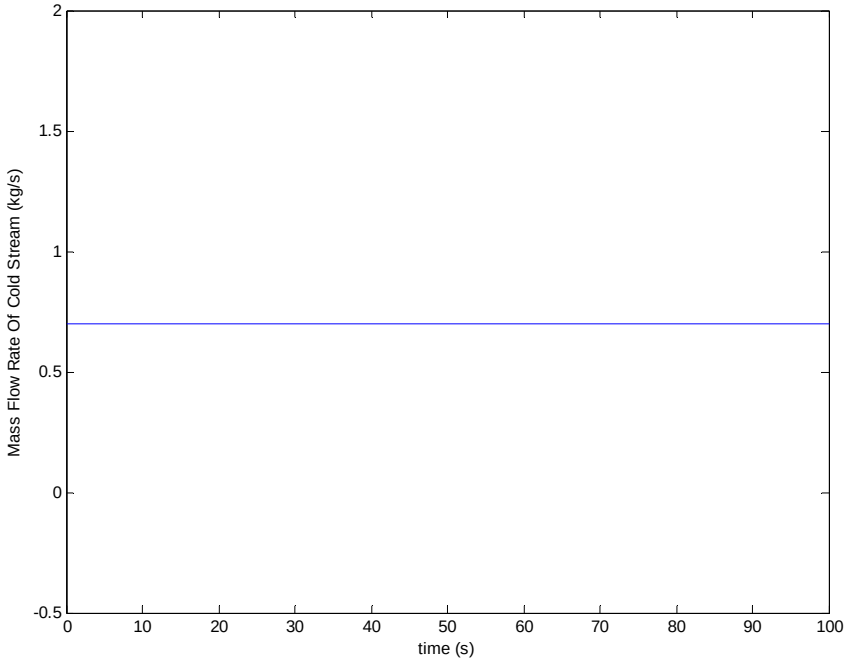

Figure 41: Mass Flow Rate of Cold Stream – Heat Exchanger Model

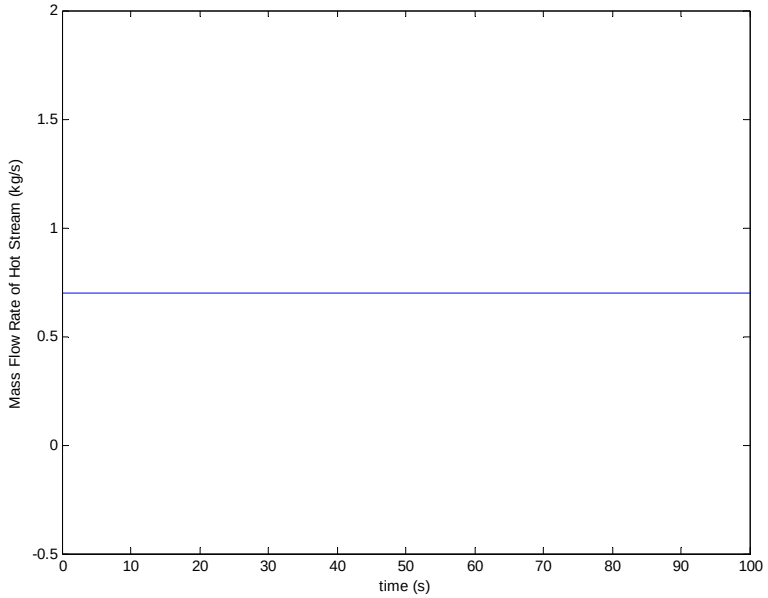

Figure 42: Mass Flow Rate of Hot Stream – Heat Exchanger Model

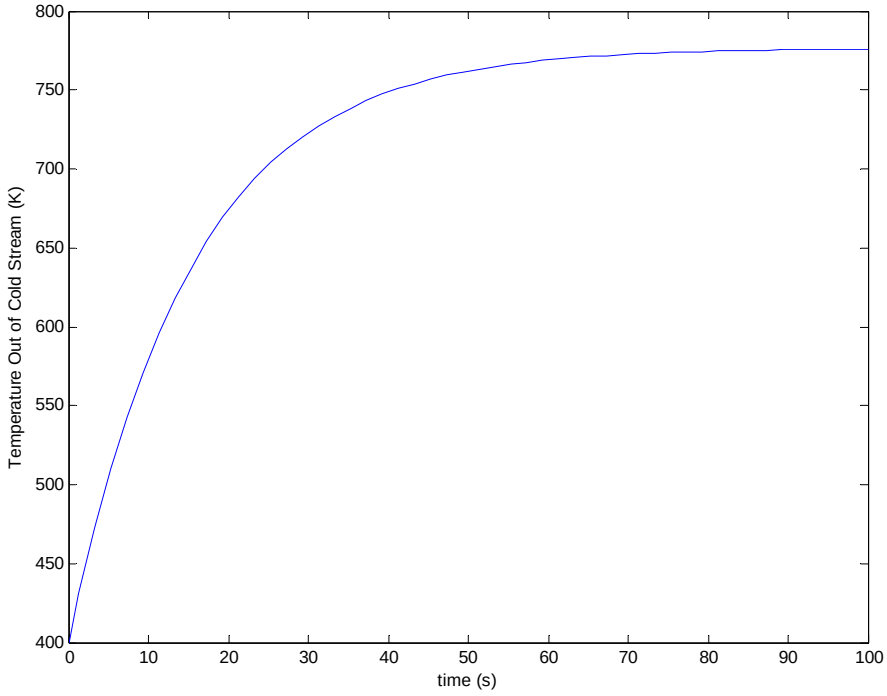

Figure 43: Outlet Temperature of Cold Stream – Heat Exchanger Model

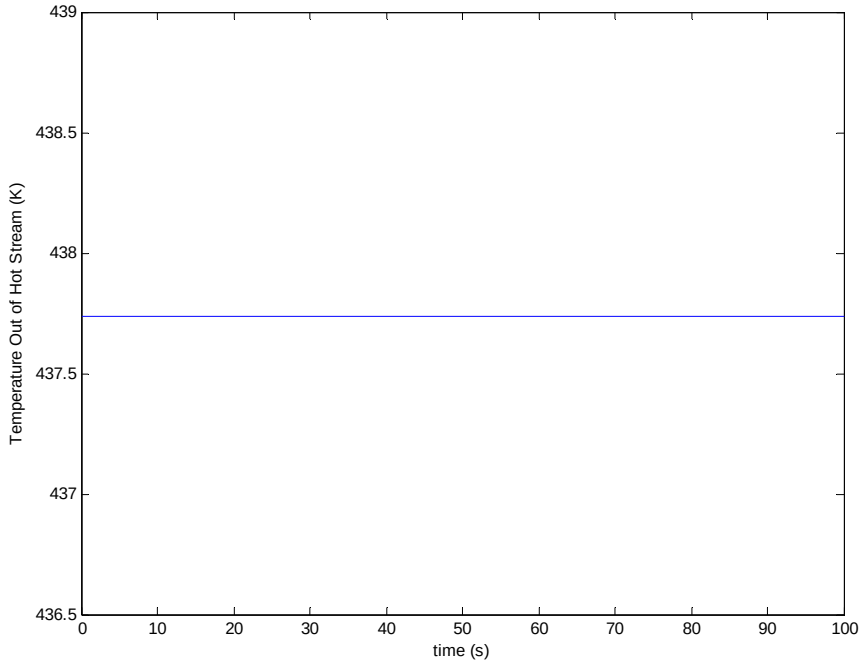

Figure 44: Outlet Temperature of Hot Stream – Heat Exchanger Model

As shown from Figure 43, the outlet temperature of the cold stream gradually increases to a steady state value of 775K while the cold and hot mass flows (Figures 41, 42) are kept constant. The flow rates are taken directly from the inputs. The outlet temperature of the hot side (Figure 44) is constant as well due to the algebraic nature of the equations. However, as stated above, it is the cold side that is of consequence in the integrated power plant model. Figures 45 - 48 show the results of the model run with a slightly higher cold stream flow rate. The outlet temperature of the cold stream is slightly lower than before. This is because the cold steam is not exposed to the heat exchanger for as long. Therefore the energy transfer rate is lower and less heat is transferred.

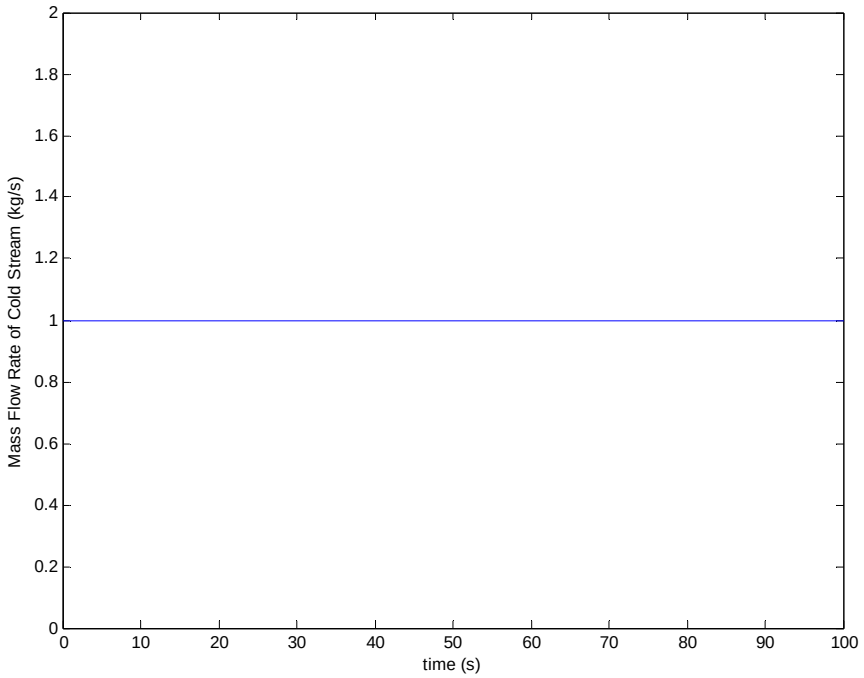

Figure 45: Mass Flow Rate of Cold Stream – Heat Exchanger Model with Higher Cold Mass Flow Rate

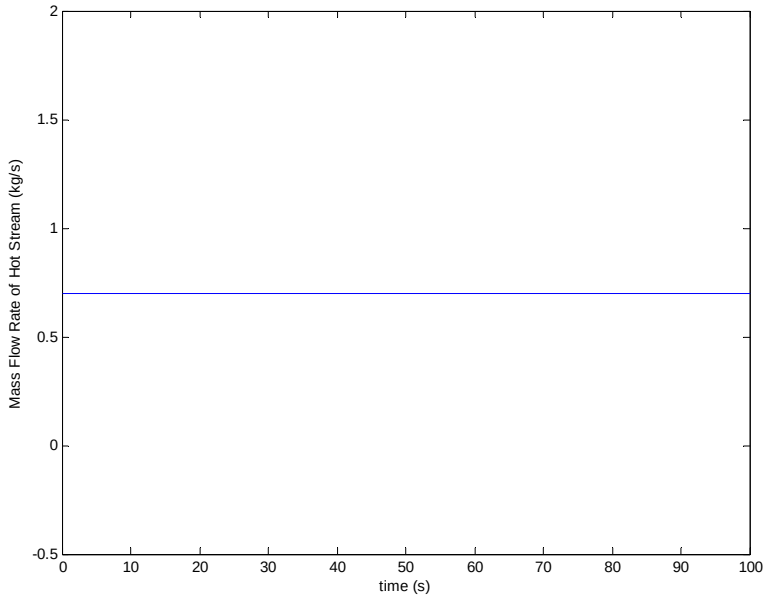

Figure 46: Mass Flow Rate of Hot Stream – Heat Exchanger Model with Higher Cold Mass Flow Rate

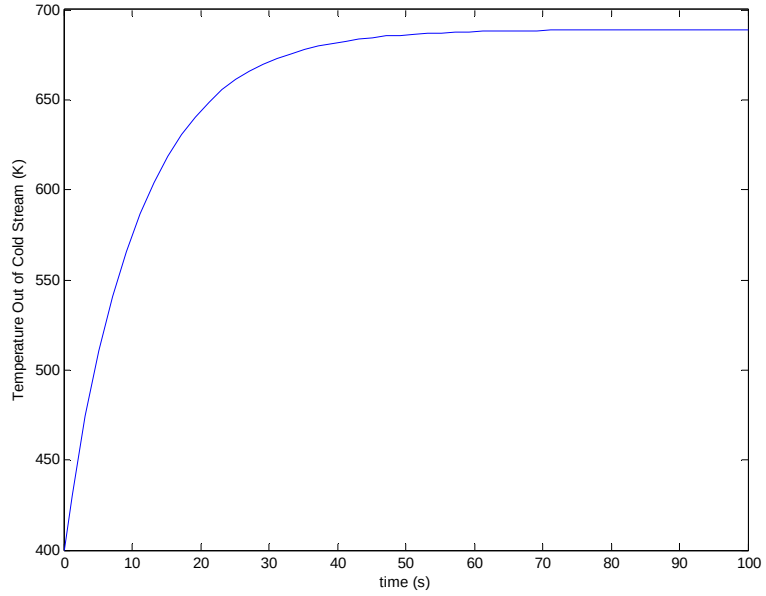

Figure 47: Temperature Out of Cold Stream – Heat Exchanger Model with Higher Cold Mass Flow Rate

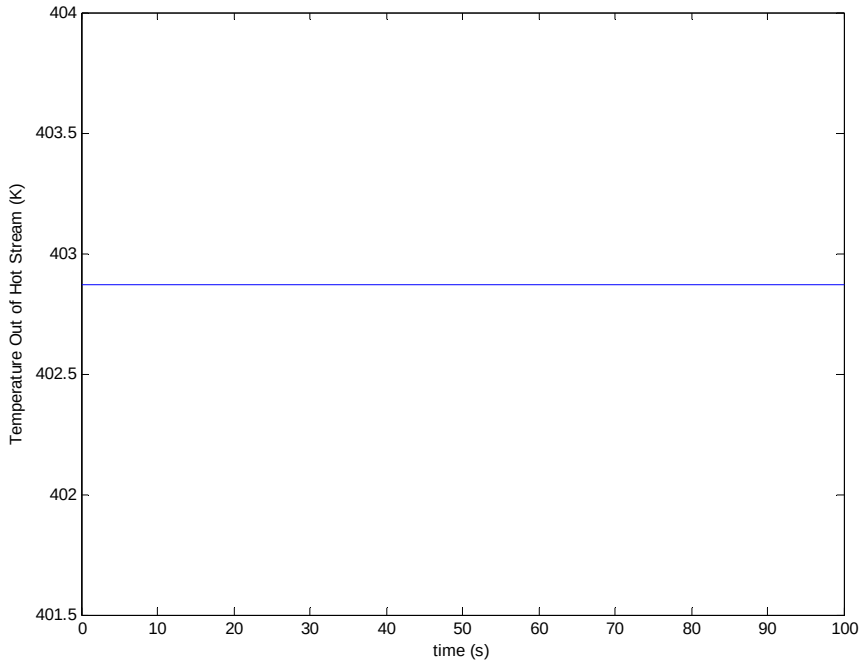

Figure 48: Temperature Out of Hot Stream – Heat Exchanger Model with Higher Cold Mass Flow Rate

3.2 FUEL CELL

3.2.1 Fuel Cell Operating Theory

The fuel cell (FC) is the main power generation system in the power plant. There are several types of fuel cells that could be integrated with a gas turbine, two of which are the molten carbonate and the solid oxide varieties, which are most suitable due to their high operating temperature. The high temperature of the fluids leaving the fuel cell is used to run the gas

turbine and create more electrical energy. A solid oxide fuel cell model was developed for this study, the basic operation of which is shown in Figure 49.

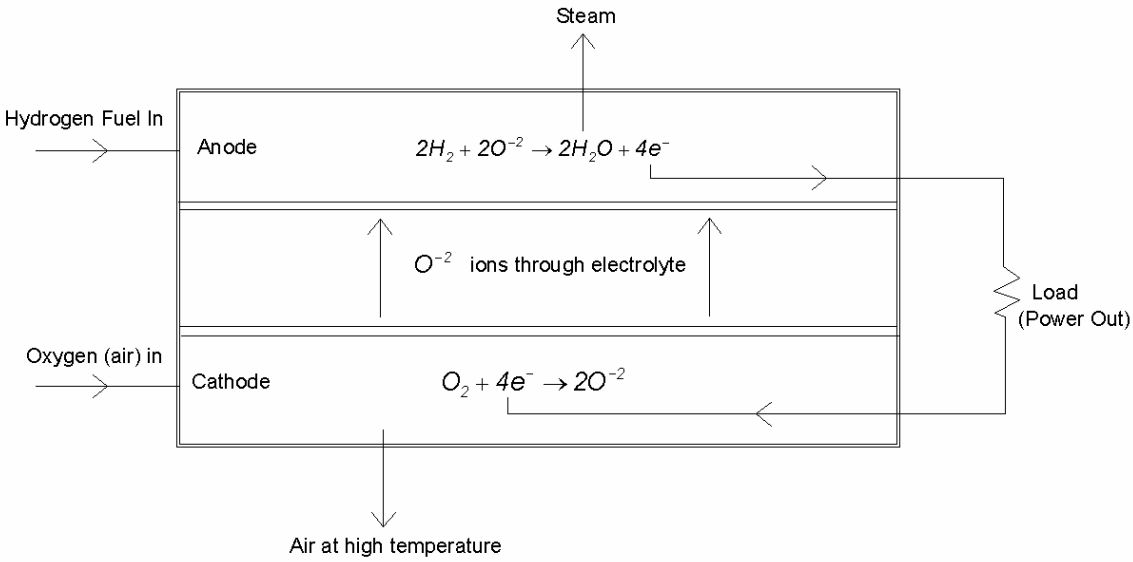

Figure 49: Solid Oxide Fuel Cell

As shown in the figure, hydrogen fuel enters the anode and combines with oxygen ions to form steam and four electrons. These electrons are forced through a load as electricity (power) and enter the cathode to combine with oxygen to produce the oxygen ions that flow through the electrolyte. The oxygen is provided by air. The excess air exits at elevated temperature and can be used to run the gas turbine. The solid oxide runs at the highest operating temperature of all the types of fuel cells. This eliminates the need for expensive catalysts and provides the possibility of including a bottoming cycle [8].

3.2.2 Fuel Cell Model

The FC model is based on a model developed by Padulles, Ault, and McDonald [9]. It was developed for dynamic power simulation of solid oxide fuel cells. The assumptions for the fuel cell model are as follows:

- The gases are ideal
- The fuel cell is fed with hydrogen and air
- The electrode channels are small enough that the pressure drop across them is negligible
- The ratio of pressures between the inside and outside of the electrode channels is large enough to assume choked flow
- The fuel cell temperature is stable
- The Nerst equation applies
- The losses are as follows
    - Ohmic
    - Activation
    - Mass Transport

The model development begins with the flow equation for choked flow [9].

$$\frac{\dot{m}_{fc}}{P_u} = K\sqrt{M} \tag{75}$$

where $\dot{m}_{fc}$ - mass flow rate

K - valve constant

P_u - pressure upstream (inside electrode channels)

M - molar mass of fluid

A utilization factor (U_f) is defined as the ratio of the amount of hydrogen that reacts with the oxygen ions ($\dot{m}_{fc,H_2,reacted}$) over the amount of hydrogen entering the anode ($\dot{m}_{fc,H_2,in}$).

$$U_f = \frac{\dot{m}_{fc,H_2,reacted}}{\dot{m}_{fc,H_2,in}} \tag{76}$$

By considering that the molar flow of any gas through the valve is proportional to its partial pressure, the following equations are derived [9]

$$\frac{q_{H_2}}{p_{H_2}} = \frac{K_{an}}{\sqrt{M_{H_2}}} = K_{H_2} \tag{77}$$

$$\frac{q_{H_2O}}{p_{H_2O}} = \frac{K_{an}}{\sqrt{M_{H_2O}}} = K_{H_2O} \tag{78}$$

where q_{H_2}, q_{H_2O} - molar flow rates of hydrogen and water respectively

p_{H_2}, p_{H_2O} - partial pressures of hydrogen and water respectively

K_{an} - valve constant of the anode

K_{H_2}, K_{H_2O} - valve molar constants for hydrogen and water respectively

By substituting equations (76), (77), (78), equation (75) can be written as:

$$\frac{\dot{m}_{fc}}{P_{an}} = K_{an}\left[\left(1 - U_f\right)\sqrt{M_{H_2}} + U_f\sqrt{M_{H_2O}}\right] \tag{79}$$

where P_{an} – the pressure inside the anode channel

The ideal gas law will be used to find the partial pressures of the gasses flowing through the electrodes. This technique will be applied to all the gasses. Only hydrogen will be derived here.

$$p_{H_2}V_{an} = n_{H_2}RT \tag{80}$$

where V_{an} – volume of the anode channel

R – ideal gas constant

T – temperature

n_{H_2} - moles of hydrogen in the channel

By isolating the pressure and taking the first time derivative, we have:

$$\frac{dp_{H_2}}{dt} = \frac{RTq_{H_2}}{V_{an}} \tag{81}$$

The hydrogen flow can be broken down to three parts and equation (81) can be rewritten as follows

$$\frac{dp_{H_2}}{dt} = \frac{RT}{V_{an}}\left(q_{H_2}^{in} - q_{H_2}^{out} - q_{H_2}^{r}\right) \tag{82}$$

where $q_{H_2}^{in}$ - molar flow of hydrogen into the channel

$q_{H_2}^{out}$ - molar flow of hydrogen out of the channel

$q_{H_2}^{r}$ - molar flow of hydrogen that reacts in the channel

According to the electrochemical relationships, the amount of hydrogen that reacts can be calculated by:

$$q_{H_2}^{r} = \frac{N_0 I}{2F} = 2K_r I \tag{83}$$

where N_0 – number of cells in the stack series

F – Faraday's constant

I – stack current

K_r – modeling constant

By substituting equations (83) and (77) into equation (82), taking the Laplace transform, and isolating the partial pressure term, the following equation can be derived:

$$p_{H_2} = \frac{1/K_{H_2}}{1+\tau_{H_2} s}\left(q_{H_2}^{in} - 2K_r I\right) \tag{84}$$

where τ_{H_2} - the system pole associated with the hydrogen flow

The stack output voltage is described by the Nerst equation [8]. The *-rI* term is the ohmis loss. This is the loss due to the resistance of the electrodes and the resistance of the flow of O^{-2} ions through the electrolyte.

$$V = N_0\left[E_0 + \frac{RT}{2F}\left(ln\frac{p_{H_2}p_{O_2}^{0.5}}{p_{H_2O}}\right)\right] - rI \tag{85}$$

where V - fuel cell output voltage

E_0 - open cell voltage (based on the Gibbs free energy)

r - ohmic losses of the stack

The activation loss is caused by the sluggishness of the reactions at the electrode surfaces. A portion of the voltage is lost in driving the chemical reaction that moves the electrons to the electrodes. A way to account for these losses is to use the Tafel equation [8]. This equation was derived by physical experimentation on various electrochemical reactions. It provides a relationship between the overvoltage at the surface of an electrode and the log of the current density. This can be used to calculate the activation voltage loss for a SOFC.

$$\Delta V_{act} = -A\ln(i) \tag{86}$$

where ΔV_{act} - activation voltage loss

A - slope of Tafel line (constant specific for SOFC)

i - current density (current / electrode area)

Mass transport losses are losses that occur due to the difference in concentration of the fuel as it passes through the electrode. The concentration will be high when the fuel and air enter the electrodes, but as they travel through, they get used in the reaction. This concentration affects the partial pressure of the reactants and has an effect on the voltage that that portion of the electrode can produce. Unfortunately this loss cannot be accurately calculated analytically. Therefore, experimental results are used to empirically estimate the loss. Equation (87) has been developed based on experiments and is accepted as a good approximation of the mass transport losses [8].

$$\Delta V_{trans} = me^{(ni)} \tag{87}$$

where ΔV_{trans} - voltage loss due to mass transfer and concentration loss

m, n – constants derived from experiment (specific to SOFC)

Combining all the losses into equation (85) gives an equation for the overall voltage of a single fuel cell. In an actual fuel cell power plant, multiple cells would be combined in series to provide the necessary voltage and current demand [8]. The total stack voltage is:

$$V = N_0\left[E_0 + \frac{RT}{2F}\left(ln\frac{p_{H_2}p_{O_2}^{0.5}}{p_{H_2O}}\right)\right] - rI - A\,ln(i) + me^{(ni)} \tag{88}$$

The total power generated from the FC (P_{FC}) is simply:

$$P_{FC} = N_0 VI \tag{89}$$

3.2.3 Fuel Cell Model Simulation

A Simulink model was created to simulate the fuel cell based on the analysis performed above (Figure 50). The model was run using parameters shown in Figures 50 and 51. Figures 52 and 53 show the voltage and power outputs of the model, respectively. The initial transients are due to the startup of the model and the initial conditions of the transfer functions being zero. It can be seen that the fuel cell produces approximately 200 kW of power with a 300 amp current demand at steady state. The model uses 20 fuel cells connected in series. The parameters used in the simulation are summarized in Table 4.

Table 4: Fuel Cell Simulation Parameters

K_r	9.95e-4
FC Temp	1273.15 K
kmol/kg_air	1/29
$Kmol / kg\_H_2$	1/2
N_0	20
K_{H2}	8.43e-4 kmol/(atm s)
K_{H2O}	2.81e-4 kmol/(atm s)
K_{O2}	2.52e-3 kmol/(atm s)
τ_{H2}	26.1 s
τ_{H2O}	78.3 s
τ_{O2}	2.91 s
r	0.126 ohms

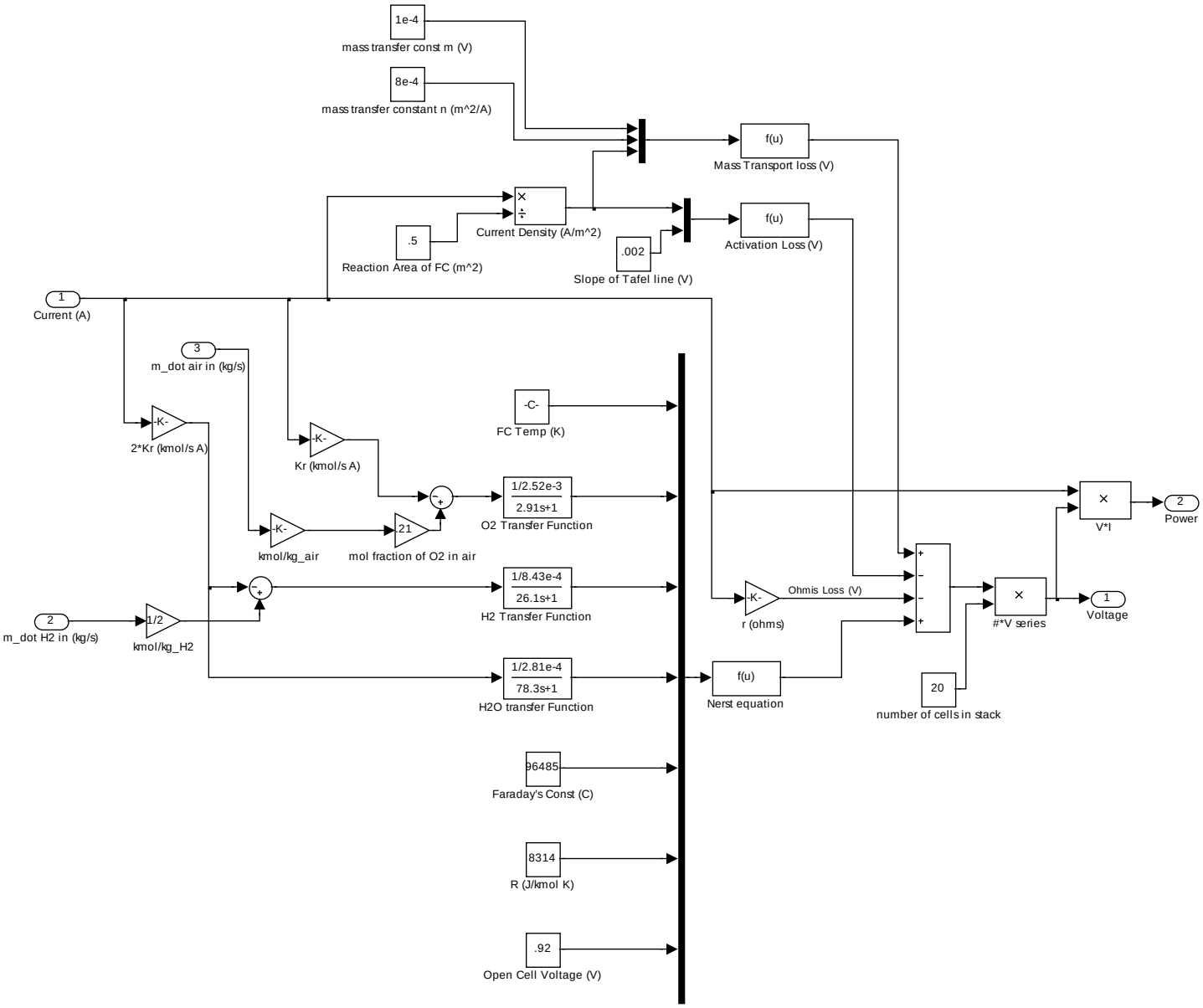

Figure 50: Simulink Fuel Cell Model

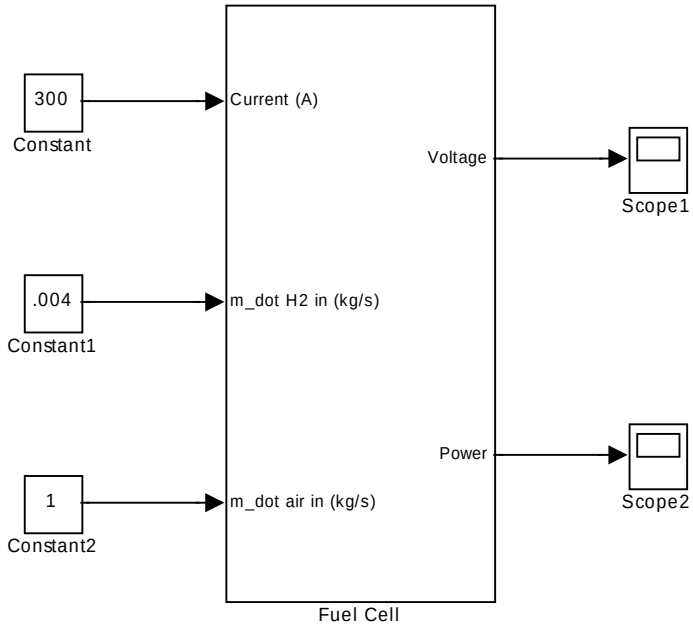

Figure 51: Fuel Cell Simulation Parameters

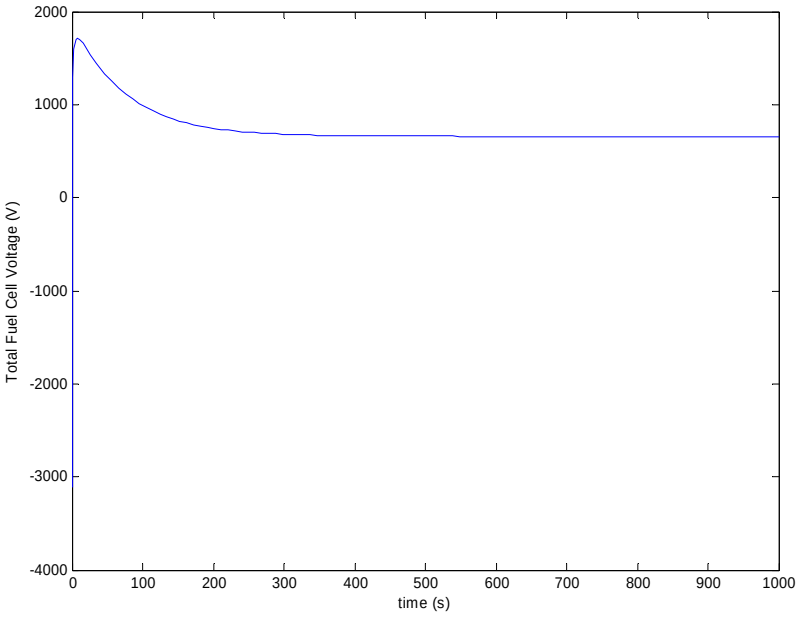

Figure 52: Fuel Cell Voltage

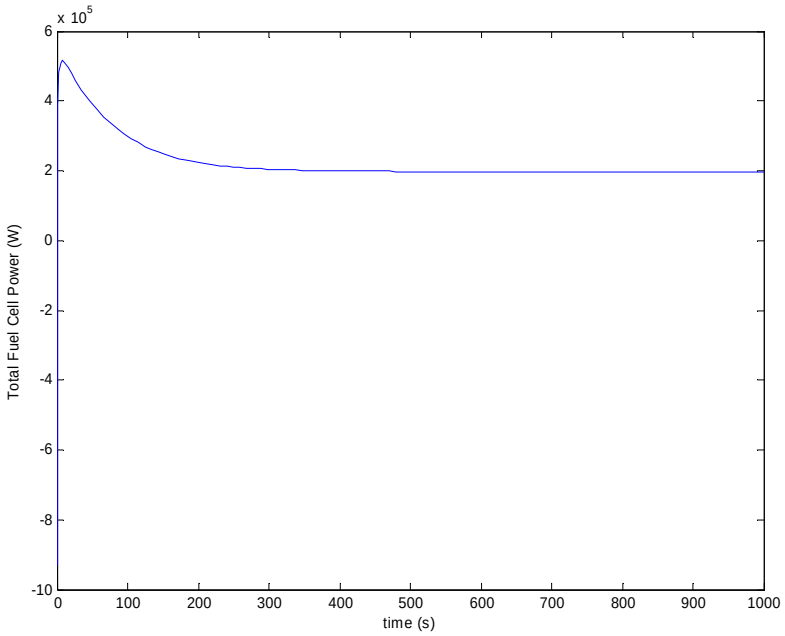

Figure 53: Fuel Cell Power

A second simulation was run using a linear current ramp starting at 10 amps with a slope of 1. Figure 54 shows the voltage response of the fuel cell. Initially, the voltage is low until the current reaches a relatively high level. This is due to the transfer functions initial conditions of zero. The voltage reached a peak just past 400 s after which it starts to drop. This is typical with fuel cells and has to do with the irreversibilities when the current reaches a certain level [8].

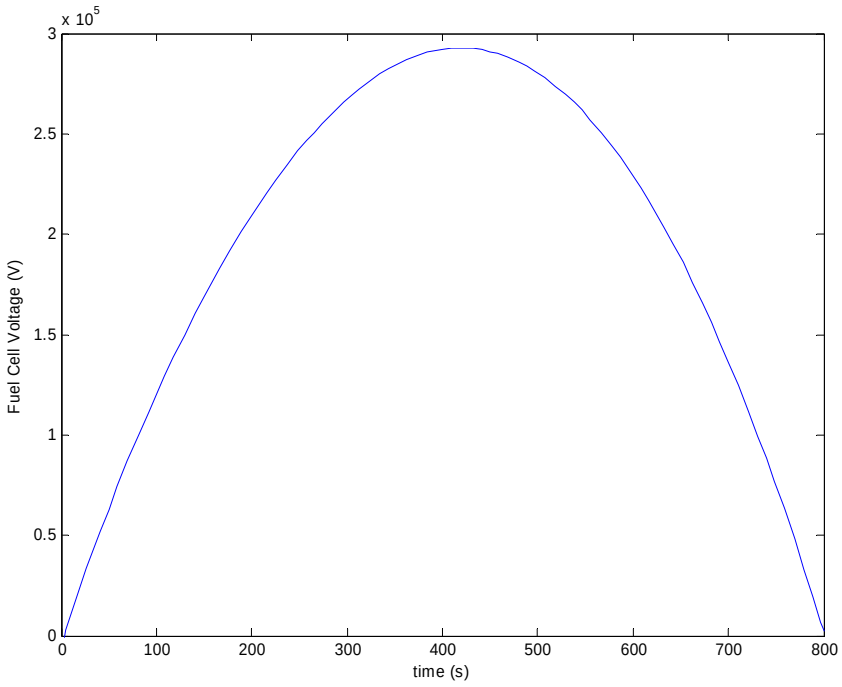

Figure 54: Fuel Cell Voltage Response Due to Linear Current Ramp

4.0 MODEL INTEGRATION

The models described above can be integrated into a number of combinations of fuel cell gas turbine power plants [13], [18], [19], [21]. The basic idea is to combine them in such a way that the high temperature of the fuel cell gases is exploited to run the gas turbine. This can be accomplished with heat exchangers or running the same fluid through the fuel cell and the gas turbine.

4.1 GAS TURBINE INTEGRATION

4.1.1 Gas Turbine Model Integration

The first step in integrating the individual component models is to construct a simple gas turbine model. This entails combining the compressor, combustor, and turbine into a system that produces a net power output. The integration of the gas turbine model is shown in Figure 22 and the thermodynamic cycle is shown above in Figure 23. By combining the Simulink models as shown in Figure 22, a complete gas turbine model is constructed (Figure 55).

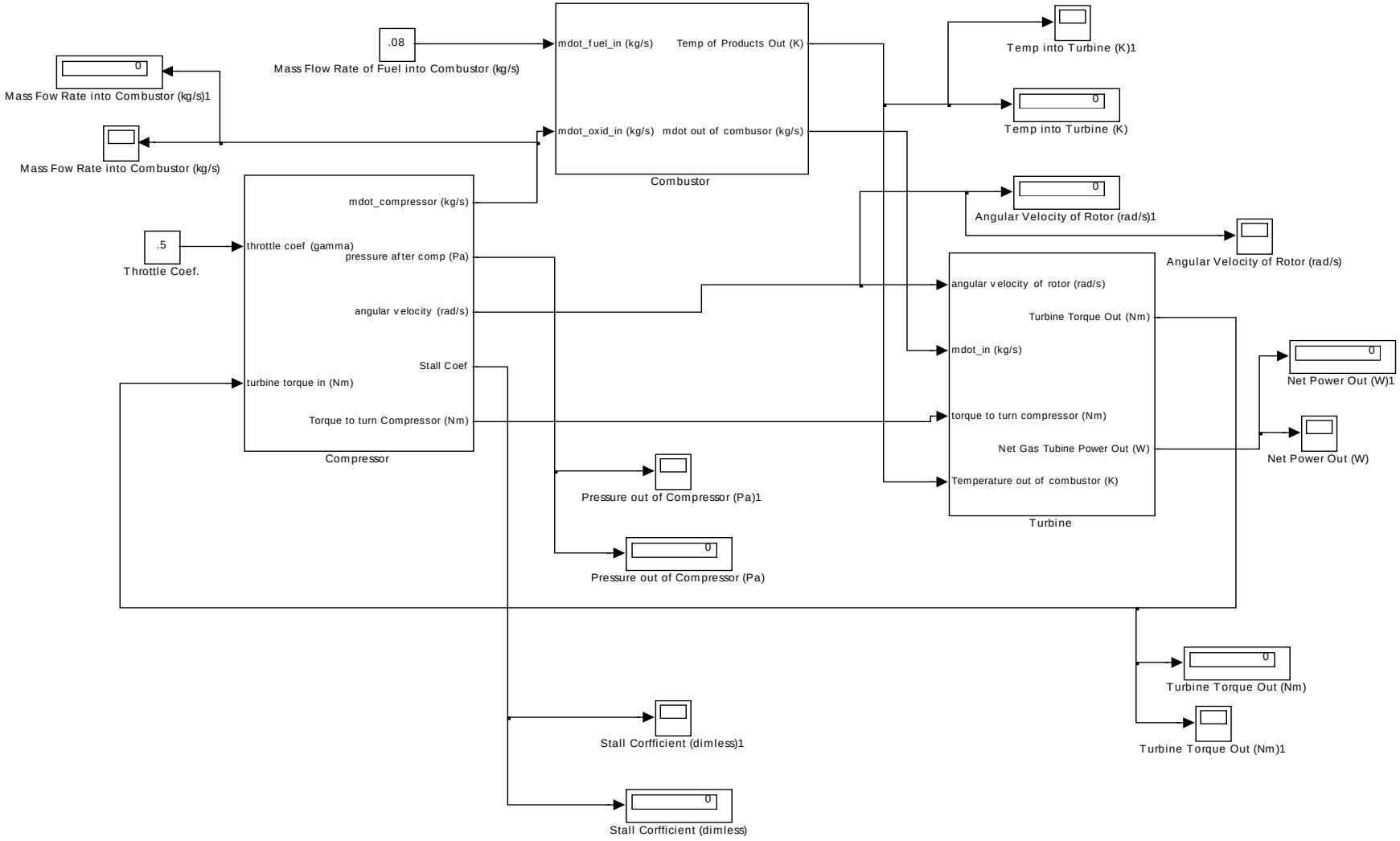

Figure 55: Gas Turbine Simulink Model

As shown in Figure 55, the inputs to the gas turbine are mass flow rate of fuel into the combustor and the throttle coefficient into the compressor model. The mass flow rate into the combustor controls the amount of fuel that is reacting. This will control the temperature of the combustion products entering the turbine. Since the power developed by the turbine is dependent on the input temperature of the working fluid, this flow rate can be used as a gas turbine control variable. The throttle coefficient can be thought of as a bleed air valve which can control the pressure drop across the turbine stage. This valve could therefore be used to control the speed of the rotor and therefore the power out of the gas turbine portion of the power plant. The outputs of the compressor model are mass flow rate, pressure, rotor angular velocity, and stall coefficient. The mass flow rate is then used as an input to the combustor and the angular velocity is connected to the input of the turbine model. This will calculate the power output of the turbine (equation (67)). The stall coefficient is used to determine if the compressor is in rotating stall. If this value is above zero, the compressor is experiencing some level of rotating stall. The temperature and flow rate out of the combustor is used to calculate the enthalpy rise of the working fluid and the power out of the turbine. The torque developed by the turbine is fed back into the input of the compressor model. As stated above, the torque balance of the turbine and compressor are calculated in the compressor model.

4.1.2 Gas Turbine Model Simulation

The gas turbine model was run using a value of 0.5 kg/s for the fuel input mass flow rate of the combustor and a value of 0.5 for the throttle coefficient [3]. The results are shown in Figures 56 – 58. Figure 56 shows that the power produced by the turbine ramps up to quasi-equilibrium in the first few seconds of operation. This is due to the initial conditions of the system at startup.

After the turbine reaches approximately 125 kW, it stabilizes and remains relatively constant throughout the simulation. Figure 57 shows that the angular velocity of the rotor is increasing throughout the simulation. This is due to the torque generated by the turbine being higher than the torque to balance the angular velocity of the rotor, therefore the rotor rotates faster. A stabilization technique for the rotor angular velocity is to control the output torque of the turbine by varying the input fuel mass flow rate of the combustor or to incorporate a cold air injection to control the inlet temperature of the turbine (Figure 58).

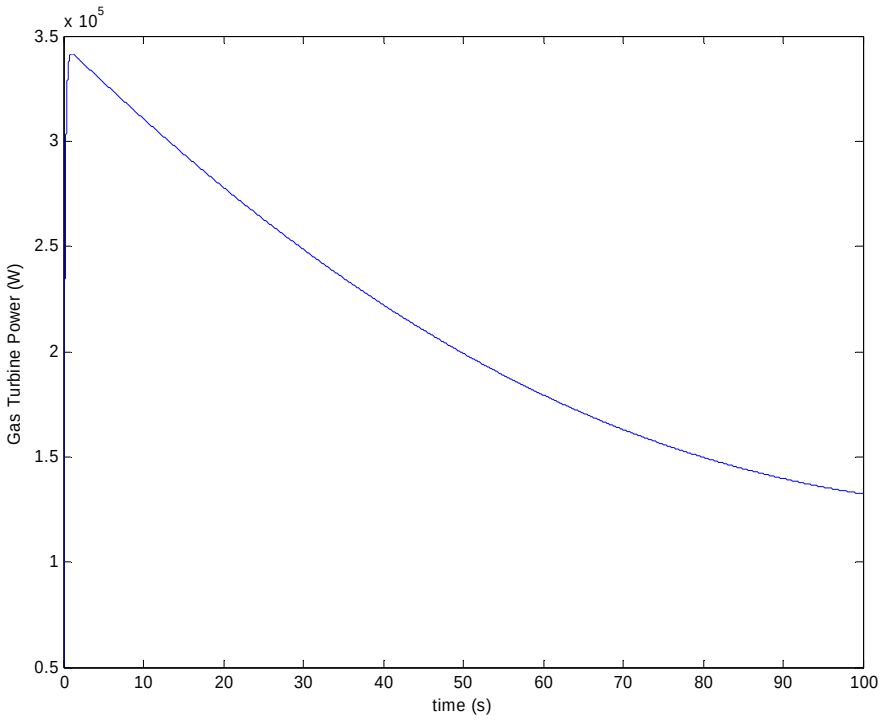

Figure 56: Gas Turbine Output Power

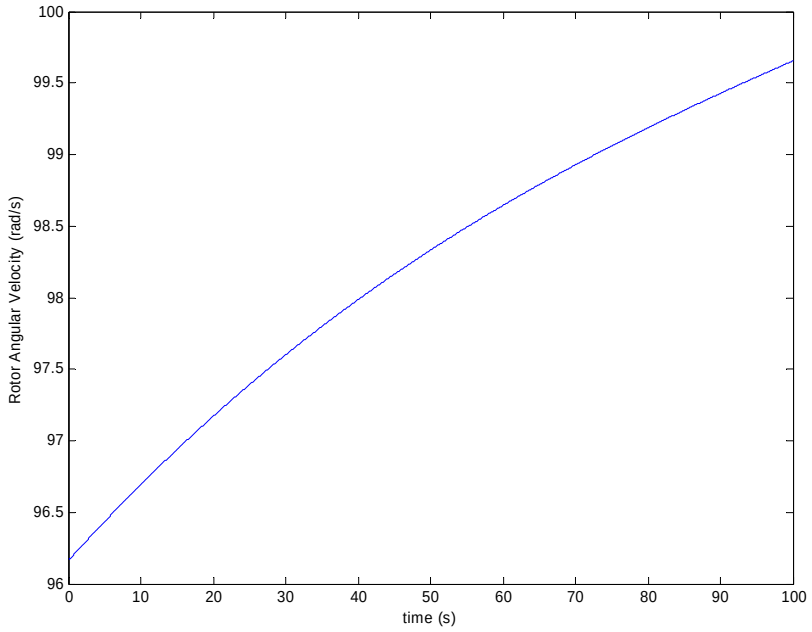

Figure 57: Gas Turbine Rotor Angular Velocity

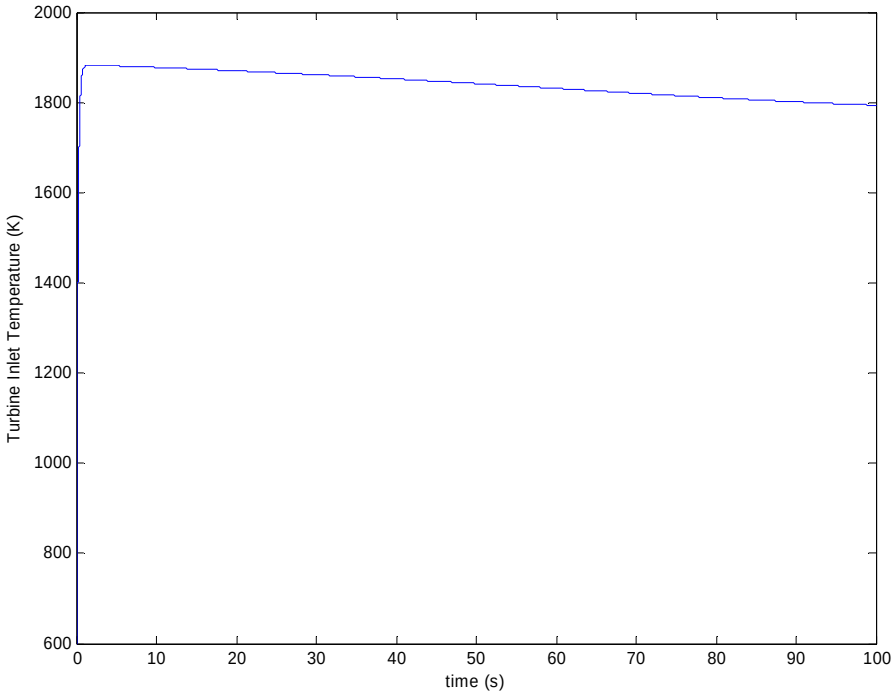

Figure 58: Turbine Inlet Temperature

4.2 FUEL CELL – GAS TURBINE

4.2.1 FCGT – Integration Configuration One

As stated above, there are several ways to combine a fuel cell and gas turbine into a hybrid power plant. One of which is to run the fuel cell independently and use a heat exchanger to transfer the heat from the fuel cell exhaust to the working fluid of the gas turbine after compression and before expansion. This eliminates the need for a combustor to raise the temperature of the working fluid before the turbine. This configuration is shown in Figure 59. An advantage to completely separating the working fluids of the fuel cell and the gas turbine is that the pressure fluctuations in the gas turbine won't affect the pressure of the fuel cell. This is not the case with configurations that have the working fluid of the gas turbine being run through the fuel cell (described later). The Simulink model for this configuration is shown in Figure 60. As previously stated, the mismatched dynamics of the gas turbine and the fuel cell will produce combined transients in the output power of the entire power plant. These transients will be evident during startup and shutdown of the system as well as transients in power demand of the grid.

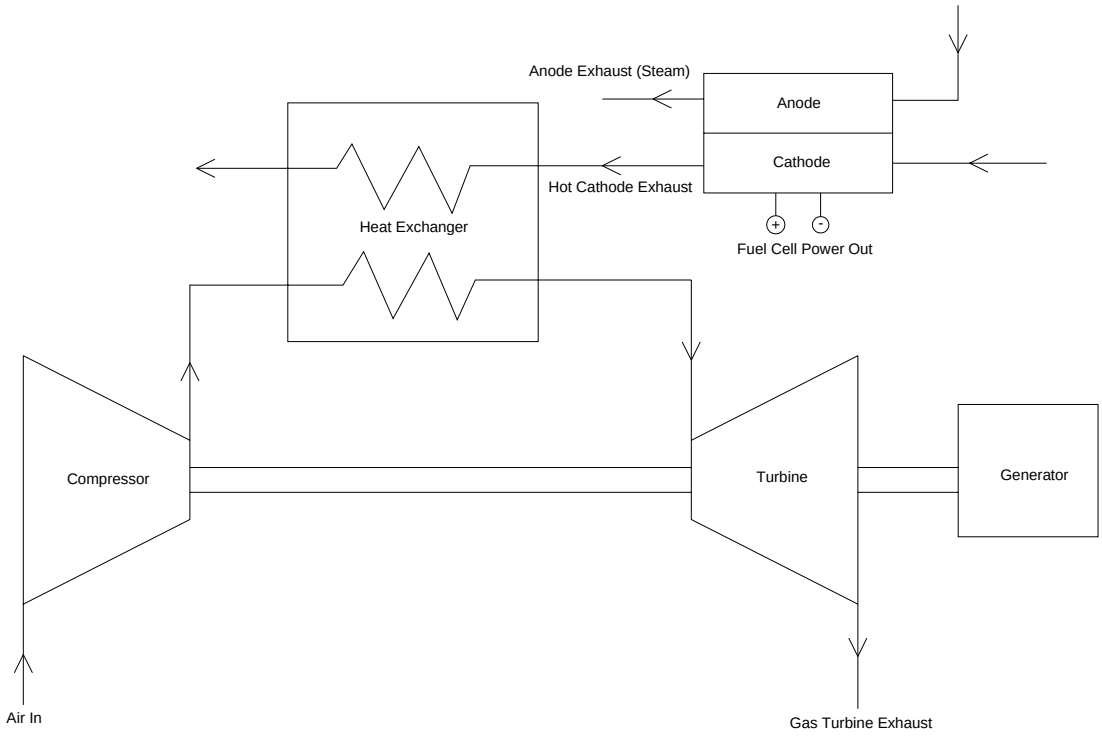

Figure 59: Fuel Cell Gas Turbine Integration using Heat Exchanger

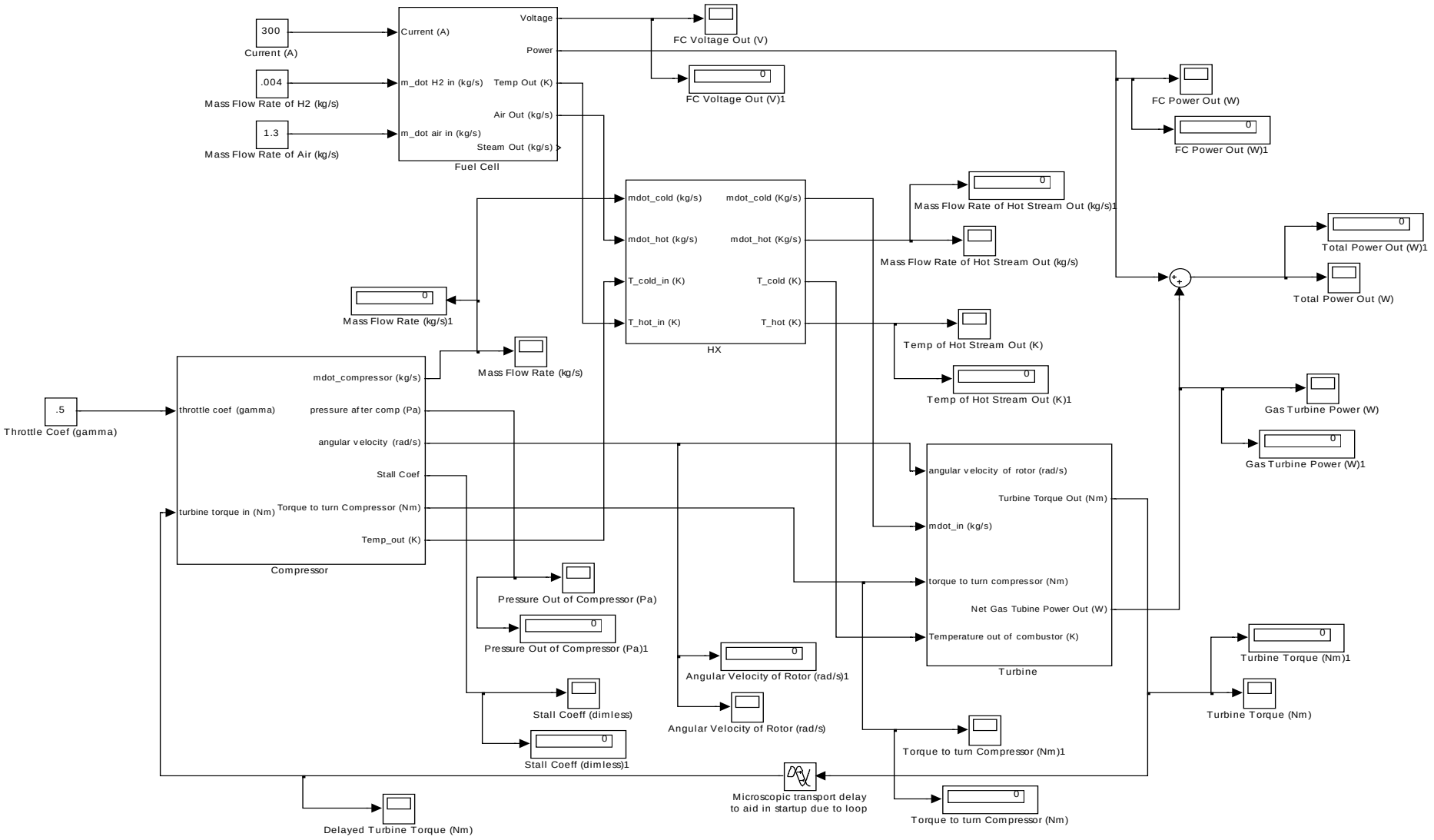

Figure 60: Fuel Cell Gas Turbine Hybrid Power Plant Simulink Model

4.2.2 FCGT – Integration Configuration One Simulation

The results of running this simulation are represented in Figures 61 – 64. The fuel cell power stabilizes at approximately 200 kW and the gas turbine stabilizes at approximately 70 kW, yielding a total plant power of 270 kW. It can be seen from Figure 61 that the fuel cell stabilizes at approximately 60 times faster (400 s) than the gas turbine (25,000 s) response shown in Figure 62. The velocity of the gas turbine rotor shown in Figure 63 is slow to reach a steady state condition due to the inertia of the turbine and compressor. It stabilizes at approximately 188 rad/s, which is equivalent to 1800 rpm. As seen from Figure 64, the convergence of the total plant power output is dominated by the turbine response, which has the slowest dynamics.

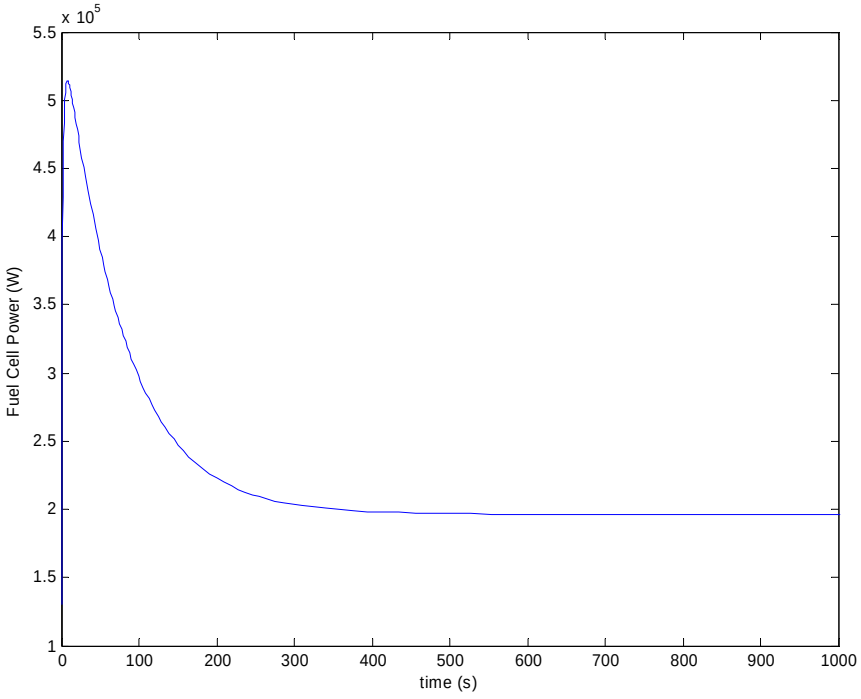

Figure 61: FCFT Power Plant – Fuel Cell Power

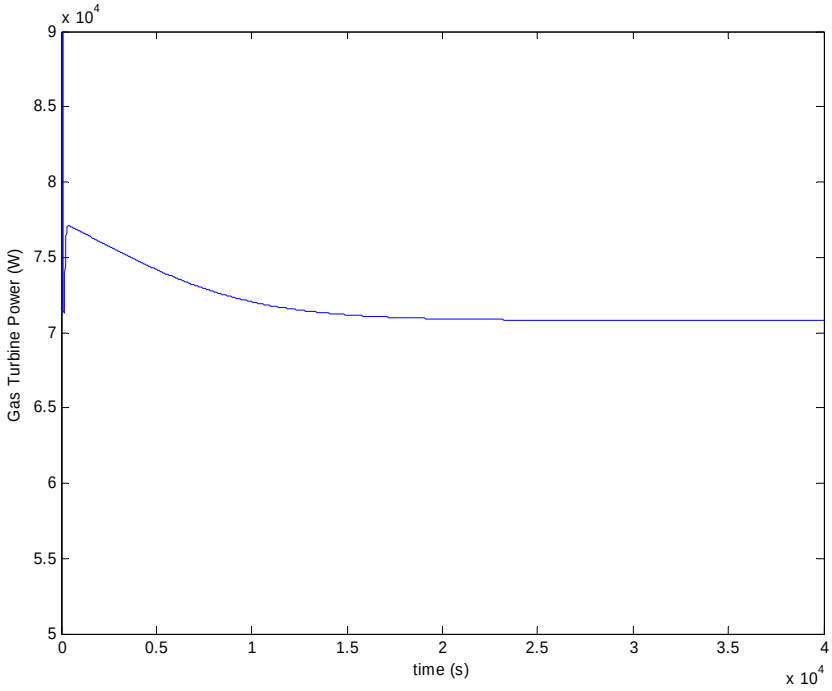

Figure 62: FCFT Power Plant – Gas Turbine Power

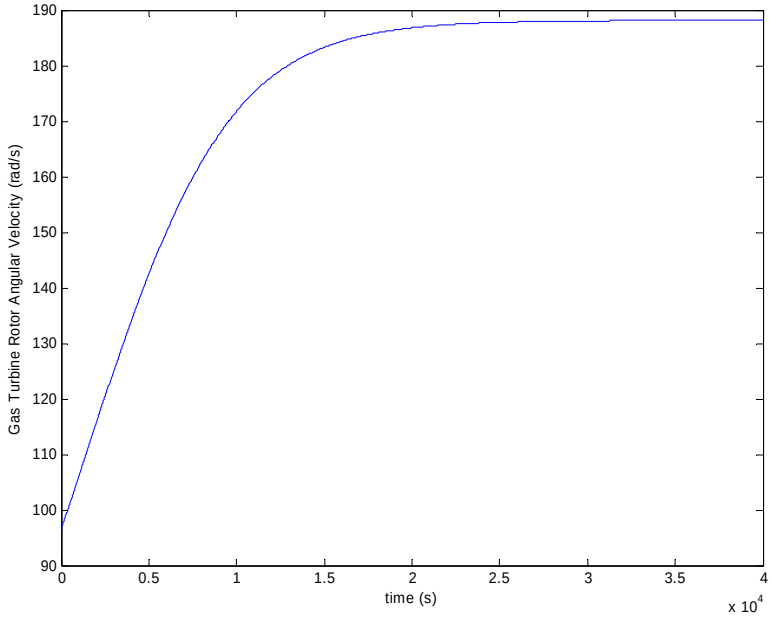

Figure 63: FCFT Power Plant – Gas Turbine Rotor Angular Velocity

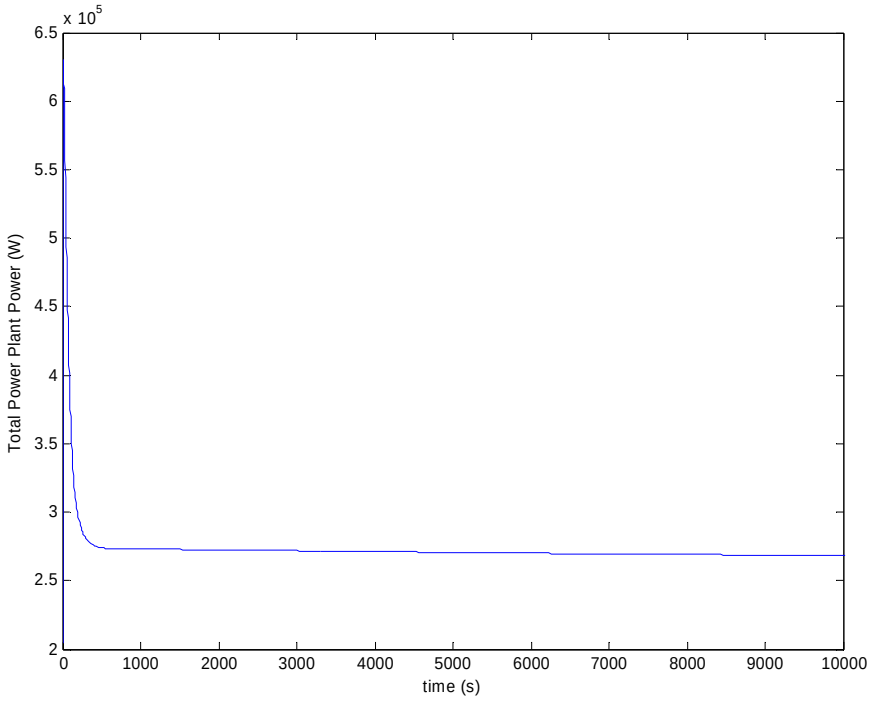

Figure 64: FCFT Power Plant – Total Plant Power

4.2.3 FCGT – Integration Configuration Two

A second configuration for a combined fuel cell gas turbine system routes run the compressed working fluid from the gas turbine directly through the cathode of the fuel cell. The output from the cathode, as well as the leftover fuel from the anode is combusted and run through the turbine. The exhaust gas of the turbine is then used to preheat the compressed air before it enters the cathode of the fuel cell (Figure 65).

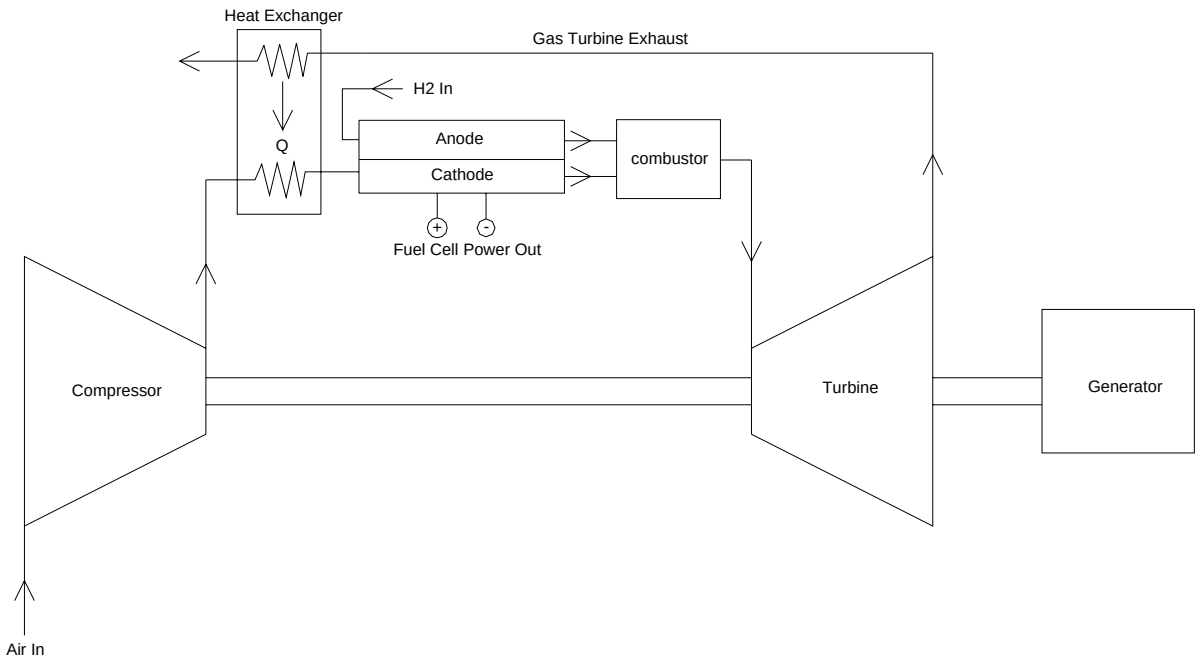

Figure 65: Fuel Cell Gas Turbine Hybrid Power Plant Configuration Two

4.2.4 FCGT – Integration Configuration Two Simulation

Figure 66 shows the Simulink Model of the above configuration. The heat exchanger model is excluded due to the fuel cell temperature assumed to be constant. Figures 67-70 show the results of running this model. The fuel cell contributes 470 kW while the gas turbine contributes 430 kW. The gas turbine contributes much more power this time because excess fuel is combusted in the working fluid before it expands through the turbine. The fluid exits the fuel cell at approximately 1300K and is combusted to a temperature of 3000K. Therefore the fluid has a much higher enthalpy than the previous configuration (Figure 59). The total power for the entire power plant is 900 kW.

Figure 67 shows that the fuel cell power reaches steady state in approximately 7 s. This is faster than the previous configuration due to the additional mass flow rate of the air being provided by the compressor into the fuel cell. Figure 68 shows the power of the gas turbine stabilizing slower than the fuel cell which is expected.

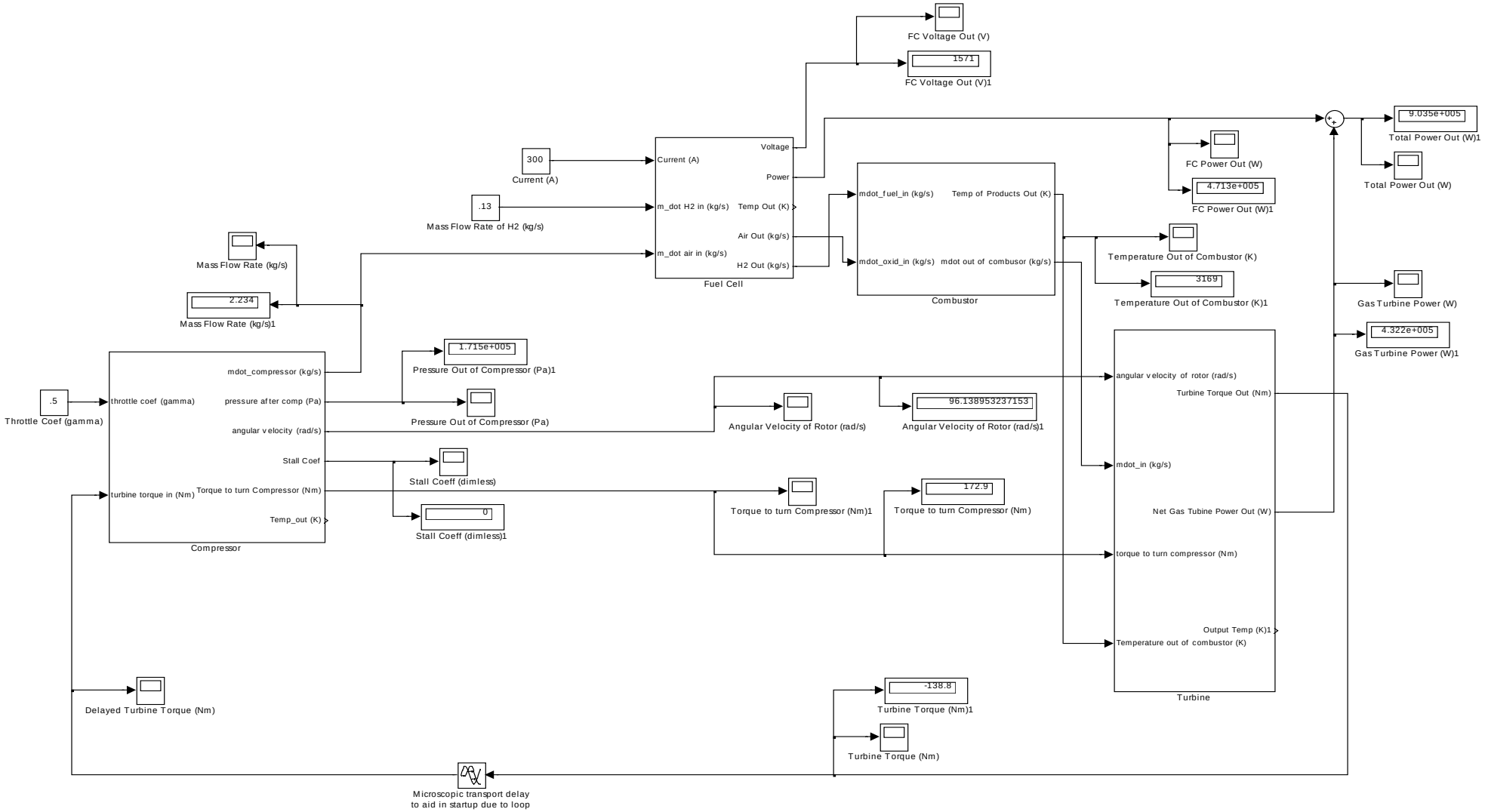

Figure 66: Fuel Cell Gas Turbine Hybrid Power Plant Simulink Model Configuration Two

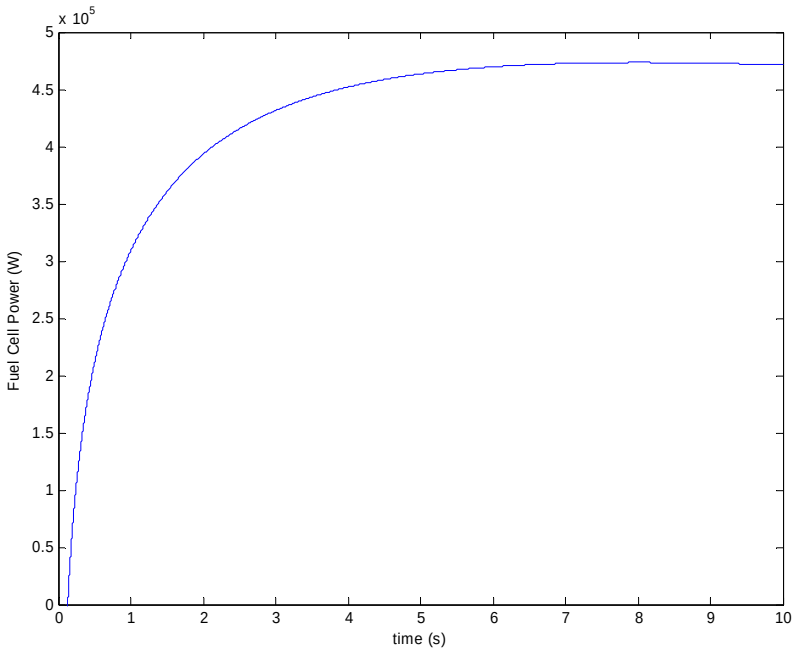

Figure 67: FCGT Configuration Two – Fuel Cell Power

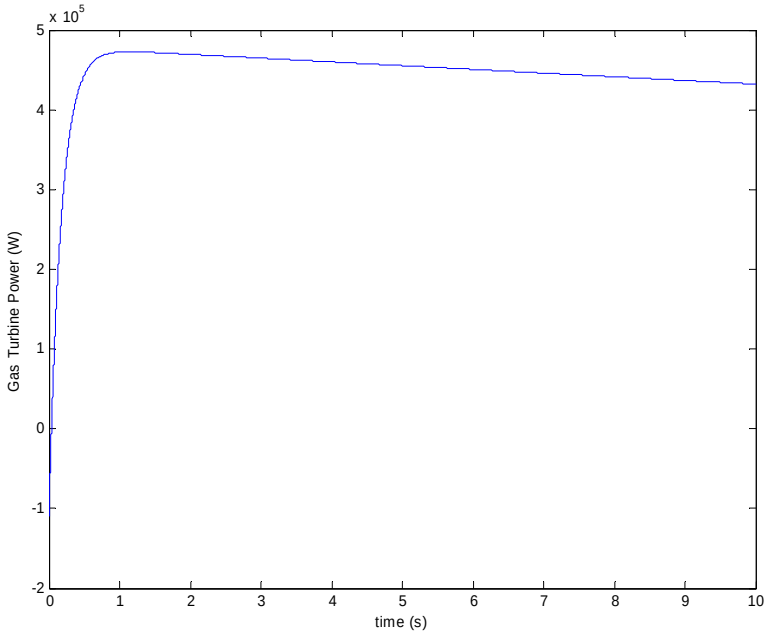

Figure 68: FCGT Configuration Two – Gas Turbine Power

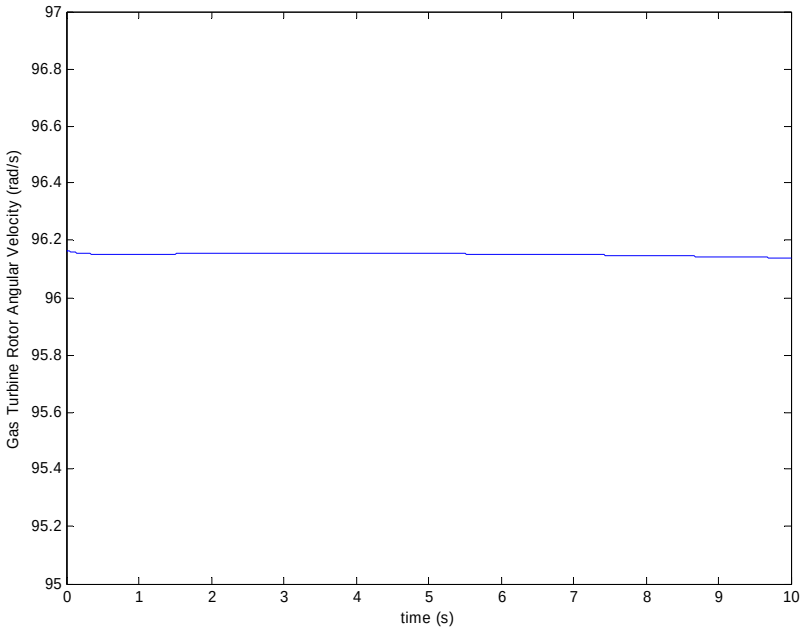

Figure 69: FCGT Configuration Two – Gas Turbine Rotor Angular Velocity

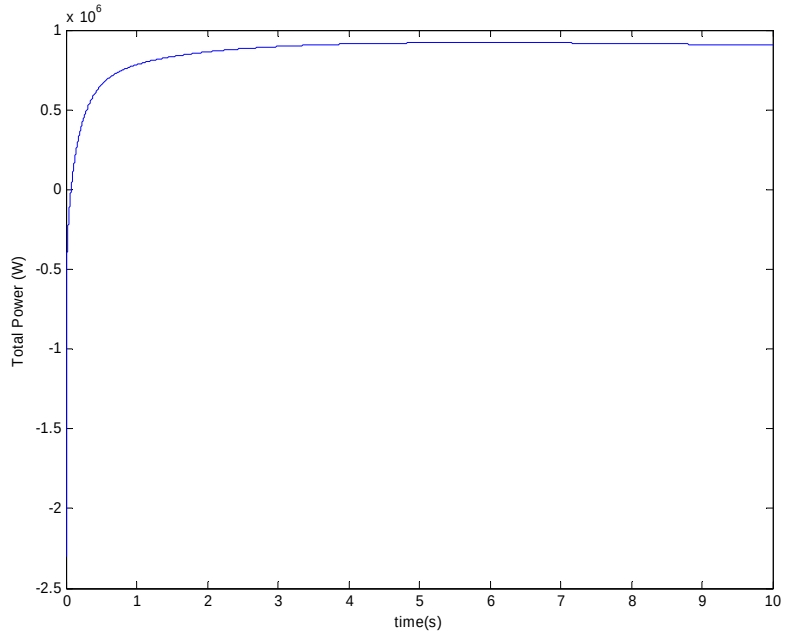

Figure 70: FCGT Configuration Two – Total Plant Power

5.0 PRELIMINARY CONTROLS

This section will discuss the control of the FCGT hybrid plant. The objective of the section is to analyze the integrated system with respect to possible control methods. This entails identifying effective control knobs based on the effect of step changes in different parameters. Once the control knobs are identified, a simple proportional, integral, differential (PID) control mechanism can be incorporated to determine if the non-linear system can be controlled. The main variable to control is the turbine rotor speed. This controls the output power of the turbine and also the air flow rate that flows through the fuel cell.

5.1 RESPONSE TO A STEP INPUT

Fuel cell – gas turbine hybrid configuration 2 will be analyzed dynamically due to its close similarity to actual hybrid systems being built and studied today [8], [13]. A step input can be attached to the inputs of the system to determine the system's response. The inputs that can be stepped are the throttle coefficient on the compressor model and the hydrogen input flow rate of the fuel cell. Table 2 shows the parameters for the dynamic step response dynamic simulations.

Table 5: Step Input Response Simulation Parameters

Input	Initial value	Step value	Step at time	Result Figure #'s
Hydrogen mass flow rate of FC	.1 (kg/s)	1 (kg/s)	5 s	71-74
Throttle coefficient	0.5	0.85	5 s	75, 76

As shown in Figure 71, the power of the fuel cell begins to decrease at the step point (5s). This is due to the increased mass flow rate decreasing the partial pressure inside the electrode. The power is related to the Nerst Equation which is dependent on the partial pressure of the species (equation (85)). The power of the gas turbine (Figure 72) sees an initial spike of performance when the additional hydrogen is added to the combustor, and then is damped out to a value slightly lower than before the step. This is due to the ratio of oxygen to hydrogen in the combustor departing from optimal. The gas turbine rotor (Figure 73) follows the power of the turbine with respect to angular velocity, exhibiting a modest increase and then decrease as a result of the step input. This is intuitive because the angular velocity calculation is based on the power generated from the enthalpy change of the working fluid through the turbine.

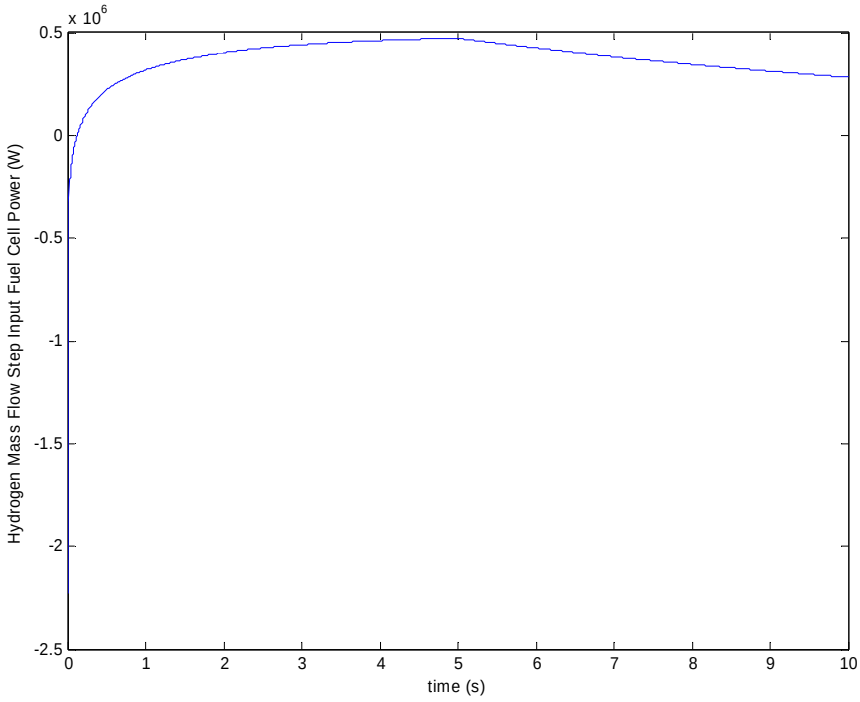

Figure 71: Fuel Cell Power during a Hydrogen Mass Flow Step Change

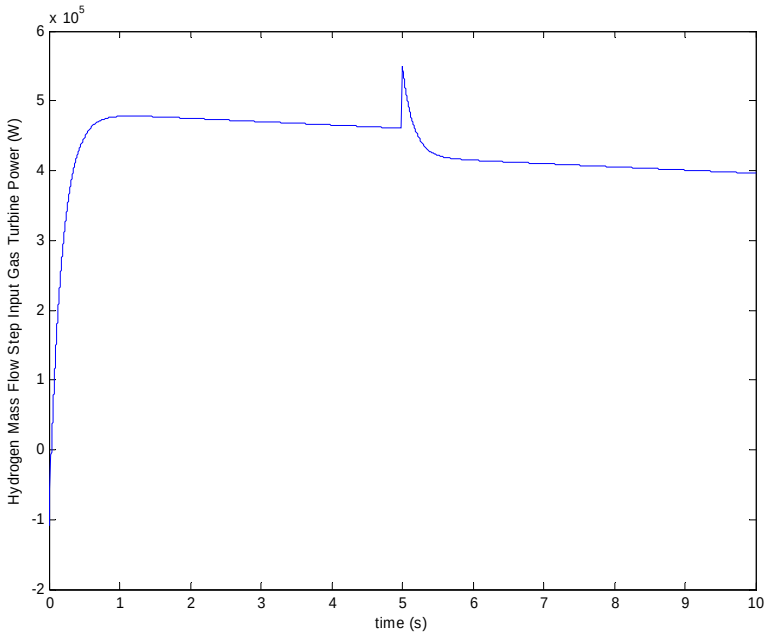

Figure 72: Gas Turbine Power during a Hydrogen Mass Flow Step Change

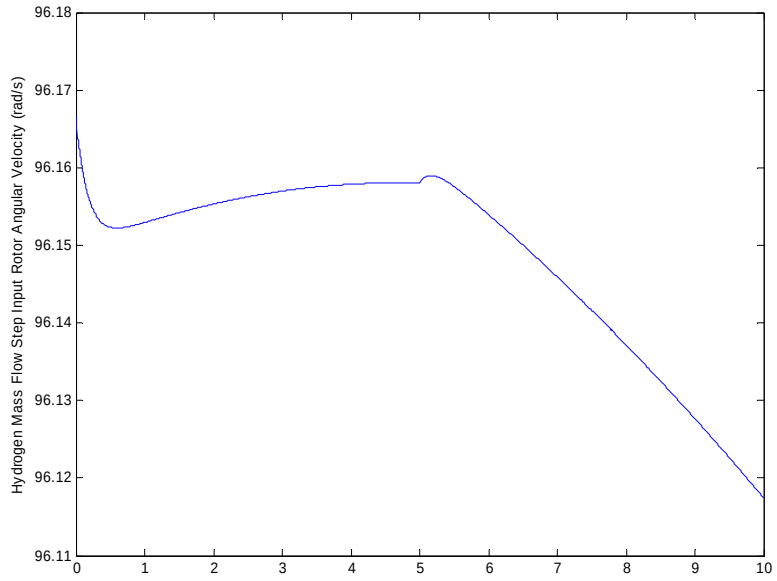

Figure 73: Rotor Angular Velocity during a Hydrogen Mass Flow Step Change

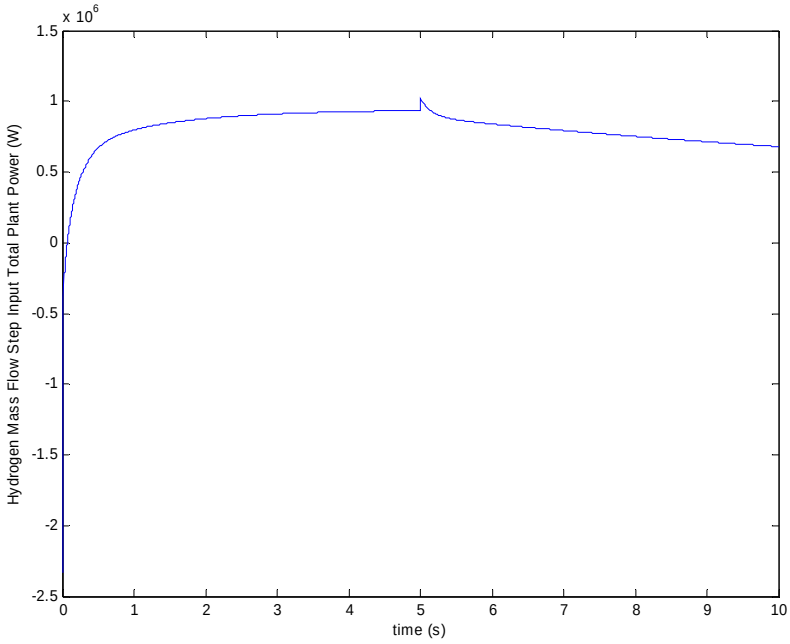

Figure 74: Total Plant Power during a Hydrogen Mass Flow Step Change

The throttle coefficient step input has almost no impact on the total power of the plant (Figure 75). This is because the throttle coefficient only slightly affects the pressure rise of the compressor (Figure 76). This change is not enough to have an impact on the overall power of the gas turbine and hence the plant. Therefore, the throttle coefficient can not be used to control the system.

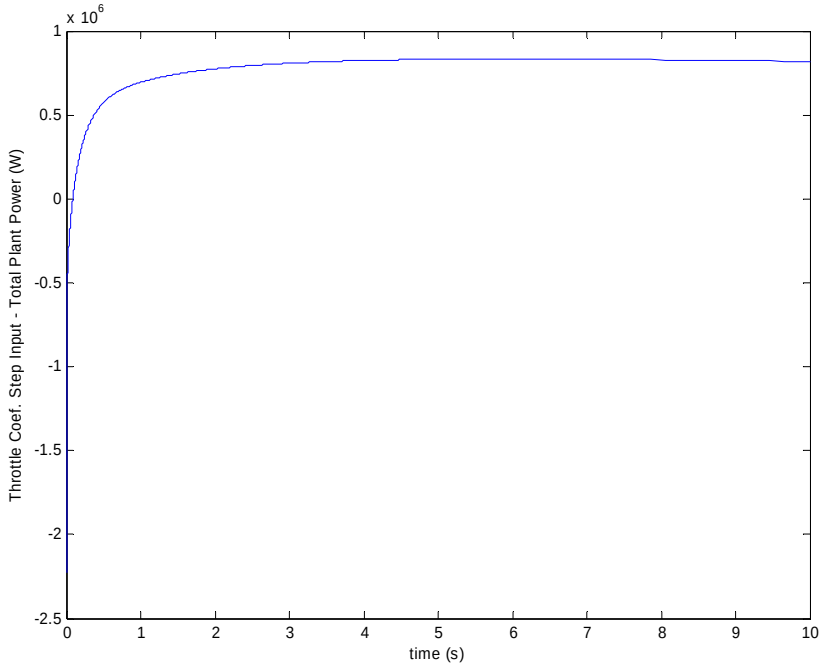

Figure 75: Total Plant Power during a Throttle Coefficient Step Input

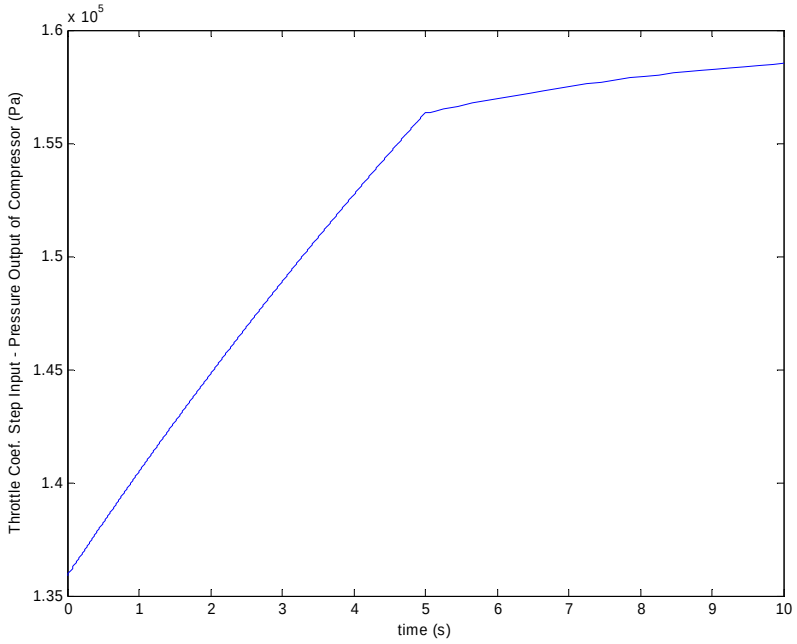

Figure 76: Pressure Output of Compressor during a Throttle Coefficient Step Input

5.2 TURBINE ROTOR SPEED CONTROL

The main control of the gas turbine would be the angular velocity of the rotor. The rotor velocity is directly proportional to the power generated by the gas turbine portion of the power plant. One way to control the angular velocity of the rotor is to introduce a temperature-controlled air input into the working fluid stream before the fluid enters the turbine. The inlet temperature of the working fluid is directly proportional to the power and torque developed by the turbine. Therefore, the overall gas turbine power can be controlled using the temperature controlled air input. This control could also be used to control the amount of fluid that runs through the fuel cell because the rotor angular velocity is a factor in the amount of air drawn into the compressor.

Since the compressed air leaving the compressor flows directly through the fuel cell (FCGT hybrid configuration 2), the air flow can also be controlled by the rotor velocity.

The temperature-controlled air input to the inlet stream of the turbine was incorporated into integration configuration 2. A PID controller was added to the Simulink plant model to control the temperature-controlled air inject signal. An angular velocity setpoint was added to have a means for varying the target value. Various PID gains were tested to determine the optimal settings for angular velocity control and are summarized in Table 3:

Table 6: Air Inject PID Control Settings

Setpoint 96 rad/s				
Run #	P Gain	I Gain	D Gain	Results Figure #
1	100000	100000	50000	77
2	100000	100000	35000	78
3	1000000	1000000	35000	79
4	1000000	1000000	500	80
Setpoint stepped 96 to 98 @ 1s, 98 to 94 @ 4s				
5	1000000	1000000	500	81, 82

As shown in Figure 77, the first run using the control scheme produced an unstable condition. The angular velocity would oscillate about the setpoint before rising asymptotically to infinity. This is due to the derivative gain being too high. It creates an “underdamped” system and the output is not controlled.

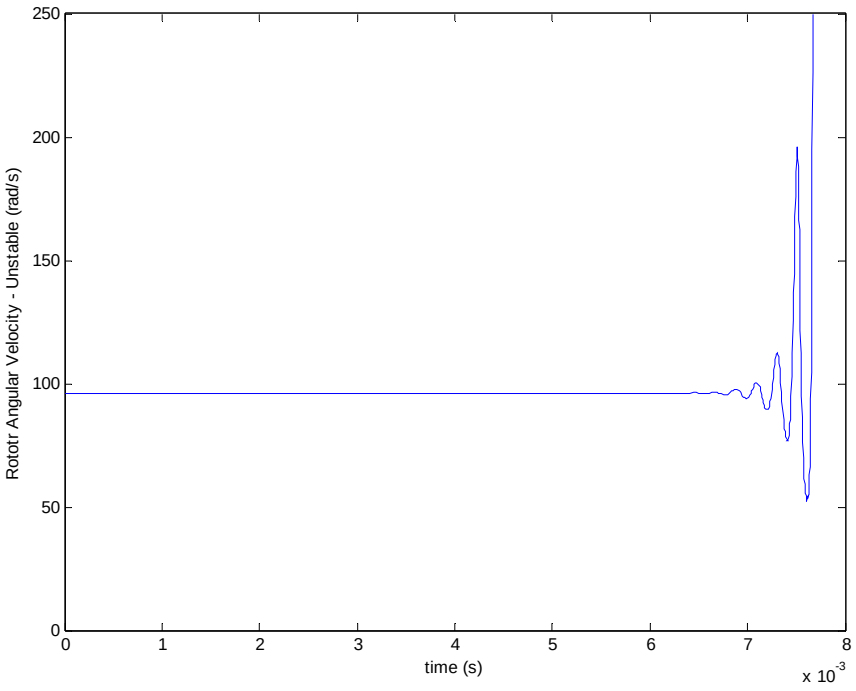

Figure 77: Angular Velocity with Control – PID gain settings 1 – Unstable

Figure 78 shows the results of the second run using different PID settings. The derivative gain was reduced in an attempt to stabilize the system. The velocity does appear to remain near the setpoint, but is still erratic with respect to the reference point (96 rad/s).

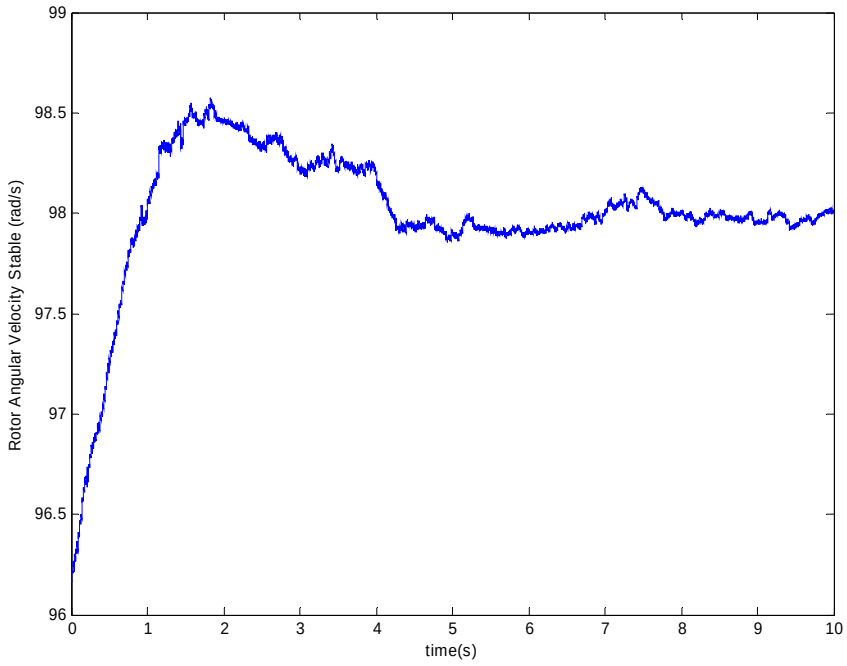

Figure 78: Angular Velocity with Control – PID gain settings 2 – Semi-stable

For the third attempt, the derivative gain was kept constant and the proportional and integration gains were increased by a factor of 10 to improve the steady state response. The output stabilized macroscopically but the small oscillations remained due to the high derivative term.

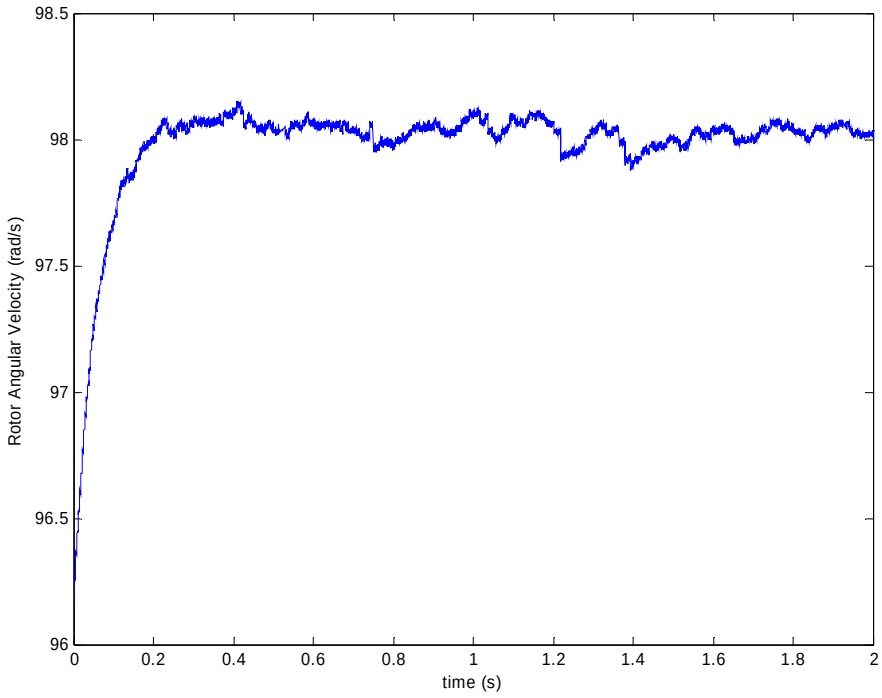

Figure 79: Angular Velocity with Control – PID gain settings 3 – Stable with Oscillations

The forth PID setting uses a high decrease in the derivative gain to try and eliminate the micro-oscillations in the output. Figure 80 shows that the signal is much less oscillatory. After a slight overshoot on startup, and slight oscillations throughout, the output reaches the setpoint in approximately 5 s.

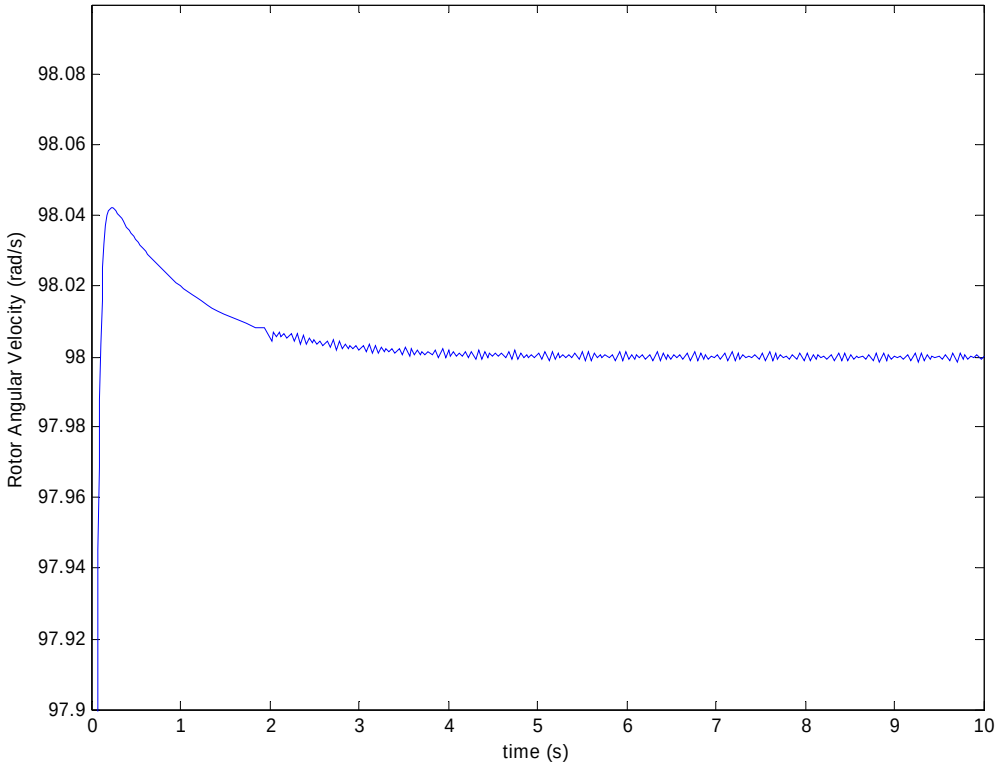

Figure 80: Angular Velocity with Control – PID gain settings 4 – Stable

To demonstrate that this type of controller can follow a stepped setpoint, a simulation was run varying the setpoint at various times throughout the simulation (refer to Table 3). Figure 81 shows the setpoint signal and the output and shows that the output can follow small oscillations in setpoint and the output power can be controlled.

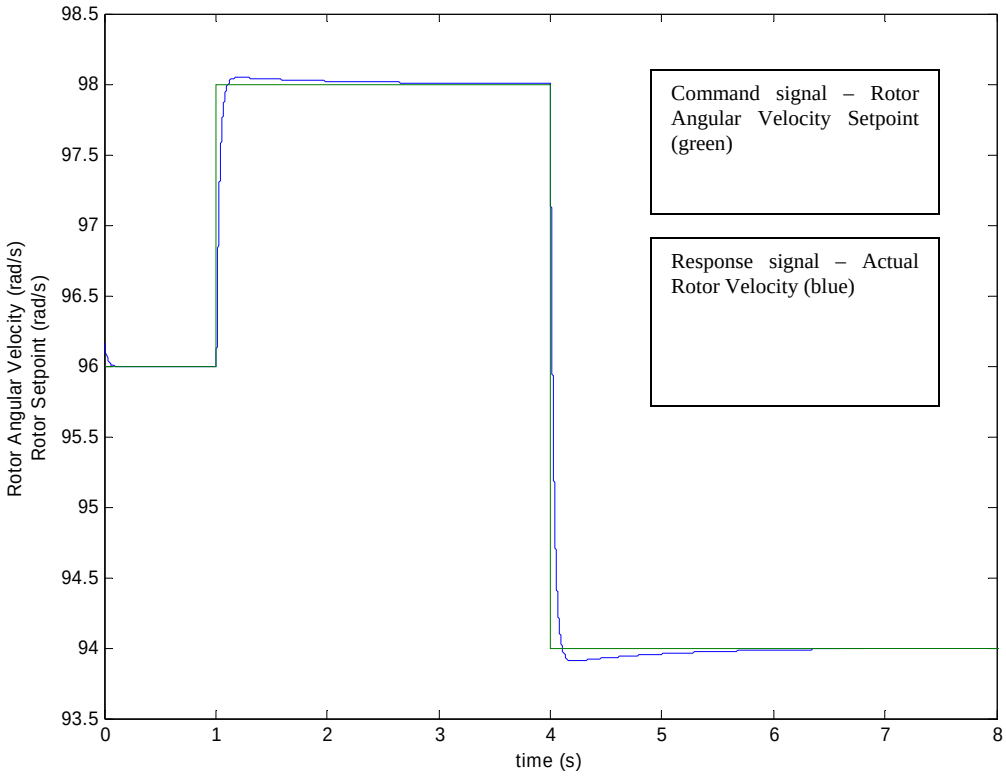

Figure 81: Angular Velocity with Control – Stepped Setpoint – Stable

Figure 82 shows the response of the deviation of the fuel cell power due to a small change in angular velocity of the gas turbine rotor. It is observed that the fuel cell power does vary slightly with respect to rotor velocity. Therefore the angular velocity of the rotor could possibly be used as a control for the output power of the fuel cell as well as the gas turbine.

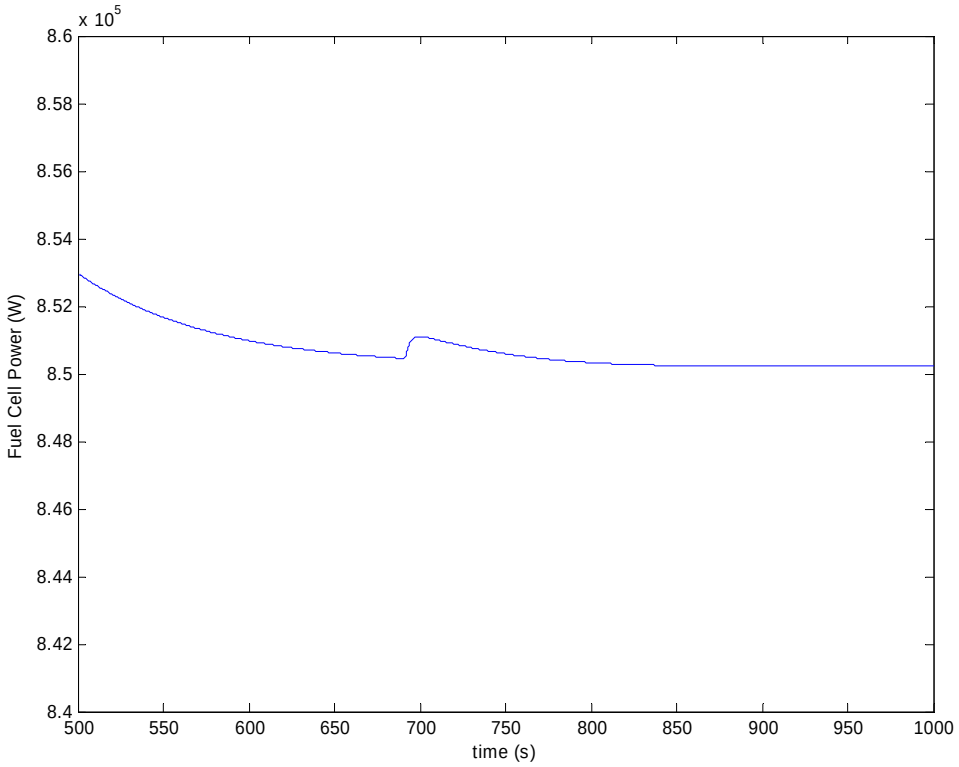

Figure 82: Fuel Cell Power Reaction to Step in Rotor Angular Velocity

6.0 CONCLUSIONS AND FUTURE WORK

Models for the various components of a fuel cell gas turbine hybrid system have been modularly developed using MATLAB and Simulink software. The component models are an axial flow compressor, combustor, turbine, heat exchanger, and solid oxide fuel cell. Each component model was developed and validated independently before incorporation into the complete system. This modularity creates a flexible framework that can be used to create a virtually limitless number of hybrid power plant combinations. Two hybrid configurations were developed here. Both were simulated to observe general plant behavior such as power, rotor velocity, and fuel cell voltage. One hybrid configuration was simulated with respect to dynamic inputs. This consisted of stepping various inputs to determine the effect on the system outputs. This can determine the control knobs that could possibly be used to control the plant. It was found that varying the H_2 input flow rate on the fuel cell had an impact on the total plant power as well as the gas turbine power and rotor velocity. Therefore, this input could possibly be used to control the output power of the plant. A separate control mechanism was implemented to control the rotor velocity, and hence power, of the gas turbine. This consisted of injecting temperature controlled air into the working fluid stream just before the turbine. This would control the inlet temperature of the turbine as well as the enthalpy of the inlet fluid. Since the power generated by the turbine is directly proportional to the change in enthalpy of the working fluid, the output power, and the rotor velocity, of the gas turbine can be controlled. This scenario

was implemented on the hybrid model using a PID controller. It was found, after some tweaking of the PID gains, that the angular velocity of the gas turbine could be controlled with respect to an input set point using the air inject method. The controls analysis performed in this study is not intended to be exhaustive, but rather to give a preliminary look at possible control methods and directions. The main achievement of this study is the development of modular models that can be used for future research. From a controls standpoint, additional studies could be performed on linearization of the individual or combined models about a steady state operating point. Standard controls analysis could then be used to characterize and design a control scheme. Other control knobs could be analyzed and simulated as well.

The models developed here do not include some additional components that could be used to better simulate a FCGT hybrid plant. For example, a fuel reformer could be incorporated into the fuel cell model. This would more accurately represent an actual fuel cell cycle. Also, a humidifier could be attached to the fuel cell. Valve dynamics could also be included to better simulate the air inject and H_2 input flow controls. In addition to the controls, these models could be used for an efficiency study of various hybrid configurations. This could involve combining multiple fuel cells and gas turbines with various heat exchangers. The study could also be expanded to include the power delivery methods, such as synchronous vs. non-synchronous turbines.

BIBLIOGRAPHY

[1] F. K. Moore and E. M. Greitzer. A Theory of Post-Stall Transients in Axial Compression Systems: Part 1 – Development of Equations. Transactions of the ASME, Volume 108, January 1986, p.68.

[2] E. M. Greitzer. Review – Axial Compressor Stall Phenomena. Transactions of the ASME, Volume 102, June 1980, p. 134.

[3] Jan Tommy Gravdahl and Olav Egeland. A Moore Greitzer Axial Compressor Model with Spool Dynamics. Proceedings of the 36th Conference on Decision and Control, San Diego, CA, USA, December 1997, p. 4714.

[4] Frank M. White. Fluid Mechanics. McGraw Hill, New York, NY, 1994.

[5] Christopher Fannin. Linear Modeling and Analysis of Thermoacoustic Instabilities in a Gas Turbine Combustor. PhD dissertation, Virginia Polytechnic Institute and State University, 2000.

[6] Michael Moran and Howard Shapiro. Fundamentals of Engineering Thermodynamics 3rd Ed. John Wiley and Sons, Inc., New York, NY, 1996.

[7] Frank Incropera and David DeWitt. Introduction to Heat Transfer. 3rd edition, John Wiley and Sons, Inc., New York, NY, 1985.

[8] James Larminie and Andrew Dicks. Fuel Cell Systems Explained. John Wiley and Sons, Inc., New York, NY, 2003.

[9] J. Padulles, G. W. Ault, J. R. McDonald. An Integrated SOFC Plant Dynamic Model for Power Systems Simulation. Journal of Power Sources, volume 86, 2000, p. 495.

[10] Shinji Kimijima and Nobuhide Kasagi. Performance Evaluation of Gas Turbine – Fuel Cell Hybrid Micro Generation System. Proceddings of ASME Turbo Expo, Amsterdam, The Netherlands, 2002.

[11] National Energy Technology Laborotory, Fuel Cell Handbook 6th edition. Morgantown, WV, 2002.

[12] Eric Liese, Randall Gemmen, Jose Rivera, Faryar, Jacob Brouwer. Development of Dynamic Modeling Tools For Solid Oxide and Molten Carbonate Hybrid Fuel Cell Gas Turbine Systems. Submitted for presentation at the International Gas Turbine Instituite meeting of the American Society of Mechanical Engineers, 2000.

[13] Eric Liese, Randall Gemmen, Faryar Jabbari, Jacob Brouwer. Technical Development Issues and Dynamic Modeling of a Gas Turbine and Fuel Cell Hybrid Systems.

[14] H. Cohen, G. F. C. Rogers, H. I. H. Saravanamuttoo. Gas Turbine Theory. John Wiley and Sons, Inc., New York, NY, 1973.

[15] The MathWorks. MATLAB and SIMULINK software. Natick, MA, 2002.

[16] Tuncer Cebeci and Peter Bradshaw. Physical and Computational Aspects of Convective Heat Transfer. Springer – Verlag, New York, NY.

[17] Trax Corporation. ProTrax Programmer's Manual. Forest, VA.

[18] Pietro Bedont, Olivia Grillo, and Aristide Massardo. Off Design Performance Analysis of a Hybrid System Based on an Ecisting MCFC Stack. Proceedings of the ASME Turbo Expo, Amsterdam, the Netherlands, 2002.

[19] Maria-Teresa Basurto, Pericles Pilidis, and Richard Hales. Molten Carbonate Fuel Cell Gas Turbine Combined Cycle for Marine Propulsion. Part A: Design Point Operation. Proceedings of the ASME Turbo Expo, Amsterdam, the Netherlands, 2002.

[20] Eric Liese and Randall Gemmen. Dynamic Modeling Results of a 1 MW Molten Carbonate Fuel Cell/ Gas Turbine Power System. Proceedings of the ASME Turbo Expo, Amsterdam, The Netherlands, 2002.

[21] Francisco Jurado. Study of Molten Carbonate Fuel Cell – Microturbine Hybrid Power Systems. Journal of Power Sources, Volume 111, 2002.

[22] A. D. Rao and G. S. Samuelsen. A Thermodynamic Analysis of Tubular Solid Oxide Fuel Cell Based Hybrid Systems. Journal of Engineering for Gas Turbines and Power, Volume 125, 2003.

[23] A. F. Massardo and L. Magistri. Internal Reforming Solid Oxide Fuel Cell Gas Turbine Combined Cycles (IRSOFC-GT) – Part II: Exergy and Thermodynamic Analyses. Journal of Engineering for Gas Turbines and Power, Volume 125, 2003.